$CdSe/CdS_xSe_{1-x}$ HETEROJUNCTIONS

by

Glenn Carl Esmond Tikasingh, M.Sc.

A thesis submitted for the degree of

Doctor of Philosphy

in the University of London

Department of Electrical Engineering,

Imperial College of Science and Technology

May 1975

ABSTRACT

Good single crystal boules of CdS, CdSe and their alloys were grown by a modified Piper-Polich vapour-phase transport technique to provide substrates for heterojunction fabrication. The alloy crystals possessed similar electrical properties to the parent materials, generally varying in magnitude in proportion to the molar ratio of S to Se. The lattice parameter varies in this way so the lattice mismatch between substrate and epitaxial layer can be changed.

A reproducible technique was devised for the fabrication of nCdSe/ $nCdS_xSe_{1-x}$ heterodiodes, the junction being formed by r.f. sputtering CdSe layers on wafers of CdS_xSe_{1-x} crystals, so that the diode characteristics were associated with the semiconductor interface rather than the technique of fabrication.

The energy band profiles were constructed from studies of the electrical properties of the constituent materials and the solution of the Poisson's equation. These studies provided theoretical values of the junction capacitance. Solutions for both abrupt and graded junctions were obtained. A mechanism of charge carrier transport will be proposed.

Measured electrical characteristics indicate a negligible role for interface states in opposition to theoretical prediction, and grading in carrier concentration of the junction.

ACKNOWLEDGEMENTS

I am greatly indebted to Dr. D. W. G. Ballentyne for his supervision, encouragement and advice throughout the course of this work. I would also like to express my gratitude to Professor J. C. Anderson for his interest and support and to Dr. M. Green for useful discussions on surface properties.

I wish to thank Mr. G. S. Holden and Mr. M. G. Bosworth of AEI Semiconductors Ltd. for their assistance in encapsulating the heterodiodes, and Mr. M. C. Petty and Mr. L. G. Hipwood of the Materials Section for their assistance in the optical measurements.

Finally I thank my wife, Julia, for her careful typing of this thesis.

LIST OF PRINCIPAL SYMBOLS

a,c	lattice constants
A,B	components in compound A^{II} B^{VI}
C	junction capacitance
D	diffusion constant
D	dielectric displacement
E_A	ionization energy of acceptors with respect to E_V
E_C	energy level at bottom of conduction band
E_D	ionization energy of donors with respect to E_C
E_G	band-gap energy
E_V	energy level at top of valence band
F	charge-carrier flux
F	electric field
I	electric current
J	mass flux of vaporized components
J	electric current density
k	Boltzmann constant
k	electron wave-number
K	equilibrum constant
K	effective electron concentration ratio
L_D	effective Debye length
m	molecular weight of vapour components
m	lattice mismatch
m_o	electron rest mass
m*	effective mass
n	molecular concentration in the vapour
n	electron concentration
N_A	acceptor concentration
N_C	effective density of state in the conduction band

N_D	donor concentration
N_V	effective density of state in the valence band
N_S	dangling bond density
p	vapour pressure
p	momentum
p	hole concentration
P_I	interfacial dipole
Q_{IS}	interfacial monopole charge density
R	resistance
R	gas constant
R_H	Hall Coefficient
S1,S2	narrow-gap and wide-gap semiconductors, respectively
T	absolute temperature
v_o	mass-average velocity of the vapour
V_i	diffusion velocity of species-i in the vapour
V	applied voltage
V_D	diffusion or built-in potential
x	anion mole fraction in mixed crystals
x	distance
X	transmission coefficient
α	non-stoichiometry coefficient
α	absorption coefficient
ϵ	dielectric constant
ϵ_o	permitivity of free-space
ξ	normalized potential
Z	normalized x
μ	mobility
ρ	space-charge
ρ	resistivity

σ electrical conductivity

ϕ electrostatic potential

χ electron affinity

ψ normalized electrostatic potential

ΔE_c discontinuity of bottom of conduction band at interface

ΔE_v discontinuity of top of valence band at interface

$\Delta \mathcal{E}_c$ normalized ΔE_c

Subscripts:-

1,2 denote narrow-gap and wide-gap semiconductors, respectively

CONTENTS

	Page
ABSTRACT	2
ACKNOWLEDGEMENTS	3
LIST OF PRINCIPAL SYMBOLS	4
CONTENTS	7
CHAPTER 1 - INTRODUCTION	10
1.1 Definition	10
1.2 Historical Survey on Heterojunction Devices	10
1.3 State of the Heterojunction Theory	14
1.4 Methods of Preparing Heterojunctions	21
1.5 Aim of the Work	25
References - Chapter 1	27
CHAPTER 2 - GROWTH OF CdS, CdSe AND THEIR ALLOY SINGLE CRYSTALS	29
2.1 Introduction	29
2.2 Crystal Growth by the Modified Piper-Polich Method	30
2.2.1 Evaporation of the Charge	33
2.2.2 Mass-Transport Via the Vapour Phase	35
2.2.3 Growth at the Crystal Surface	40
2.3 Experimental Details	43
2.3.1 The Charge	45
2.3.2 The Growth Ampoule	45
2.3.3 The Furnace and Temperature Profile	46
2.3.4 Growth of the Crystal Boule	46
2.4 Conclusion	49
References - Chapter 2	50
CHAPTER 3 - PROPERTIES OF CdS, CdSe AND THEIR ALLOYS	51
3.1 Introduction	51
3.2 Crystal Lattice Structure	52
3.3 Energy Band Structure	57
3.4 Some Transport Properties of CdS_xSe_{1-x}	61

		Page
3.4.1	Effective Mass	61
3.4.2	Carrier Mobility	62
3.4.3	Dielectric Constant	67
3.5	Imperfections in CdS and CdSe	68
3.6	Surface Properties of CdS, CdSe and CdS_xSe_{1-x}	71
3.7	Ohmic and Rectifying Contacts to CdS and CdSe	75
3.8	Space-Charge-Limited Currents	77
3.9	Optical Properties	80
References - Chapter 3		87
CHAPTER 4 - EXPERIMENTAL DETAILS		92
4.1	Introduction	92
4.2	Substrate Preparation and Electrical Assessment	92
4.3	Preparation of the CdSe Layer	95
4.4	The Fabrication of the Heterojunction Devices	98
4.4.1	Ohmic Contacts to the CdSe Layer and CdS_xSe_{1-x} substrate	99
4.4.2	Top Metallization	99
4.4.3	Back Metallization	99
4.4.4	Scribing and Dicing	100
4.4.5	Encapsulation	100
4.5	Electrical Measurements	103
References - Chapter 4		106
CHAPTER 5 - THEORY OF ISOTYPE HETEROJUNCTIONS		107
5.1	Introduction	107
5.2	Theoretical Band Profile and Junction Capacitance	107
5.2.1	Abrupt Model without Interface States	109
5.2.2	The Model with Interface States	124
5.2.3	The Graded Junction Model	135
5.3	Transport Mechanisms in Isotype Heterojunctions	141
5.3.1	Emission and Diffusion Models	141
5.3.2	Tunnelling Model	144
5.3.3	Reverse Bias Conduction	146
5.3.4	Effect of Interface States on Current Transport	147
5.4	Photo-electronic Properties	150

	Page
5.5 Conclusions	152
References - Chapter 5	154
CHAPTER 6 - RESULTS AND DISCUSSIONS	156
6.1 C-V Measurements and Deduction of Energy Band Profiles	158
6.1.1 C-V Measurements	158
6.1.2 Deduction of Energy Band Profiles of $CdSe/CdS_xSe_{1-x}$ Heterodiodes	165
6.2 I-V Characteristics	167
6.3 Spectral Photoresponse	174
References - Chapter 6	176
CHAPTER 7 - CONCLUSIONS	177
APPENDICES	180
A.1 Purity of CdS Starting Material	180
A.2 Purity of CdSe Starting Material	180
B Purity of CdSe of Sputtering Target Material	181

CHAPTER 1 - INTRODUCTION

1.1 Definition

A semiconductor heterojunction is defined as a junction between two mono-crystalline semiconductor materials having different energy band structures. It is required that the two lattices should be bonded together chemically i.e. one material is grown epitaxially onto the other. However, in most practical heterojunction devices defects occur at the junction due to the mismatch of lattice parameter and thermal mismatch, that is there is a difference in the coefficient of expansion of the two materials resulting in lattice strain on cooling from the growth temperature.

The term 'isotype heterojunction' is applied to devices having the same conductivity type i.e. n-n or p-p, while those with different conductivity types are called 'anisotype heterojunction' i.e. n-p or p-n. It is conventional to devote the first symbol to the material with the smaller energy band-gap.

The junction which exists between the two homogeneous semiconductor materials may either be 'abrupt', in which there is a sharply defined interface, or 'graded', in which the two materials are joined by an alloy of continuously varying composition.

The electronic and optoelectronic properties of the junction will be dominated by the interaction of charge carriers and photons with the discontinuities existing at the interface. Devices possessing suitable energy band structure differences will therefore be expected to exhibit pronounced electronic and optoelectronic characteristics e.g. improved injection, rectification and window-effect.

1.2 Historical Survey on Heterojunction Devices

Interest in heterojunctions began in the late 1950's when Kroemer (1957) postulated that a wide-gap emitter heterojunction transistor

would exhibit a higher injection efficiency than the homojunction counterpart. But it was not until Anderson (1960, 1962) proposed the abrupt heterojunction model, supported by experimental results on Ge-GaAs devices that interest in the heterojunction as a potential device grew. Intensive work was performed by many investigators on the Ge-GaAs system, and their ideas were then extended to many other heterojunction pairs.

The application of heterojunctions fall basically into two groups; the first utilizing the electrical properties i.e. rectification and injection and the other, the optoelectronic properties.

Isotype heterojunction devices closely resemble the metal-semiconductor (Schottky) devices, where the narrow band-gap material plays the role of the metal. A rectifying barrier is developed in the conduction band edge at the interface (for n-n heterojunctions) due to electron affinity differences in the two semiconductors. This is virtually a majority carrier device and can be utilized in switching operations. Oldham and Milnes (1963) Fang and Howard (1964) reported switching speeds of nearly 1 n-sec for their Ge-GaAs diodes. It is, however, doubtful if these devices can ever compete with the modern Schottky barrier devices (GaAs Schottky diodes fabricated by the author exhibited switching speed of smaller than a n-sec), being at present slower and more difficult to fabricate than the latter.

Anisotype heterojunction devices, on the other hand, resembles the p-n homojunction diodes and work, at forward bias, by injection of minority carriers from the wide-gap material. Due to the difference in the barrier heights for holes and electrons, it was hoped to use such a junction as the emitter-base junction of a transistor, thereby increasing the emitter injection efficiency by increasing the barrier for charge flow from the base to emitter, compared with emitter to base.

The heterojunction transistor, since first being suggested by Shockley (1951) and then by Kroemer, has received considerable interest. It was hoped that the emitter injection efficiencies could be improved by the use of the heterojunction rectifying barrier compared to homojunctions, but so far there has been little success.

Wright (1962) proposed the heterojunction transistor as a space-charge limited dielectric triode where only one contact is injecting. The first successful attempt to fabricate this type of structure was made by Brojdo (1963) using CdS on Si. Since then considerable work has been performed on heterojunction transistors by Jadus (1967), Jadus and Feucht (1969) on nGaAs-pGe-nGe structures, by Hovel and Milnes (1969) on nZnSe-pGe-nGe structures and Sleger (1971) on nZnSe-pGaAs-nGaAs structures in attempts to improve the current gain and high frequency performance of transistors. The results so far have not been very promising.

It is in their optoelectrical properties that heterojunctions come into their own. Both isotype and anisotype devices can exhibit photoelectronic properties, the effect being more pronounced in the latter.

The idea of a heterojunction injection laser consisting of a radiating base, sandwiched between two heavily doped wide-gap injectors, was proposed by Kroemer (1963). The injected carriers are confined in the narrow base region by the heterojunction barriers and, as a result, population inversion occurs i.e. injected carrier density is in excess of that in the injectors at relatively low current densities. The injection efficiency of such lasers is, however, lowered due to the presence of interface states, acting as recombination centres, caused by dangling bonds - a direct result of lattice mismatch. In an attempt to minimise the effect of these states, Alferov and Co workers (1969, 1970) Hayashi and Panish (1970) developed the close lattice match system $Al_xGa_{1-x}As$-GaAs, and have achieved much success. Room temperature C-W operation with threshold below 1000 A cm^{-2} has been reported.

Other optoelectrical devices make use of various other unique properties. One such property is the 'window effect' first reported by Preston (1950) and is the basis of detector devices. Its principle of operation is that photons incident on the wide-gap material are transmitted through this material with very little attenuation but are heavily absorbed near the interface of the low-gap material where their quantum conversion efficiency is greatest, with photon energies between that of the two energy band-gaps. This effect has been observed by Anderson (1962), Rediker et al (1964) and many other investigators. This effect is also utilized in the phototransistor heterojunction which is expected to produce a high injection efficiency in the window range of energy allowing generation within the base region Milnes and Feucht (1972).

Perhaps the most promising application of the heterojunction is in light conversion devices as solar cells and photodetectors. Emtage (1962) postulated that a graded heterojunction can theoretically create up to 40% light conversion efficiency. Solar cells operate on a reverse principle to the window effect. Again interface states cause considerable degradation of properties and energy conversions of only up to 11% have been reported (Tansley, 1969).

Another application of heterojunction devices is in the up-conversion of infra red radiation to visible light. Van Ruyven and Williams (1967a) termed the devices anti-stoke light converters. The basic structure of this converter is a graded band-gap semiconductor heterojunction in which the majority carrier density is constant. The principle of operation is that as the small band gap region is irradiated with infra-red light, the induced minority carriers drift under the external field to the wide-gap material creating higher energy photons.

A null detecting frequency meter for use in the infra-red has been described by Hampshire et al (1970) which uses the bias dependent

optical properties of nCdSe -nGe heterojunctions. At a given bias there is a particular frequency within the photoresponse range where the photo-emf is zero. The frequency at which the cross-over of sign of the photo-emf can be varied by the biasing voltage.

Further applications of heterojunction devices have been made but few have yet so far offered any advantages over the well established homojunction counterpart.

1.3 State of the Heterojunction Theory

Heterojunction theory can be explained in terms of two types of models, namely, the energy-band model in the region of the interface and a charge carrier transport mechanism through this region.

The abrupt heterojunction theory was first proposed by Anderson as an extension of the metal-semiconductor and p-n homojunction theories. He proposed energy band diagrams for both isotype and anisotype heterojunctions and explained current flow mechanism in each. It is an idealised case of two different bulk crystalline semiconductors being brought into intimate contact. The two lattices are similar so that lattice periodicity is continuous across the interface. The interface width is no more than a few atomic dimensions and the effect of interface mismatch is neglected. The quantities of interest are energy gasp, E_G, electron affinity, χ, and work function, ϕ_w. Since E_G and χ are different in most heterojunction pairs, a discontinuity in the conduction and valence bands will arise at the interface.

Anisotype Heterojunction Model

The equilibrum band diagram of Anderson for the anisotype heterojunction is illustrated in fig. 1.1. If the two semiconductors are brought into intimate contact to form the junction, at equilibrum, the Fermi level must be equalized by a net flow of carriers across the interface i.e. electrons from the lower work function material (semiconductor 1, say) and holes from the other (semiconductor 2).

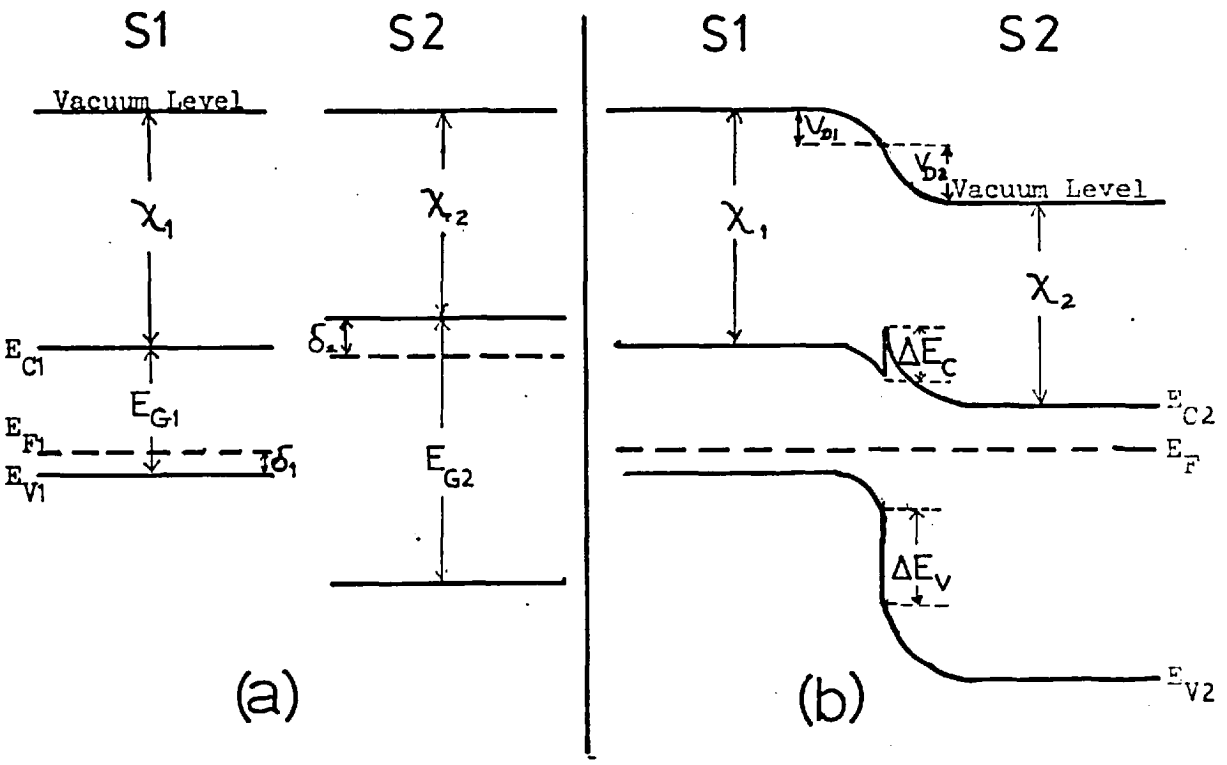


Fig. 1.1 Equilibrum Band Profile of a p-n Heterojunction

(a) Before Contact (b) After Contact

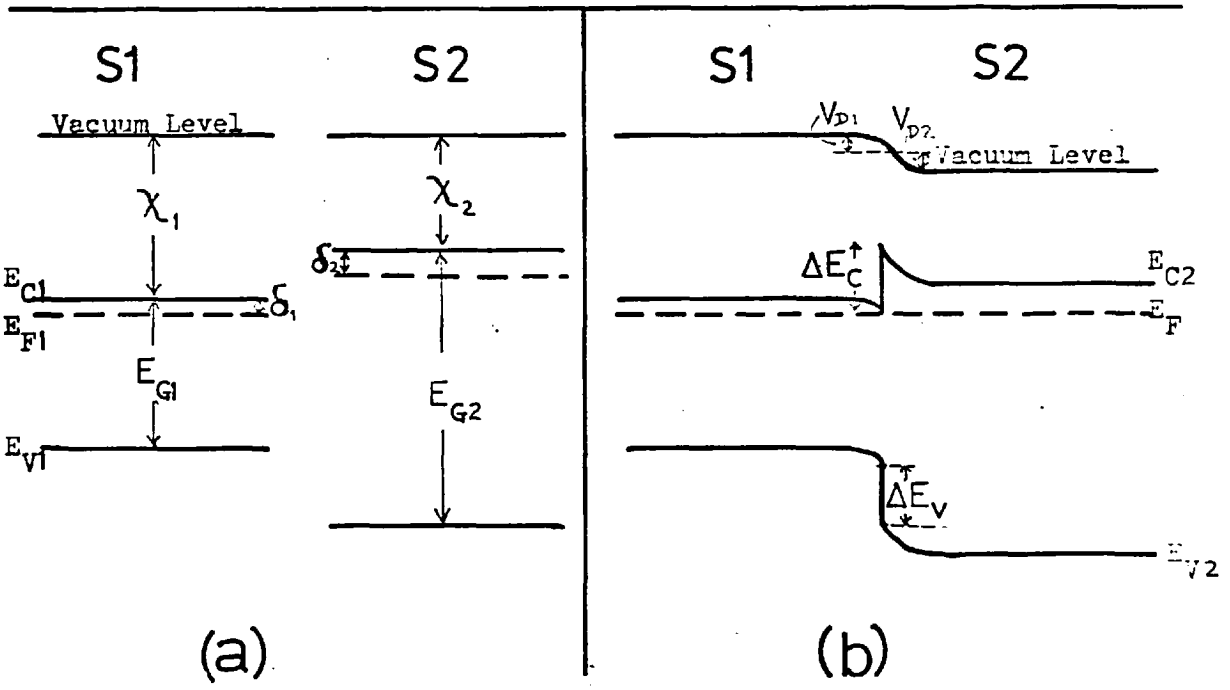


Fig. 1.2 Equilibrum Band Profile of an n-n Heterojunction

(a) Before Contact (b) After Contact

This charge transfer creates a partial depletion of electrons near the junction in semiconductor 1 corresponding to a bending upwards of the band-edge, while a redistribution of charge in semiconductor 2 corresponds to a bending down of the band-edge. A depletion region is therefore formed on either side of the interface with opposite but equal charge.

The total built-in voltage, V_D, is the difference in the work function of the two materials and equals the sum of the partial built-in voltage supported by each semiconductor. The dielectric displacement, D, and vacuum level are continuous, but the conduction band and valence band edges are discontinuous by the amounts ΔE_C and ΔE_V, respectively, where ΔE_c is the electron affinity difference for the two semiconductors.

In order to explain the charge carrier transport mechanism, Anderson adopted the Shockley diffusion theory for homojunctions. In the diagram, the barrier to hole flow is greater than that due to electron flow, so only electron flow need be considered.

The current flow in Anderson's Ge-GaAs diodes did not vary as described by the Shockley equation, being smaller and showing neither the predicted temperature nor voltage dependences. Since then, several models have been presented in an effort to give better agreement with experimental observations. However, Anderson's idealised model is a basic one from which many new heterojunction models can be developed. If the arrays of interface states, arising from the lattice and thermal mismatches and the adsorption of impurities, are included many possible transport models can be obtained.

Perlman and Feucht (1964) adopted the basic model of Anderson and assumed two modes of operation - homojunction type and metal-semiconductor type operations. The majority carriers are first injected by thermal emission over the spike barrier, piling up at the edge of the depletion region which limits the passage of current. Then by a Schottky type operation, the carriers diffuse in the conduction band of the narrow-

gap material. In the latter type of operation, carrier reflection at the interface has little affect on the total current. However, the magnitude of current predicted from this model is still too small and does not describe most heterojunction behaviour over the whole or part of the voltage range. Both this and Anderson's models describe current flow by carriers surmounting the potential barrier and are therefore termed 'thermal currents'.

Rediker et al (1964)proposed a different model in which the electrons tunnel through the spike barrier from the conduction band of the wide gap material into the narrow-gap material where they combine with holes. This tunnelling current, termed 'non-thermal current' is given by the product of the tunnelling probability and the incident electron flux. Rediker et al do not describe the temperature dependence of the excess current although tunnelling currents are very weakly temperature dependent.

Riben and Feucht (1966) assumed a tunnelling - recombination mechanism to explain device characteristics and suggested total recombination at the interface states which prevent injection of minority carriers. They observed that in addition to the very small current temperature dependence, the I-V characteristics were similar to the excess current observed in Esaki tunnel diodes. They concluded non-thermal currents were dominant and the transport mechanism involved band-to-band tunnelling of both type of carriers.

Riben and Feucht (1966) extended the idea of single-step to multi-step recombination where interface states are spacially distributed in the space-charge region. However, since the interface state distribution is not known, it is not possible to determine quantatively the magnitude of the currents.

Donnelly and Milnes (1966) observed that none of the previous models predicted I-V values in agreement with real device characteristics.

So they combined previous transport models to produce simultaneous thermal emission and tunnelling transport mechanisms. This model has been used to interpret observed I-V characteristics for many anisotype devices and six possible major transport processes have been presented (Donnelly and Milnes, 1966).

Isotype Heterojunction Model

The earliest isotype heterojunction energy band profile was presented by Anderson (1962) in the same paper as the anisotype heterojunction. When the two semiconductor materials are brought into intimate contact a charge transfer takes place as described for the anisotype structures, giving space-charge regions at the interface. This space-charge region is now presented as a depletion region in semiconductor 1 (lower work-function) and an accumulation region in S2 shown in Fig.1.2. In this model there is no minority carrier injection.

Anderson neglected the affect of interface states and adopted the transport mechanism of Schottky diodes. This model is in fair agreement with only a few heterojunction pairs, where lattice mismatch is small ($<1\%$).

In the case of isotype heterojunctions having large mismatch e.g. Ge-Si, some observed I-V characteristics show a tendency to current saturate for both polarities of voltage. Oldham and Milnes (1964) postulated that for such devices, a net interface charge is produced by interface states in the forbidden gap arising from lattice mismatch. If sufficient interface states are generated to form a monopole layer, the energy-band at the interface must move up or down. If the density of electrons at the interface is high the band bending in the accumulation layer is reduced or even a depletion layer may be formed e.g. for Ge-Si junctions, two positively charged depletion regions on either side of the interface will result because of the acceptor - like nature of the interface states. This double-depletion

model is commonly referred to as 'two Schottky diodes back-to-back,' where the surface states play the role of the metal. These interface states act as recombination centres of large capture cross-section and greatly affect the transport of carriers across the junction. For high interface state density, all carriers traversing this region are trapped and subsequently re-emitted. Oldham and Milnes neglected tunnelling of carriers and derived I-V characteristics from the emission theory.

Van Orpdorp and Kanerva (1967) and Van Orpdorp (1969) extended this idea of double Schottky diodes and presented a mathematical analysis of this model. They observed for both polarities, a Schottky type characteristic at low voltages followed by a soft breakdown at higher voltages. The I-V curve has a point of inflection which can be seen as a displacement of the origin of the I-V axes.

Van Ruyven (1964) introduced a dipole arising from the difference in free surface work-functions in addition to the monopole of the previous model to account for the discrepancy between observed and predicted energy discontinuities. In this model, the two surfaces are brought into contact - i.e. each material having the band structures of their free surfaces. On contract, these states will partially cancel in the bonding of one material to the other (complete cancellation is equivalent to Anderson's model), leaving interface states, and a dipole, resulting in a discontinuity in the vacuum level. This model differs from the previous ones only in magnitude of the band discontinuity, ΔE_C.

Carrier transport in isotype heterojunctions has received considerable attention, especially those devices not exhibiting double current saturation. The simplest approach has been to consider Schottky-type operation in the absence of interface states. But because of the discrepancy between observed and predicted I-V values, it has been suggested that tunnelling effectively reduces the barrier height.

Oldham and Milnes included interface states as lying in the band gap in a thin layer between two depletion regions and presented a kinetic treatment describing electron fluxes for this class of device. The effect of tunnelling and images are neglected in his treatment.

Graded Heterojunction Model

There has been relatively little theorectical work on graded heterojunctions. An early theoretical study on the photovoltaic effect in semiconductor structures with linear variations of band gap and electron affinity with distance was made by Emtage (1962), who used a number of simplifying assumptions to solve the transport equations.

Oldham and Milnes (1963) presented a model for graded heterojunctions with continuously varying band-gap and electron affinity and emphasized a basic requirement for rectification that a certain degree of 'abruptness' of the junction is necessary.

The earliest graded model was presented by Kroemer (1957) for inhomogeneous graded regions in which he introduced quasi-electric and quasi-magnetic fields due to the grading of band-gaps in order to describe charge carrier motion through the junction. However, he did not separate the effects of grading on the band edge and from built-in or external field due to the space-charge both effects of which cause the band bending. Van Ruyren and Williams (1967b) extended this treatment and separated these effects by considering the transport of charge carriers in inhomogeneously doped non-uniform semiconductors so that there is no space-charge. The graded region is macroscopically graded and is treated as comprising of homogeneous layers to form a series of microscopic adjacent abrupt heterojunctions. Gora and Williams (1969) theorectically describe carrier transport in graded junctions $\gtrsim$ 100 lattice spacings of inhomogeneous systems where the constituent materials have same structure and lattice constant. The

effective mass is also treated as a position dependent parameter in their study. Roth and Bennett (1972) presented a relatively simple one-band one-dimensional model to study the electrical properties of more realistic graded heterojunction where composition varies over a few lattice spacings. However, lattice mismatch is ignored in their study in which two bulk materials are represented by 15 atoms. A qualitative discussion of heterojunction theory will be presented in Chapter 5.

1.4 Methods of Preparing Heterojunctions

The preparation of heterostructures involves the growth of an epitaxial layer of one semiconductor onto a single crystal substrate of another semiconductor. It is desirable that for good hetero-epitaxial growth, the crystal structure of the two materials are similar and the lattice parameters closely matched. It is important that the crystal substrate should be chemically treated after being cut, lapped and mechanically polished to remove damage and contamination from the surface, leaving it virtually flat and clean prior to epitaxy.

The choice of epitaxy will depend on factors as layer thickness, desired abruptness of the junction, stoichiometry of composition, degree of lattice misfit and technological advances. Not all the heterojunction systems can be fabricated using the same growth methods, and it is necessary that the experimentalist should consider the effect of the growth method on the particular system as it is found that the heterojunction properties are correlated to the manner in which the devices are fabricated. The main methods of growth are interface alloying, vapour phase growth, evaporation and r.f. sputtering. These techniques will be outlined below giving their merits and indicating some disadvantages.

(i) Interface Alloying

This technique involves placing the two semiconductor materials

in contact with each other on a strip heater, with the higher melting point material under the other. This is normally done in a hydrogen or inert gas ambient. The heater produces a temperature gradient across the interface and at a particular temperature, the bottom of the low melting-point material melts. As soon as wetting is observed and before the rest of the low melting point material becomes liquid, the temperature is reduced, resulting in recrystallisation of the melt on the substrate material.

This method is relatively simple and inexpensive and has been used to fabricate a large number of heterostructures. Using materials of significantly different melting points, the technique produces virtually an alloy of the two materials at the interface and will give rise to graded junctions. It is therefore important to keep the alloying time as short as possible to avoid excessive impurity cross-diffusion and hence preserve rectification. Only relatively thick epitaxial layers can be obtained from this method.

(ii) Vapour Phase Growth

Vapour phase growth has been used quite satisfactorily to produce epitaxy in both open and closed tube systems. In the closed tube system an evacuated tube containing the semiconductors is held in a two-zone furnace so that the source, which may or may not include dopants, is transported via the vapour phase from the high temperature region onto a substrate in the low-temperature region. Transport reagent e.g. hydrogen and halides, are often used, and these flow back to the source after deposition to start a new cycle, thus producing continuous epitaxy. The open tube system is similar to the above except the transport reagent flows over the heated source.

Contamination of the epitaxial layer by the transport reagent has been reported by several works (Riben et al, 1965; Zeidenbergs and Anderson, 1967). These impurities may act as donor or acceptor in some of the semiconductors (e.g. I_2 acts as donor centres

in CdS crystals). The process involves lengthy growth periods at elevated temperatures, increasing the probability of graded junctions.

(iii) Solution Growth

Heterojunctions have been successfully fabricated using the solution growth method which involves the solution of one semiconductor material by a suitable solvent metal to form a saturated solution. The solution is allowed to flow over the second semiconductor (substrate) while the system is allowed to cool slowly, thereby precipitating the semiconductor solute onto the substrate to form an epitaxial layer. An example of this method is the exchange of Ga for In atoms in a bismuth melt in the fabrication of $Ga_x In_{1-x}As$-GaAs structures.

Because the process takes place at high temperatures and for long periods while the precipitate is in contact with the solution, the junction 'abruptness' can be expected to degrade.

(iv) Evaporation

The evaporation technique has invoked considerable interest over the past years (Oldham and Milnes, 1964; Muller and Zuleeg, 1964) mainly because it is a simple technique involving low substrate temperatures. The source material is conveniently evaporated by resistance of r.f. heating, or by electron bombardment (in an evacuated chamber where the background pressure is $< 10^{-5}$ torr.)

The major advantages of this technique are the controllability of substrate temperatures and evaporation rates so that layers of thicknesses from monomolecular to several microns can conveniently be produced. The technique can be used for a wide range of elemental or compound semiconductors. Two important disadvantages using this method are the formation of polycrystalline and non-stoichiometric films. It is possible to overcome the first problem by using high substrate temperatures with the risk of degrading the junction. A 'flash evaporation' technique has been developed in an attempt to improve the stoichiometry of the

epitaxial layer, (e.g. Holloway et al, 1966)

(v) Sputtering

This process involves removal of atoms or molecules from the target material (to be deposited onto a suitable substrate) by momentum transfer under the bombardment of positive ions accelerated by an applied field. These positive ions are normally generated by an electron flow from a hot cathode through a gas or by r.f. excitation of the gas to form a plasma. Ions are used instead of neutral atoms because they can conveniently be accelerated.

R.F. sputtering developed by Davidse and Maissel (1966) has been used to produce good quality semiconductor films. It has the advantage over d.c. sputtering of operations at lower gas pressures so that sputtered particles make fewer collisions with gas molecules resulting in increased growth rates.

Sputtering is more versatile than evaporation as different materials can be used (e.g. insulators, semconductors as well as conductors). Better stoichiometric films are obtained with the elimination of spitting, and in general a better quality film is obtained. One of the main disadvantages of sputtering is the low growth rate, hence epitaxial layers are limited in thickness.

The techniques and difficulties in the fabrication of heterojunction devices are numerous and it is not possible practically to grow epitaxial layers under the most ideal conditions e.g. while attempting to enhance the abruptness of the junction using either evaporation or sputtering a low substrate temperature is chosen but this can result in decreasing the surface mobility of the deposited film - an undesirable effect. It is therefore necessary to obtain a compromise between surface mobility and junction abruptness.

Two main problems involved in heterojunction epitaxy are the

formation of large numbers of interface states at the junction and loss of abruptness of the junction. In fabricating some devices it is found that one or both faults are present resulting from the choice of the heterojunction pair or the method of epitaxy. In order to fabricate devices with favourable heterojunction properties, it is therefore desirable to conform to the following properties.

(a) Surface damage and impurities are to be reduced or eliminated from the substrate before epitaxy.

(b) Lattice mismatch should be less than 1%.

(c) Materials should have similar coefficients of expansion impurity cross-diffusion must be minimised.

1.5 Aim of the Work

The main aim of the work involved firstly growth of good qualtiy single crystals of CdS, CdSe and their alloys to obtain good substrates for epitaxy. This was achieved using a modified Piper-Polich vapour transport technique under the conditions of Ballentyne et al (1970). Secondly, the heterostructures were obtained by r.f. sputtering CdSe from a compressed powder target under conditions which gave good epitaxial growth. Finally, the device properties were investigated with special regards to variations in lattice mismatch and rectification with composition of the substrate material. The heterojunction theories developed in this study were applied to the CdSe/CdS_xSe_{1-x} devices in order to derive a model to explain their properties.

The flow diagram of Fig. 1.3 describes the step-by-step processing involved in the fabrication of these heterodiodes from which reliable measurements could be made.

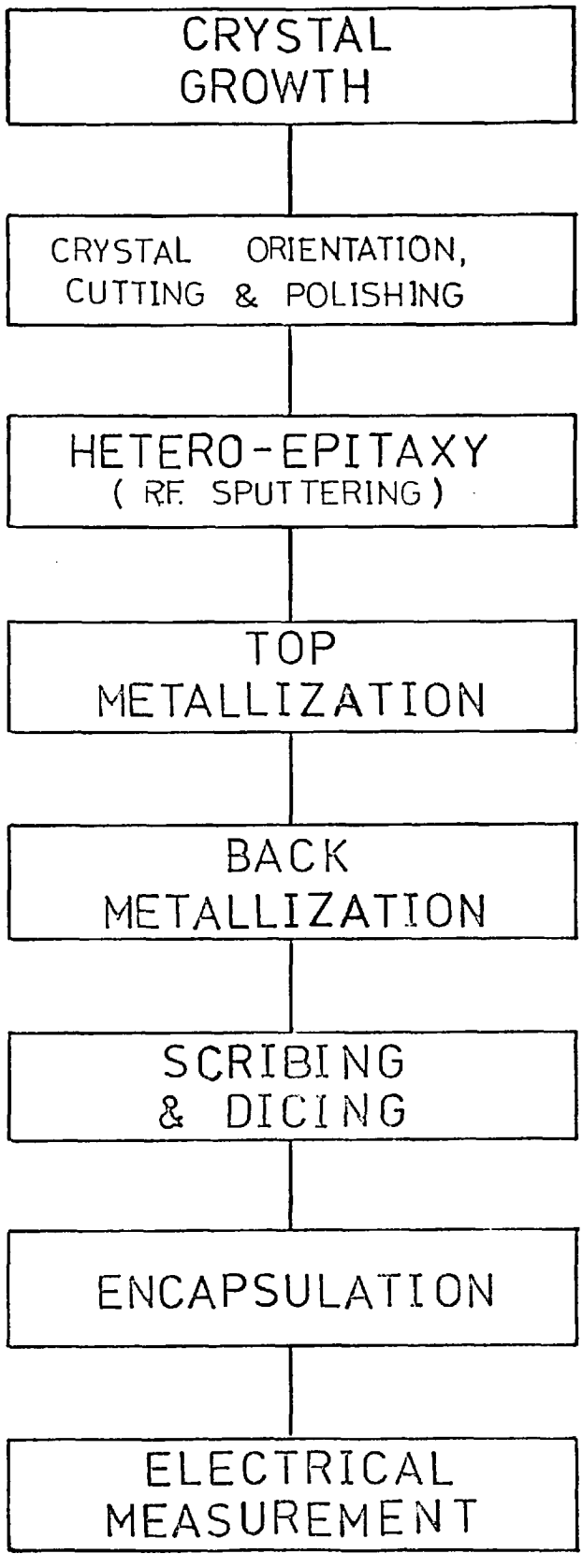


Fig. 1.3 Flow Chart of the Experimental Work

REFERENCES - CHAPTER 1

Alferov, Zh. I., Andreev, V. M., Korol'kov, V.I., Portnoi, E. L., Tret'yakov, D. N. (1969) Sov. Phys.-Semicond. 2, 843.

Alferov, Zh. I. (1970) J. Luminescence 1,2, 869.

Anderson, R.L. (1960) IBM J. Res. Develop. 4, 283.

Anderson, R.L. (1962) Sol. St. Electron 5, 341.

Ballentyne, D.W.G., Wetwatana, S., White, E.A.D. (1970) Crystal Growth 7, 79

Brojdo, S. (1963) Sol. St. Electron. 6, 611.

Davidse, P. D. (1967) Vacuum 17, 139.

Donnelly, J. P., Milnes, A. G. (1966) Proc. IEE. 113, 1468.

Emtage, P. R. (1962) J. Appl. Phys. 33, 1950

Fang, F. F., Howard, W. E. (1964) J. Appl. Phys. 35, 612.

Gora, T., Williams, F. E. (1969) Phys. Rev. 117, 1179

Hampshire, M. J., Pritchard, T. I., Tomlinson, R. D. (1970) Sol. St. Electron 13, 1073.

Hayashi, I., Parish, M. B. (1970) J. Appl. Phys. 41, 150.

Holloway, H., Richards, J. L., Bobb, L.C., Perry, J., Zinnerman, E. (1966) J. Appl. Phys. 37, 4694.

Hovel, H. J., Milnes, A. G. (1969) IEEE ED-16, 766.

Jadus, D.K. (1967) Ph.D. Thesis, Carnegie-Mellon Univ., Pittsburg, Pennsylvania.

Jadus, D.K., Feucht, D. L. (1969) IEEE Trans. Electron Devices ED-16, 102.

Kroemer, H. (1957) Proc. IRE 45, 1535

Kroemer, H. (1963) Proc. IEEE 51, 1782.

Miles, A. G., Feucht, D. L. (1972) Heterojunctions and Metal-Semiconductor Junctions, Academic Press, p.16.

Muller, R. S., Zuleeg, R.(1964) J. Appl. Phys. 35, 1550.

Oldham, W. G., Milnes, A. G. (1963) Sol. St. Electron. 6, 121.

Oldham, W. G., Milnes, A. G. (1964) Sol St. Electron. 7, 153.

Perlman, S. S., Feucht, D. L. (1964) Sol. St. Electron. 7, 911.

Preson, J. S., (1950) Proc. Roy. Soc. A202, 449.

Rediker, R. H., Stopek, S., Ward, J. R. H. (1964) Sol. St. Electron. 7, 621

Riben, A. R., Feucht, D. L. (1966) Int. J. Electron. 20, 583

Riben, A. R., Oldham, W. G., Feucht, D. L. (1965) J. Appl. Phys. 36, 3685

Roth, L. M., Bennett, A. J. (1972) Phys. Rev. B 6,6, 2238

Shockley, W. (1951) U.S. Patent 2, 569, 347.

Sleger, K. (1971) Ph.D. Thesis, Carnegie-Mellon Univ.

Tansley, T. L. (1971) Semicond. and Semimetals 7A, 293.

Van Opdorp, C., Kanerva, H. K. J. (1967) Sol. St. Electron. 10, 401.

Van Opdorp, C. (1969) Philips Res. Rep. Suppl. 10, 1.

Van Ruyven, L. J. (1964) Phys. Stat. Solidi 3, K109.

Van Ruyven, L. J., Williams, F. E. (1967a) Sol St. Electron 10, 1159.

Van Ruyven, L. J., Williams, F. E. (1967b) Amer. J. Phys. 35, 705.

Wright, G. T. (1962) Sol St. Elecrron. 5, 117.

Zeidenbergs, G., Anderson R. L. (1967) Sol. St. Electron 10, 113.

CHAPTER 2 - GROWTH OF CdS, CdSe AND THEIR ALLOY SINGLE CRYSTALS

2.1 Introduction

In order to fabricate good quality heterojunction devices, good single crystals are required for the substrates.

There are three main methods for growing single crystal boules:-

1. growth from the melt,
2. growth from solution, and
3. growth via the vapour phase.

Large cadmium sulphide crystals have successfully been grown from the melt (Takahashi et al, 1963). Sublimation of the cadmium sulphide below its melting point is a major difficulty in using this technique. High pressures of an inert gas can be applied over the melt to prevent loss of charge by evaporation and to lower the melting point (1800°C at 50 atmospheres).

Growth from solution has received less attention, mainly because crystals grown by this method are usually small. Rubenstein (1966) first reported growth of CdS from bismuth solution while other metallic solvents as Cd, Sn and Pb have been used to grow CdS and other II-VI compound crystals.

The vapour phase method has invoked considerable interest mainly because high quality single crystals can be grown with relatively simple apparatus. There are two vapour phase methods, the dynamic flow method and the static or sealed-tube method. The former produces needles or platelets of crystals and is therefore not suitable in this work. The static method was first devised by Reynolds and Czyzak (1950) for growing ZnS crystals and was later modified to grow bigger crystals (Green et al, 1958). Two further but significant modifications were introduced by Piper and Polich (1961) and involves (a) the growth tube traversing the temperature gradient of the furnace and (b) a conical tip at the growth surface for the initial nucleation. Several variations of this method

have been offered (Clark & Woods, 1966; Toyama, 1966) but these are only minor. The method of Wetwatana (1969), Ballentyne et al (1970) was adopted for growth of single crystal boules of cadmium sulphide, selenide and sulpho-selenide and will be discussed in this chapter.

A further variation of the vapour phase method is based on the principle of chemical transport reaction and was proposed by Nitsche (1960). Iodine is included in the ampoule which acts merely as a transport reagent. CdS reacts with the iodine to produce gaseous species of cadmium iodide and sulphur which diffuse to the cold region of the tube where CdS crystal reforms, regenerating iodine to return to the hot zone to start another cycle. A disadvantage of this method is that transport reagent impurities are included in the crystal and often act as dopants, hence this method is not suitable for producing crystals for this work.

In this chapter the theoretical work of Ballentyne et al, with simplifications by Tempest (1974) will be reviewed, and the derived experimental conditions of Ballentyne et al will be used to grow single crystals of CdS, CdSe and their alloys. The reproducibility of crystal growth and their quality grown under these conditions will be discussed.

2.2 Crystal Growth by the Modified Piper-Polich Method

The sublimation method devised by Czyzak et al (1952) was established by Piper and Polich (1961). Toyama (1966) developed growth kinetics for II-VI compounds using the experimental method of Piper. The growth process in a sealed ampoule is divided into three steps viz

(i) Evaporation of the charge.

(ii) Mass transport via the vapour-phase.

and (iii) Condensation of the vapour at the crystal surface.

Ballentyne et al developed these ideas further and although their equations are accurate in predicting growth rates, they are very tedious to derive. In their treatment, the vapour species are assumed to be in

mutual equilibrum with the solid at the charge and crystal interfaces. Faktor and Garrett (1971) developed the theory one step further by assuming activated absorption of the vapour species at the crystal surface. Tempest adopted this idea and making suitable simplifying assumptions (e.g. uni-diffusion coefficient for all vaporized species) and simplified the growth rate equation of Ballentyne et al without losing a great deal of accuracy.

The modified Piper method is as follows:-

A high purity quartz tube, termed, the 'growth ampoule' is sealed with high purity polycrystalline lumps of charge in an inert gas of a pressure 20 torr, illustrated in Fig. 2.1. The inert gas simply controls the diffusion process and, hence, growth of the crystals and neither reacts chemically with the compound $A^{II}B^{VI}$, nor alter the partial pressures of A(g) and B_2(g) vapours. The ampoule is held vertically in a two-zone furnace with the desired temperature gradient (Fig. 2.1) and then pulled smoothly through this temperature gradient to match the crystal growth rate. Here, the tip of the ampoule traverses the temperature gradient and becomes cool while the charge remains virtually at a constant temperature, T(0), resulting in evaporation of some of the charge which fills the whole tube. This gives rise to vapour pressures which reach a thermal equilibrum value, depending on the value of T(0). Nucleation of the solid AB occurs at the conical tip of the ampoule where suitable sites are available, and held at a lower temperature T(1) where the vapour is sufficiently supersaturated. This forms a seed for subsequent growth and a crystal grows out at the tip. The pulling speed of the ampoule has to match the growth rate of the crystal.

The crystal growth theory is applied to CdS but is equally applicable to CdS_xSe_{1-x} since, under the conditions of diffusion-limited growth

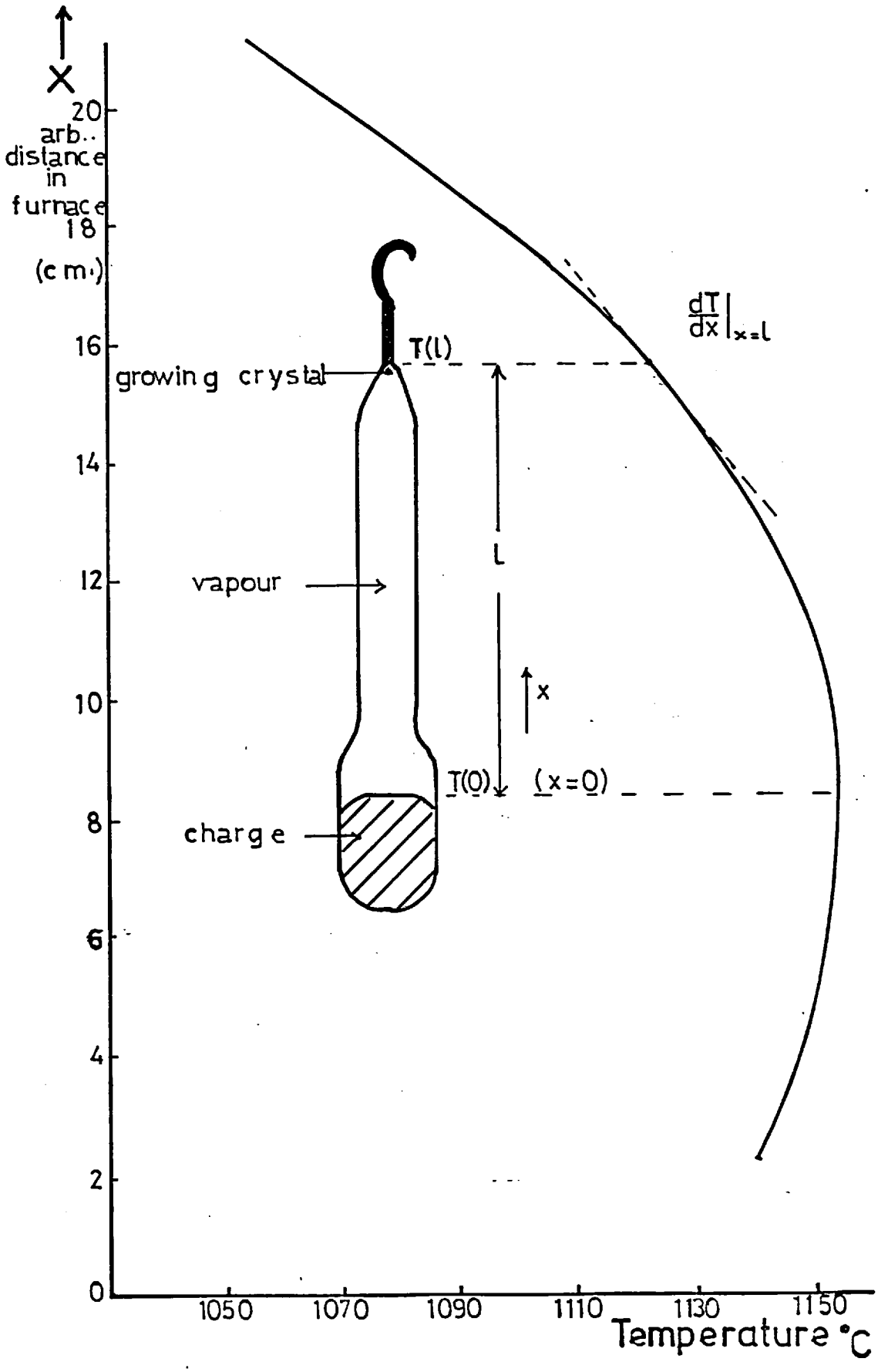


Fig. 2.1 Temperature Profile of Furnace and Position of Ampoule along the Temperature Gradient

(discussed in paragraph 2.2.2 from which the crystals were grown) because growth parameters especially the equilibrum vapour pressures and diffusion coefficient of CdS and CdSe are so similar, then the predicted growth rates for CdS and CdSe are almost identical. If, however, crystals are grown under condensation-limited conditions (though none were grown in this work) growth rates would be higher for CdSe.

The crystal growth proceeses of CdS_xSe_{1-x} can be represented by the equation

$$x\ CdS(s) + (1-x)\ CdSe(s) \longrightarrow Cd(g) + \frac{x}{2} S_2(g) + \frac{1-x}{2} Se_2(g)$$

$$\longrightarrow CdS_xSe_{1-x}(s)$$

where the charge consists of a mixture of CdS and CdSe in molar ratio x : (1-x). Under diffusion-limited conditions, the selenium molecule behaves similarly as a sulphur molecule.

2.2.1 Evaporation of the Charge

Stoichiometric II-VI compounds dissociate on sublimation at high temperatures according to

$$AB\ (s) \rightleftharpoons A(g) + \tfrac{1}{2}B_2(g) \qquad (2\text{-}1)$$

It has been shown that the molecular species AB(g) does not exist in the vapour state (Ban, 1972). The partial pressures of the two vaporized components is given by

$$P_{1S} \cdot P_{2S}^{\frac{1}{2}} = K \qquad (2\text{-}2)$$

where K is the equilibrum constant of the equation. The total pressure P_S is the sum of the two partial pressures.

$$P_S = P_{1S} + P_{2S} \qquad (2\text{-}3)$$

At equilibrum, it follows that

$$\frac{\partial P_S}{\partial P_{1S}} = 0 = \frac{\partial P_S}{\partial P_{2S}} \qquad (2\text{-}4)$$

From equations (2) and (3) $P_{1S} = 2P_{2S}$ (2-5)

and $P_S = (\frac{3}{2})\ 2^{\frac{1}{3}}\ K^{\frac{2}{3}}$ (2-6)

K can be expressed in terms of the free energy change, ΔG and temperature T as

$$K = \exp\left(-\frac{\Delta G}{RT}\right) = \exp\frac{\Delta S}{R} \quad \exp\ -\frac{\Delta H}{RT} \qquad (2\text{-}7)$$

where ΔS is the change in entropy, ΔH, the change in enthalpy and R, the gas constant.

The total pressure can be expressed in the form

$$P_S = A \exp\ (-\ b/T) \qquad (2\text{-}8)$$

where A and b are constants, which can be evaluated from experimental data for K.

If, however, the charge is non-stoichiometric, then the vapour would be rich in one species (Cd in CdS or CdSe), making the condition $P_1 = 2P_2$ invalid. Wetwatana applied the Gibb-Duhem equation to obtain new partial pressures

$$P_1 \cdot P_2 = P_{1S} \cdot P_{2S} = 2/9\ \ P_S^{\,2} \qquad (2\text{-}9)$$

or in terms of the concentration of species 1 and 2

$$n_1(0)\ .\ n_2(0) = 2/9\ \ A^2/(RT(0))^2\ \ \exp\ (-2b/T) = K_{NS}(0) \qquad (2\text{-}10)$$

The effect of an excess component is to reduce the rate of vaporization of the charge due to the diffusion of Cd or S atoms from the bulk to the surface (Somorjai and Jepsen, 1964).

When an inert gas is included with the vaporised components in equilibrum with a stoichiometric charge, the sum of the partial pressures is only a little higher than P_S, giving

$$P = P_{1S} + P_{2S} + P_3 = P_S + P_3 \qquad (2\text{-}12)$$

The vacuum evaporation rate of the c-face of undoped or uncompensated CdS at 1150°C has been measured by Somarjai (1962) as 2.88×10^{-1} gm cm^{-2} sec^{-1}. The rate of evaporation of polycrystalline material will be about this value. However, if the charge contains excess Cd the rate will be reduced by about an order of magnitude (Wetwatana). But the

growth-rate, corresponding to mass-transfer in a Piper method is < 1% of this rate, therefore the evaporation rate in the ampoule is sufficient to maintain the thermal equilibrum partial pressure.

2.2.2 Mass- Transport Via the Vapour Phase

After the charge evaporation process, the ampoule contains mixed vapours of species i, with average velocity v_i (relative to a fixed axis, x, in space along the length of the ampoule), such that $v_i > 0$, due to a change in molecular concentration, n_i, at the crystal surface, and thus serves as a driving force.

For each component, the mass-flux J_i is expressed as

$$J_i = n_i v_i \qquad (2\text{-}13)$$

After obtaining steady state condition, $\frac{dJ_i}{dx} = 0$ for a stoichiometric vapour, the vapour moves as a whole with mass average velocity, v_o, given by $v_o = J_i / n_i$ and $v_i = v_o$. If the ampoule contains a vapour (Ar) which does not condense, this vapour will try to accumulate at the crystal surface (where its vapour pressure is greatest) but will eventually diffuse back along the tube. The diffusion velocity will then be given by $V_i = v_i - v_o$, but since V_i is in the direction of its negative concentration gradient $v_i = -\frac{D_i}{n_i}\frac{dn_i}{dx}$, where D_i is the ternary diffusion velocity of the i^{th} component, the mass-flux of the i^{th} component in a three component vapour is

$$J_i = n_i v_o - D_i \frac{dn_i}{dx} \qquad (2\text{-}14)$$

In trying to solve the mass-flux and growth equations it is necessary to make certain simplifying assumptions viz

(i) The solid AB is isotropic - only one phase is present

(ii) Constant diameter ampoule, therefore a 1-D analysis can be made.

(iii) Charge and crystal have same density.

(iv) Only the vapours A(g), B_2(g) and Ar(g) are present and they behave as perfect gases.

(v) The pulling speed is identical to the crystal growth rate making T(1) and T(0) constant during growth.

(vi) In calculating the mass-flux, temperature, total pressure and diffusion coefficient are constant throughout the vapour.

Tempest made further simplifying assumptions:-

(a) The concentration of the vapour species at the charge surface $n_1(0)$ and $n_2(0)$, are fixed. This was assumed on the basis of spectrographic data in the vapour at different temperatures.

(b) $n_1(0)$ and $n_2(0)$ must satisfy the equilibrum condition given by equation (2-10).

(c) All diffusion coefficients are equal and a function of temperature only i.e.

$D_i = D_j = D_k = D$ where D is an average value. The binary diffusion coefficient D_{ij} was calculated from the formula of Reid and Sherwood (1966).

Since $A^{II}B^{VI}$ dissociates to form one mole A and $\frac{1}{2}$ mole B, then $J_1(s) = 2J_2(s)$, and since there is no nett flow of argon, $J_3 = 0$. Hence, at the charge surface $J_1(0) = 2J_2(0)$ and at the crystal surface $J_1(1) = 2J_2(1)$. Under steady state conditions $J_1 = 2J_2 = J$ (2-15) is the mass flux of AB molecules, is the boundary conditions used to solve equation (2-14).

The value of concentration n along the tube is considered constant (from viscous flow theory), so

$$n = n_1 + n_2 + n_3 \qquad (2\text{-}16)$$

Applying the boundary condition of equation (2-15) to the mass-flux rate equation (2-14), and fulfilling the above conditions, Tempest obtained the mass-flux as

$$J_d = \frac{2nD}{3l} \ln \left[\frac{n - 3n_2(1)}{n - 3n_2(0)}\right] \qquad (2\text{-}17a)$$

$$\text{where } n_2(1) = \frac{n}{2}\left[\frac{c-2}{3c}\right] + \left[\frac{n}{2}\cdot\left(\frac{c-2}{3c}\right)^2 + \frac{K_{NS}(1)}{c}\right]^{\frac{1}{2}} \qquad (2\text{-}17b)$$

If the growth rate is limited by the rate of diffusion of the vapours, the above expression can be used to determine the value of J_d, this is shown in Fig. 2.2 for CdS, as a function of temperature difference, ΔT, along the tube. As mentioned previously, the equilibrum vapour pressure (Lorentz, 1967) and diffusion coefficient of CdS and CdSe are very similar, also, the collision integral and force constant of these materials too are very similar (Tempest), then Fig. 2.2 also represents the growth rate of CdS_xSe_{1-x} crystals. (Similar curves of Wetwatana and Faktor are included in the diagram for comparison. The value obtained by Tempest was 20% smaller than the value of Wetwatana as a result of these simplifications. The larger discrepancy with the curve of Faktor was attributed to the use of different data in calculating D.

Instability of the growing surface can result from constitutional supersaturation and gives rise to dendritic growth under non-stoichiometric conditions. If the concentration of condensing and saturated species are n_i and n_{iT}, respectively, then stable growth will result if the condition

$$\left.\frac{d\ n_{iT}}{dx}\right|_{x = L} \geqslant \left.\frac{dn_i}{dx}\right|_{x = L}$$

is fulfilled.

The concentration gradient of $B_2(g)$ molecules is given (from equation (2-16) as

$$\left.\frac{d_{n2}}{dx}\right|_{x = L} = -\frac{J}{2nD}\ (n - 3n_2(1)) \qquad (2.18)$$

The equilibrum concentration of B_2 molecules, n_{2T}, given by the equation (2-17b) is used with the gas equation, $P_S = A\exp - b/T$, to obtain an expression for the critical growth rate as

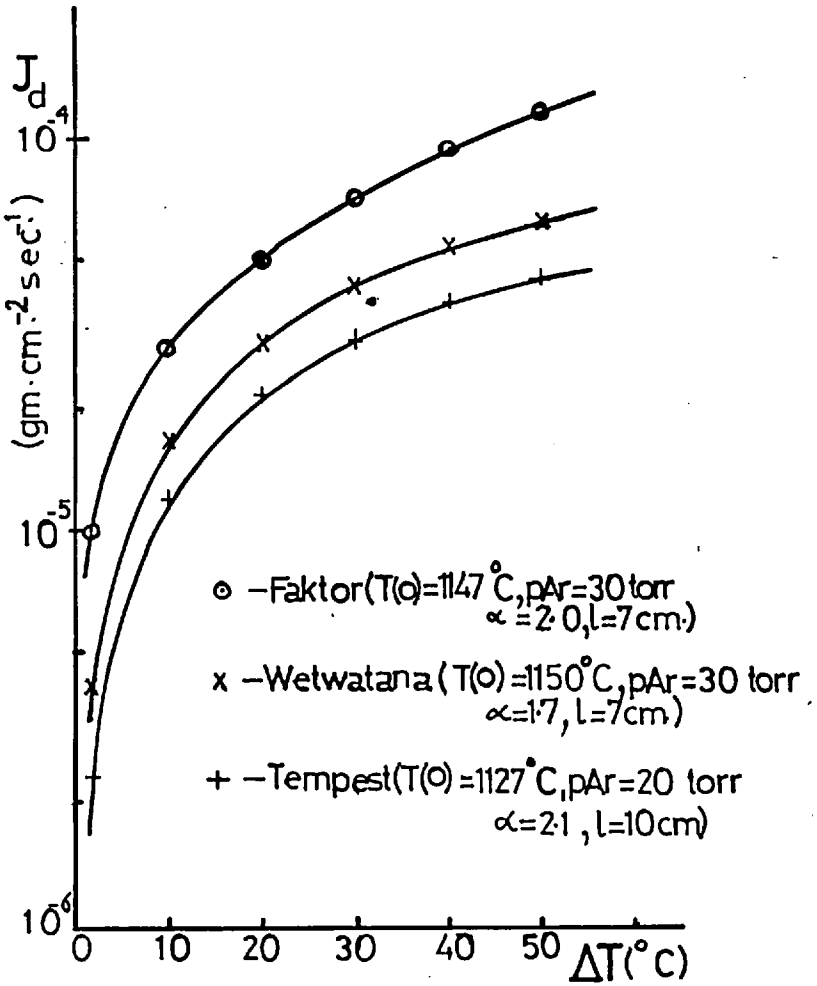


Fig. 2.2 Diffusion-Limited Growth of CdS (and CdS_xSe_{1-x})

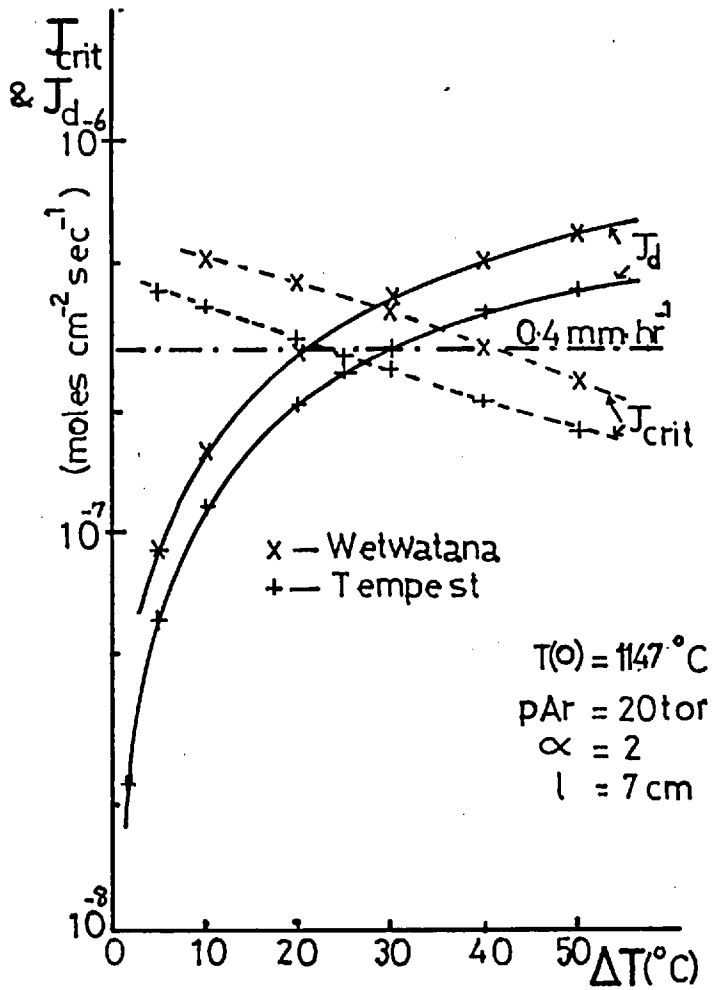


Fig. 2.3 Variation of J_d and J_c with T for CdS (and CdS_xSe_{1-x})

$$J_{Crit} = \frac{2nD\, K_{NS(1)} \left[\frac{b/T(1) - 1}{T(1)} \right] \frac{dT}{dx} \Big|_{x=1}}{c(n-3n_2(1)) \left[\left(\frac{n}{2} \frac{(C-2)}{3C} \right)^2 + \frac{K_{NS}(1)}{C} \right]^{\frac{1}{2}}} \qquad (2\text{-}19)$$

For stable growth $J_d > J_{crit}$. The value of J_{crit} for CdS (and also applies for CdS_xSe_{1-x}) as a function of ΔT is illustrated in Fig. 2-3 together with the J_d curve. Again J_{crit} is ~20% lower than that of Ballentyne et al.

The limiting condition for stable growth can then be obtained from the graph of Fig. 2.3, and the pulling speed can be chosen to match a growth rate of a lower value J_d than the intersect of the J_d and J_{crit} curves. The pulling speed for CdS (CdS_xSe_{1-x}) growth, limited by diffusion, was estimated by Wetwatana to be $\simeq$ 0.4mm/hr. Unfortunately, this would lead to unstable growth as determined from the Tempest analysis, but this is a direct result of the generalization of conditions made by Tempest. These conditions of Wetwatana for (diffusion limited growth) were applied to CdS, CdSe and CdS_xSe_{1-x} (see Section 2.3) and led to stable growth.

It is also interesting to observe the effect of non-stoichiometry given by the term $\alpha = \frac{n_1(0)}{n_2(0)}$ and the argon pressure P_{Ar} on the growth rate. This is illustrated in the Fig. 2.4 for $T(0) = 1420^{\circ}K$, $\Delta T = 25^{\circ}K$ and L = 7.0 cm, while argon pressure is the parameter at 1, 20 and 100 torr. The growth rate is largely reduced, especially at low pressures, when $n_1(0)$ is only just greater than $n_2(0)$. The other effect is obvious, that as the argon pressure increases, growth rate reduces. A value of $P_{Ar} \simeq$ 20 torr is chosen in the experimental work, to minimise the influence of α on growth rate. The value of α is, however, not expected to vary more than a value of 5 so that the growth rate is less sensitive to variations of α and P_{Ar}.

The quality of the grown crystal will depend on parameters as T(0), ΔT,L and crystal pulling speed i.e. the value of J_d relative to J_{crit}. To reduce the probability of constitutional supersaturation without a

great reduction in growth rate, J_{crit} can be increased by maximizing $dT/dx\Big|_{x = L}$. The quality of the crystal depends, not only when the vapour is slightly supersaturation but on the adsorption of molecules on the growing surface such that the molecules will have sufficient time to diffuse to the lattice sites and form an orderly array or when the vapour - crystal interface is near chemical equilibrum.

2.2.3 Growth at the Crystal Surface

Condensation at the crystal surface can be treated as an activated chemisorption process whose rate is a function of the actual concentration of the vapour species $n_i(1)$ (Faktor and Garrett, 1971). Condensation of CdS can be diffusion limited or condensation limited depending on degree of non-stoichiometry, α, charge temperature and the energy barrier is growth at the crystal surface.

Crystal surfaces are divided into three main classes. The first class is growth on a perfect singular surface corresponding to a cusp in the plot of surface energy as a function of orientation. This process requires that steps are generated by nucleation, and occurs at high vapour saturation ratio. The second type is growth on a nearly perfect singular surface containing either a limited number of steps from screw dislocations normal to the surface or a vincinal surface (making a small angle with the singular surface). This type of surface can grow at relatively low vapour supersaturation ($\sim$ 1.01). The third class is growth at a non-singular surface; a surface at a large angle to a singular surface and which are atomically rough, requiring lower vapour saturation than class one or two. Unlike the first two classes of crystals which grow a mono-layer at a time, class three crystals grow relatively quickly due to the presence of corner sites where the condensing atoms need not diffuse much to find such sites.

Imperfections such as stacking faults, grain boundaries and dislocation can result from high vapour supersaturation since the growth

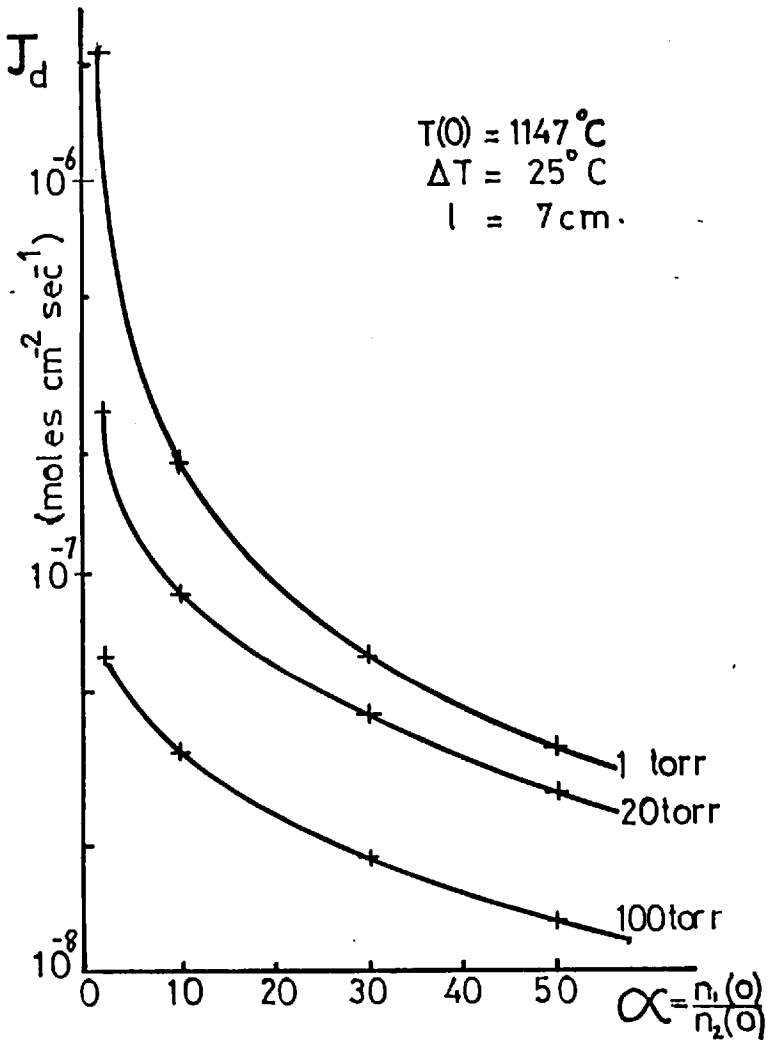


Fig. 2.4 Effect of Non-stoichiometry (α) and Inert Gas Pressure on J_d

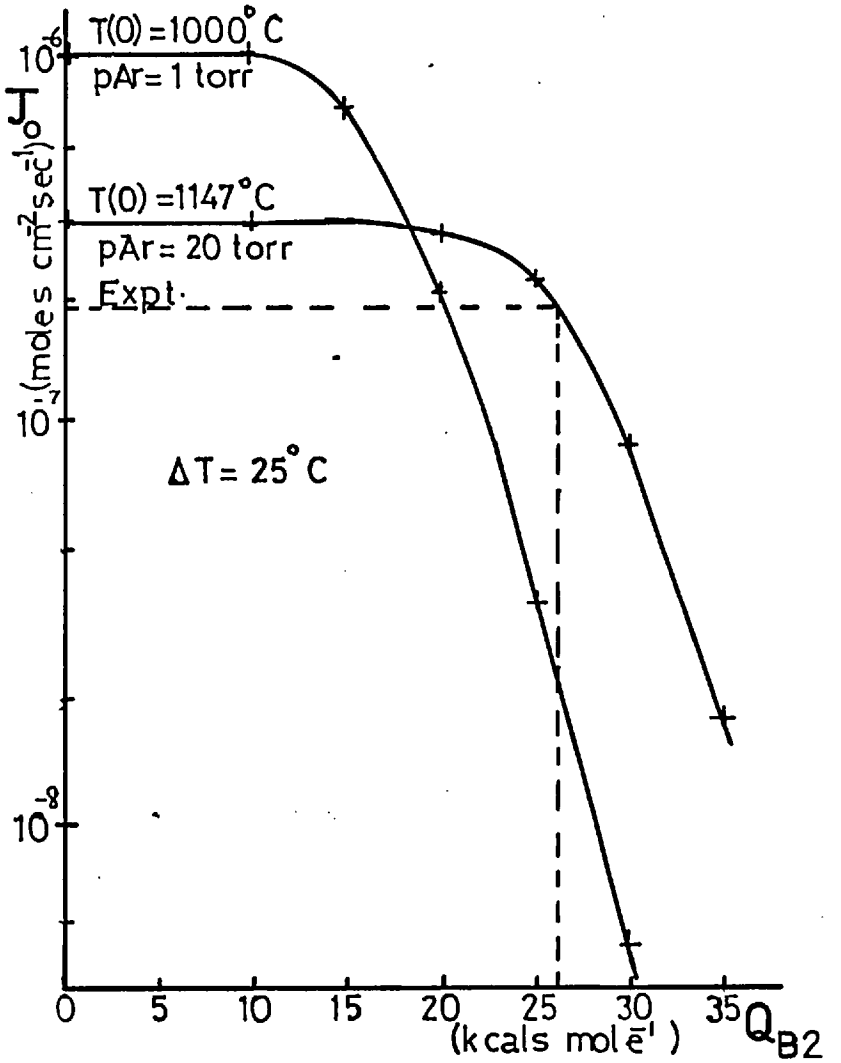


Fig. 2.5 Variation of J_o with Activation Energy Q_{B2}

rate becomes high and the condensing molecules do not have sufficient time to occupy corner sites.

If the condensation process is limited only by activated chemisorption of B_2 molecules (absorption of A atoms being non-activated), then the approach by Tempest may be used to determine the growth rate. Equating chemisorption rate and desorption rate, the velocity constant of desorption at equilibrum can be obtained, whose value may be assumed to remain constant for slight departure from equilibrum. The condensation rate is given by the expression

$$J_{cond.} = \frac{RT(1)}{X_2}\left[n_2(1) - n_{2eq}(1) \exp\left(-Q_{B2}/RT\right)\right] \qquad (2\text{-}20)$$

where $$X_2 = \frac{N\left[2\pi m_2 kT\,(1)\right]^{\frac{1}{2}}}{2\beta_2\,(1-\theta_2)}$$

β_2 is the condensation coefficient and θ_2 is the surface coverage of B_2 atoms, n_{2eq} is the equilibrum concentration of B_2 molecules, Q_{B2} is the activation energy of B_2 molecules.

The condensation rate is expected to be higher for CdSe than CdS since the Q_{B2} is a little smaller for selenium molecules (Tempest).

The overall growth rate can be expressed in terms of diffusion and condensation parameters as

$$J_o = \frac{n_1(0)}{2A_1} + \frac{n_2(0)}{2A_2} - \left[\frac{n_1(0)}{2A_1} + \frac{n_2(0)}{2A_2} - \frac{K_{NS}(0) - L_{NS}(1)}{A_1 A_2}\right]^{\frac{1}{2}} \qquad (2\text{-}21)$$

where $K_{NS}(1) = n_{1eq}(1)\, n_{2eq}(1)$

$A_1 = (3l/2nD)\left[2/3n - n_1(0)\right]$

$A_2 = (3l/2nD)\left[1/3\,n - n_2(0)\right] + (X_2/RT)\exp(Q_{B2}/RT)$

The parameter, A_2, depends on the diffusion term only at high argon pressure or the condensation term only at low temperature, and therefore determines the type of growth. There is, however, a large range of conditions over which both types of growth mechanisms contribute

simultaneously.

The variation of overall growth rate, J_o, for CdS as a function of Q_{B2} is illustrated in Fig. 2.5 for (a) low temperature and pressure, (b) higher temperature and pressure at fixed $T = 25^{\circ}K$ and $Q_A = 0$. It is observed that the diffusion limited region is greatly reduced in size as conditions are changed from (b) to (a). A value of Q_{B2} between 25 and 30K cal $mole^{-1}$ was determined by Tempest from experimental growth rates, for both CdS and ZnS verifying that the condensation process is limited by the chemisorption of S_2 molecules. Also, this value of Q_{B2} is less than the dissociation energy of S_2 molecules. The value of J_o for CdS_xSe_{1-x} is expected to increase with decreasing x, by less than an order of magnitude when x = o which, in crystal growth terms, is a small amount.

Comparing diffusion limited growth rate J_d with the overall growth rate, J_o, for CdS under the same conditions (Fig. 2.6) it can be seen that the two curves are similar suggesting that the crystal growth is limited by diffusion of the vapours. However, the growth rate is more accurately represented by J_o than J_d.

2.3 Experimental Details

Single crystals of CdS, CdSe and their alloys were grown using the experimental method of diffusion limited growth described above.

Since the equilibrum vapour pressure of pure CdS and CdSe and diffusion coefficient are similar then the growth conditions for CdS are not much different to that of CdS_xSe_{1-x} i.e. the diffusion rate would not be much altered by the Se_2 species at $1150^{\circ}C$, for crystals grown under diffusion limited conditions. However, the presence of a 4th species, Se_2 molecules, would be important if crystals were to be grown under condensation limited conditions.

Practical limitations for growing good quality crystals restricted the ideal growth rate; a value of $\sim 10^{-7}$ moles cm^{-2} sec^{-1} (or 5-10 gm/week)

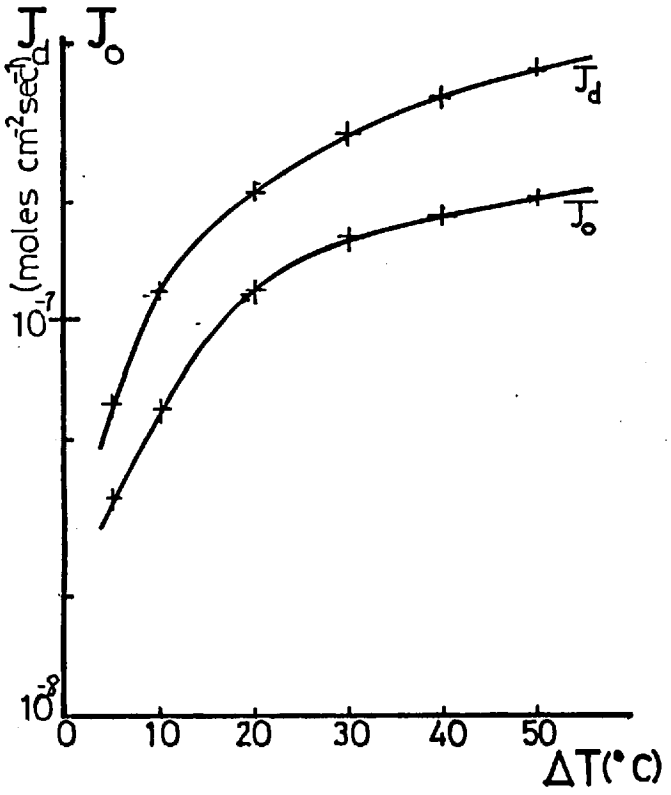
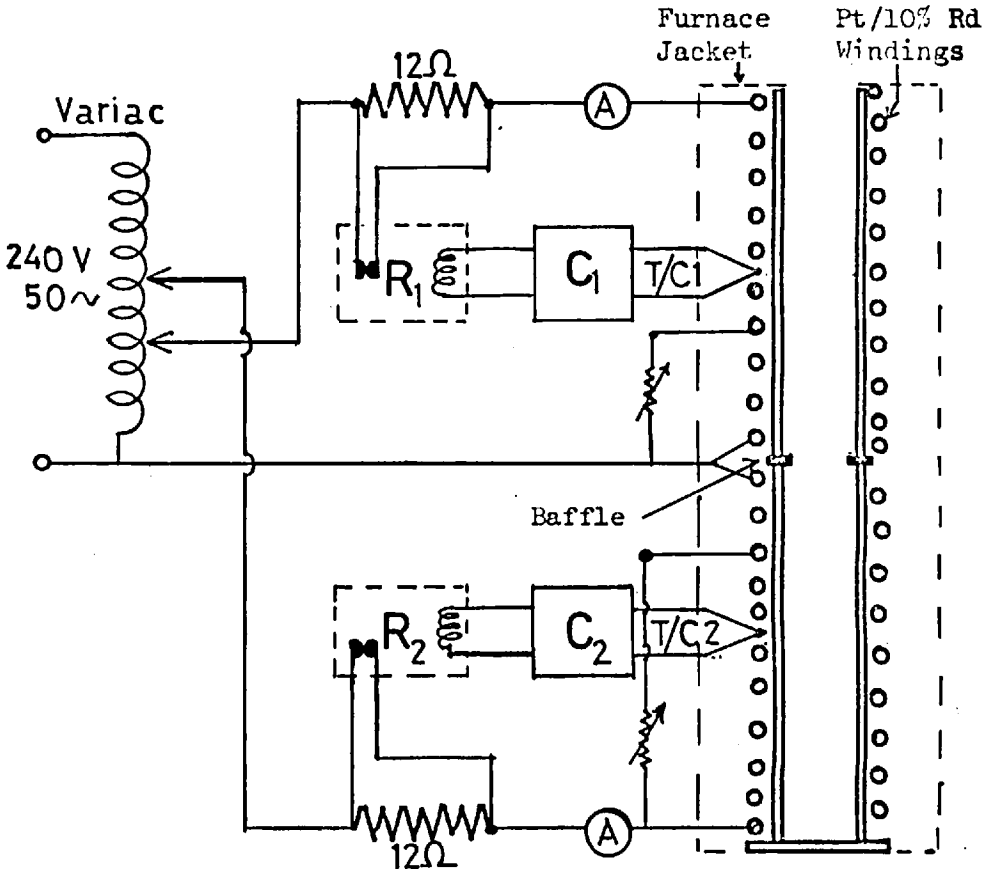


Fig. 2.6 Comparison of J_d and J_o with ΔT



R_1, R_2 — Thermostatic Relays

C_1, C_2 — Eurotherm Temperature Controllers (type LP96)

T/C1, T/C2 — Pt - Pt/13% Rd Thermocouples

Fig. 2.7 Heater Circuit Arrangement for the Two-Zone Vertical Furnace

was sought since the lifetime of the ampoule at elevated temperatures is limited $\sim$ 1 week.

2.3.1 The Charge

Polycrystalline lumps of (BDH 'optran' grade II) CdS and 4-40 mesh CdSe (BDH 'Vactran' grade) were used as the charge. The purity of these materials are given in table A1 and A2 of Appendix A. The charge of CdS or CdSe was placed in a high purity alumina boat and heat treated separately at $\sim$ 900°C in a quartz tube through which argon gas flowed at 1 litre/min for 7 hours. This step, termed a 'pre-heat' was necessary to remove adsorbed gases and volatile impurities and to improve the stoichiometry of the charge. Approximately 1/3 of the charge was lost in this step.

2.3.2 The Growth Ampoule

The growth ampoule was made from high purity tubing of standard wall thickness 20cm in length and 1 cm in diameter joined to a close ended tube 3-5 cm in length and 1.6 cm diameter. The tube was then treated with hot 'Decon 90' under ultrasonic agitation, rinsed in distilled water, then etched with 10% HF for 20 minutes, rinsed in D.I. water and finally dried in an oven. The tube was flame polished to smooth the interior surface and thus removing unwanted nucleation sites.

A pre-heated charge of 10 grammes of CdS, CdSe or a mixture of both was carefully placed in the growth tube, avoiding contact with the walls of the narrow part of the tube. A constriction approximately 8 cm from the closed end was made in the narrow bore length. The tube was evacuated to a pressure $\sim 10^{-5}$ torr, then argon was bled into the ampoule until the pressure was $\simeq$ 20 torr, after which the ampoule was sealed off. A quartz hook of 4mm diameter rod and $\sim$ 10 cm length was joined to the tip of the ampoule. The ampoule was suspended with 15 thou. Pt wire attached to the pulling motor and lowered into a furnace possessing a suitable temperature profile.

2.3.3 The Furnace and Temperature Profile

The growth furnace consisted of 2" i.d. alumina tubes, around which 1 mm 10% Rh/Pt heater wire was wound to give a two-zone vertical furnace structure. The required temperature gradient was obtained from a non-uniform winding density with about a 25% tapping of each heater coil from the lower terminal to the upper heater coil and from the upper terminal to the lower heated-coil. Two Pt-Pt/13% Rh thermocouples were positioned midway between each heater to actuate the Eurotherm temperature control units (type LP96), using the arrangement illustrated in Fig.2.7 which controlled the temperature to better than 1°C.

The current in each coil was adjusted to give the desired temperature profile. The profile was determined by pulling a Pt-Pt/13% Rh thermocouple ($\simeq$ 10cm/hr) through the furnace and recording the temperature on a chart recorder. A typical profile is shown in Fig. 2.1. An asbestos cover placed over the top open-end of the furnace tube prevented convection and gave a more stable profile.

2.3.4 Growth of the Crystal Boule

Using the following conditions calculated in Section 2.2 as mass charge = 10 gm, argon press = 20 torr, T(0) = 1150°C, ΔT = 25°C, temperature profile of Fig. 2.1, pulling speed 0,4 mm/hr, (these being the conditions necessary for diffusion limited growth), single crystals of CdS, CdSe and CdS_xSe_{1-x} were grown.

The ampoule was initially lowered into the furnace to the desired position relative to the temperature profile, and after 15 minutes, when thermal equilibrum has been re-established, the ampoule was smoothly pulled through the profile at the determined pulling speed. After 5-6 days, the furnace was allowed to cool slowly by reducing the current in the furnace windings (initially at a cooling rate of $\lesssim$ 5°C/min).

Most runs showed some transport i.e. complete or nearly complete transport in which the boules were 2-3 cm long. The photograph of Fig. 2.8

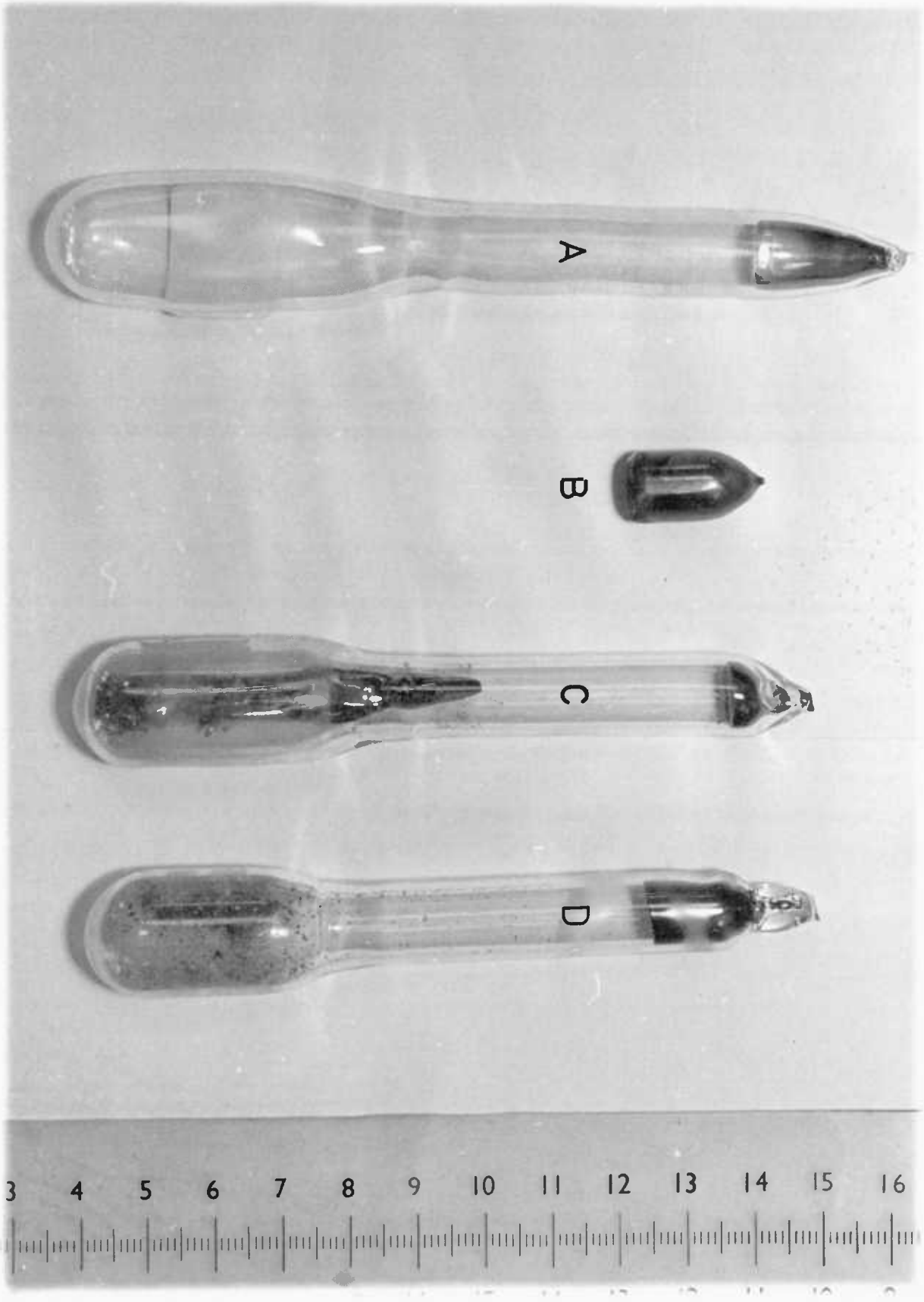


Fig. 2.8 Monocrystal Boules of CdS, CdSe and CdS_xSe_{1-x} Grown Under Diffusion-Limited Conditions

show CdS, CdS_xSe_{1-x} and CdSe crystals from runs A,B,D obtained from complete transport while run C failed (partial transport) showing facetted residual charge, due to insufficient supersaturation, the crystal growing on top of the charge. Runs A,B,D produced single crystal determined from Laue X-ray diffraction.

Most crystals appeared uniform in colour ranging from amber for CdS, red for $CdS_{.75}Se_{.25}$ brown for other CdS_xSe_{1-x} to grey-black for CdSe. Only a few crystals contained macroscopic cracks (due to stresses in the cooling cycle caused by differences in coefficient of expansion). Run A and B produced typical good quality boules possessing a smooth free surface, slightly curved and normal to the growth ampoule while run D produced a crystal facetted on the $(10\bar{1}0)$ and basal plane.

The carrier concentration determined by the differential capacitance method (see section 3.7) indicated approximately uniform carrier concentration across the boules. Microprobe analyses (SEM) revealed that the alloy crystals grew in molar ratios S:Se similar to the charge molar ratios, also there was only slight variations in the ratios across the boules.

The crystal quality was dtermined mostly by inspection by reflected and transmitted light under a microscope, though one CdS sample, briefly studied by X-ray topography (transmission method) possessed defects similar to those of Tempest. The main defects occuring in the crystals were stacking faults and dislocations (density $\sim$ 500 lines/cm^2) mainly in the basal plane. Microcracks appear in some samples and were apparently caused (during the cooling cycle) by the difference in coefficient of expansion of quartz and CdS_xSe_{1-x}.

The growth plane of CdS crystals was measured, using the Laue X-ray diffraction method as 18° to 19° to basal plane.

2.4 Conclusion

Good quality crystal boules of CdS, CdSe and their alloys have been reproducibly grown under diffusion-limited conditions along the ampoule. The conditions are calculated using the method of Ballentyne et al (1970).

REFERENCES - CHAPTER 2

Ballentyne, D. W. G., Wetwatana, S., White, E. A. D. (1970)
J. Crystal Growth 7, 79.

Ban, V. S. (1972) Private Communication. Now at R.C.A./David Sarnoff Research Centre, Princeton, N.J.

Clark, L., Woods, J. (1966) Brit. J. Appl. Phys. 17, 319.

Czyzak, S. J., Craig, D. G., McCain, C. E., Reynolds, D. C. (1952)
J. Appl. Phys. 23, 932.

Faktor, M. M., Garrett, I. (1971) J. Cryst. Growth 9, 12.

Green, L. C., Reynolds, D. C., Czyzak, S. J., Baker, W. M. (1958)
J. Chem. Phys. 29, 1375.

Lorentz, M. R. (1967) Physics & Chemistry of II-VI Compds, Ch.2, edited by Aren, M., and Prener, J. S., North-Holland.

Nitsche, R. (1960) J. Phys. Chem. Solids, 17, 163.

Piper, W. W. and Polich, S. J. (1961) J. Appl. Phys. 32. 1278.

Reid, R.C., Sherwood, T. K. (1966) The Properties of Gases and Liquids, 2nd ed., McGraw-Hill, p.523.

Reynolds, D.C., Czyzak, S. J. (1950) Phys. Rev. 79, 543.

Rubenstein, M. (1966) J. Electrochem. Soc. 113, 623.

Somorjai, G. A. (1962) Proc. of the Inter. Symp. on Evaporation and Condensation of Solids., Dayton, Ohio, 1962.

Somorjai, G. A., Jepsen, D. W. (1964) J. Chem. Phys. 41, 1389.

Takahashi, M., Shoji, H., Funisaki, H., Matsumura, T., Tanabe, Y. (1963)
Jap. J. Appl. Phys. 2, 666.

Tempest, P. A. (1974) Ph.D. Thesis, Univ. of London.

Toyama, M. (1966) Jap. J. Appl. Phys. 5,12, 1204.

Wetwatana, S. (1969) Ph.D. Thesis, Univ. of London

CHAPTER 3 - PROPERTIES OF CdS, CdSe AND THEIR ALLOYS

3.1 Introduction

Early work on II-VI compounds used powdered samples, and it was not until recent years that single crystals were successfully grown enabling reliable experimental data to be acquired. The high melting points of II - VI compounds has been a drawback in the development of these materials.

The physical and chemical properties of CdS and CdSe have been extensively investigated during the past two decades. The high photo-conductivity of these materials have made these two compounds perhaps the most interesting of the II-VI compounds for device application e.g. photodetectors, electromechanical transducers, thin film transistors and lasers.

These two compounds crystallise in two forms, hexagonal wurtzite and cubic sphalerite with, in some cases, a certain degree of polymorphism. The bonding varies from ionic to covalent and for most II-VI compounds both types are involved. Suchet (1965) suggested that for CdS and CdSe the proportion of ionic bonding is 74% and 64% respectively. With the exception of HgTe and HgSe, they have direct, relatively wide band gaps.

The alloy crystals or solid solutions of CdS and CdSe exhibit similar properties to those of the constituents and variables such as band-gap and lattice constants can be chosen to give any values in between those of CdS and CdSe. As the band gap varies in these alloys, luminescent emission goes from green (CdS) to infra red (CdSe). At present, relatively little is known about these alloys and conflicting data has been presented in the literature. Further investigation is, therefore, required in order to understand their behaviour.

In this chapter ideas relating to the lattice structure energy band structure, electrical transport of bulk and surface and electrodes to these materials will be discussed. Only a very brief mention of

optical properties will be made.

3.2 Crystal Lattice Structure

Single crystals of CdS and CdSe grow basically in the wurtzite structure when pure but can attain the closely related sphalerite structure if grown in film form on suitable crystalline substrates. Excess Cd atoms increase the stability of the hexagonal phase in CdS (Chopra and Khan 1967) and CdSe (Shamilova et al, 1966). Any polymorphism will be omitted in this study.

The two ideal structures illustrated in fig. 3.1 show the atoms are tetra-hedrally bounded. The wurtzite structure is formed by the hexagonal close - packing (hcp) of successive atomic layers displaced a distance $\frac{3}{8}c$ along the x-axis with respect to each other. The nearest neighbour atoms are at distances $\frac{3}{8}c$ (or $\sqrt{\frac{3}{8}}$ a), where and c are the lattice constants, a being the side of the hexagon and c, the height of the unit cell. For a specified atom, A, there are twelve next-nearest neighbours, six of these are at the corner of a hexagon in the same plane as A (basal plane), while the other six are at the corners of a triagonal prism at a distance $\sqrt{\frac{a^2}{3} + \frac{c^2}{4}}$ from A.

The sphalerite structure is formed by the cubic close-packing of successive atomic layers such that each atom is surrounded tetrahedrally by four atoms of opposite type. This structure is referred to as face-centre cubic (fcc), and if the bias was one rather than two, the structure would be that of diamond. The atoms are situated at the corners of the unit cell consisting of four molecules with the site at the centre of the cell $(0, \frac{1}{2}, \frac{1}{2})$. The nearest neighbours are separated a distance of $\sqrt{\frac{3}{4}}$ a. For a specified atom, B, there are twelve next-nearest neighbours all of which are at a separation of $\frac{\sqrt{2}}{2}$ a; six of these are at the corners of a hexagon in the same plane as B while the other six form a trigonal antiprism (with three above and three below the plane of the hexagon).

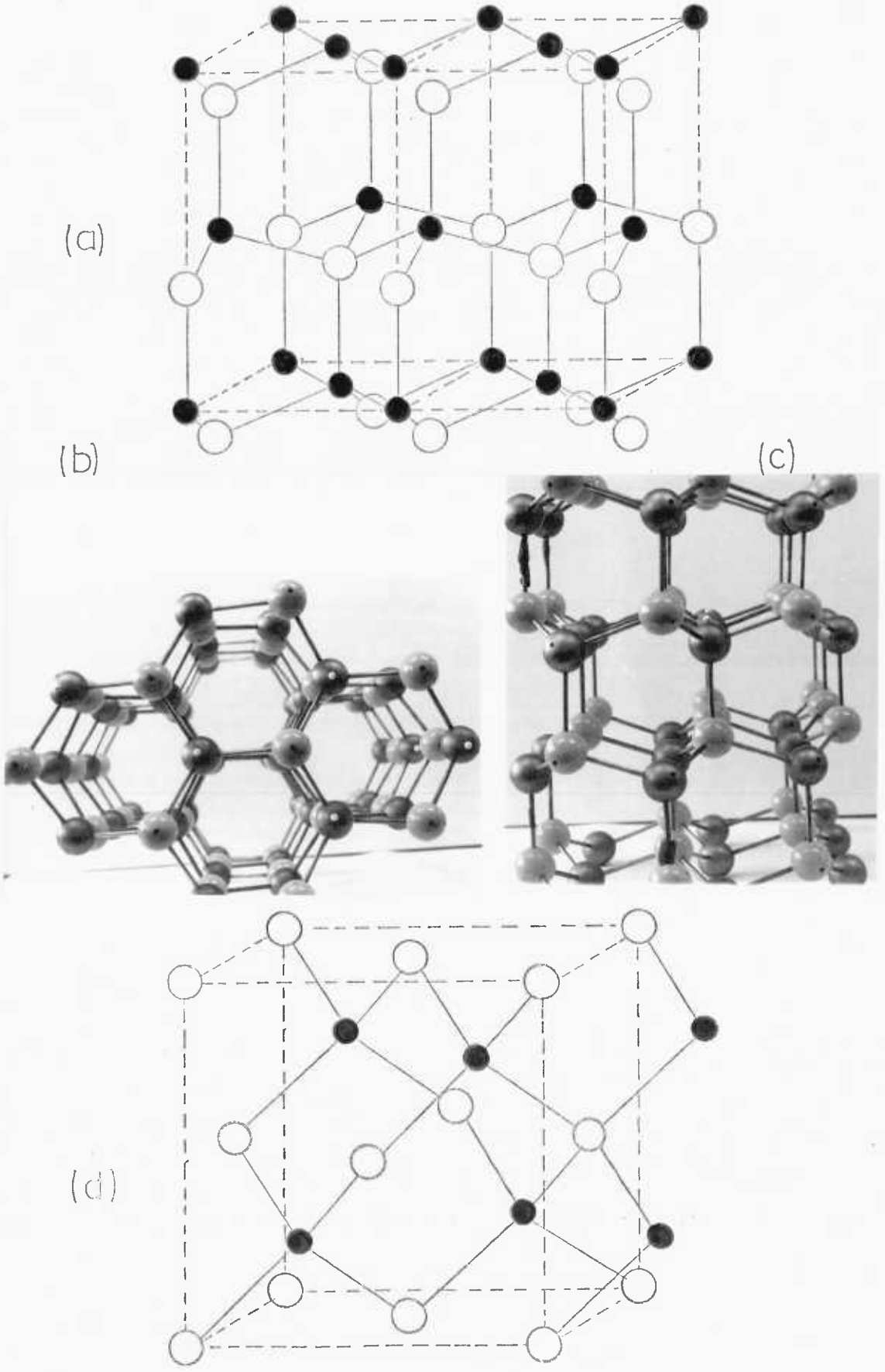


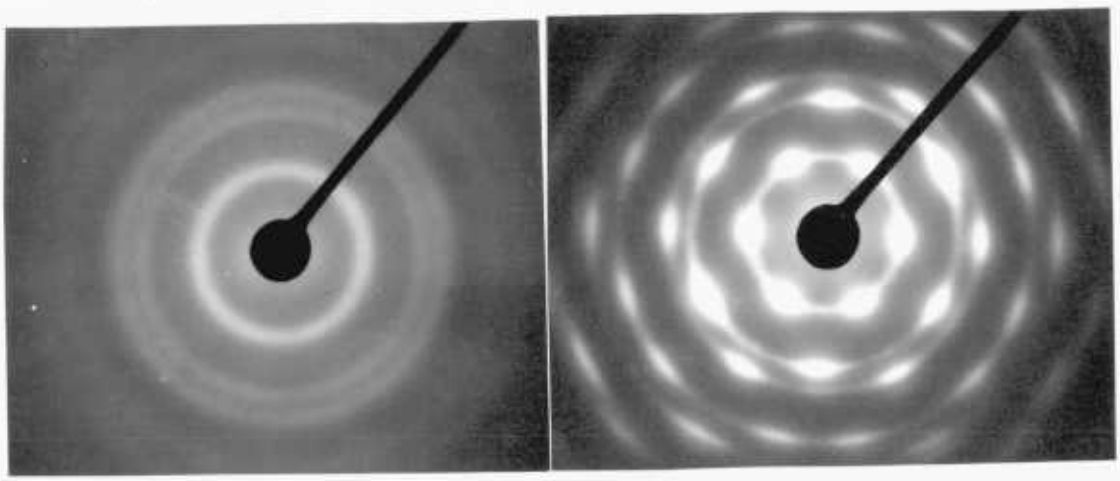
Fig. 3.1 (a) Wurtzite Structure, (b) ⊥ C-face, (c) // C-face
(d) Sphalerite Structure

These two types of structures are closely related, and geometrically the sphalerite can be converted to the wurtzite by changing the stacking sequence. By rotating the interpenetrating tedrahedra in the sphalerite about the (111) axis, it becomes the (001) hexad axis of wurtzite. Neither of these structures have a centre of symmetry.

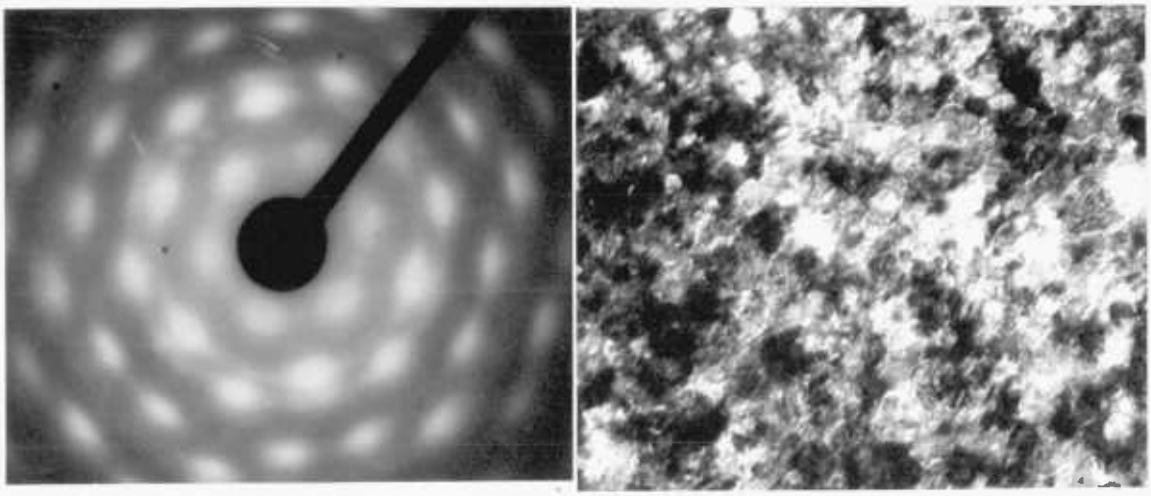
Both CdS and CdSe crystalline under most growth conditions as the wurtzite structure. In the case of CdS_xSe_{1-x} grown from the vapour phase, all crystals attain the stable wurtzite structure. However, for thin films the real structure will depend on substrate cystallographic orientation and temperature. Simple experiments were performed by growing thin CdSe films ($\sim$ 500 Å thick) by r.f. sputtering on substrates of soda-glass, mica, sapphire, KCl and CdS at temperatures up to 350°C in order to study their crystallographic structures in the electron microscope. (The thin films were lifted from most substrates by exposing the substrates to HF fumes and immersing in water). Selective area diffraction pattern (SADP) analysis revealed that the CdSe films grew

(i) Very poorly crystalline (hexagonal) on soda-glass at temperature 200°C, characterised by a SADP ring-pattern (Fig. 3.2 a) but became more crystalline, characterised by a spot-ring-pattern as the substrate temperature was increased above 250°C. Micrograph studies showed crystallites slowly increasing in size up to 400 Å at 300°C, but then nearly double in size as the temperature approached 400°C.

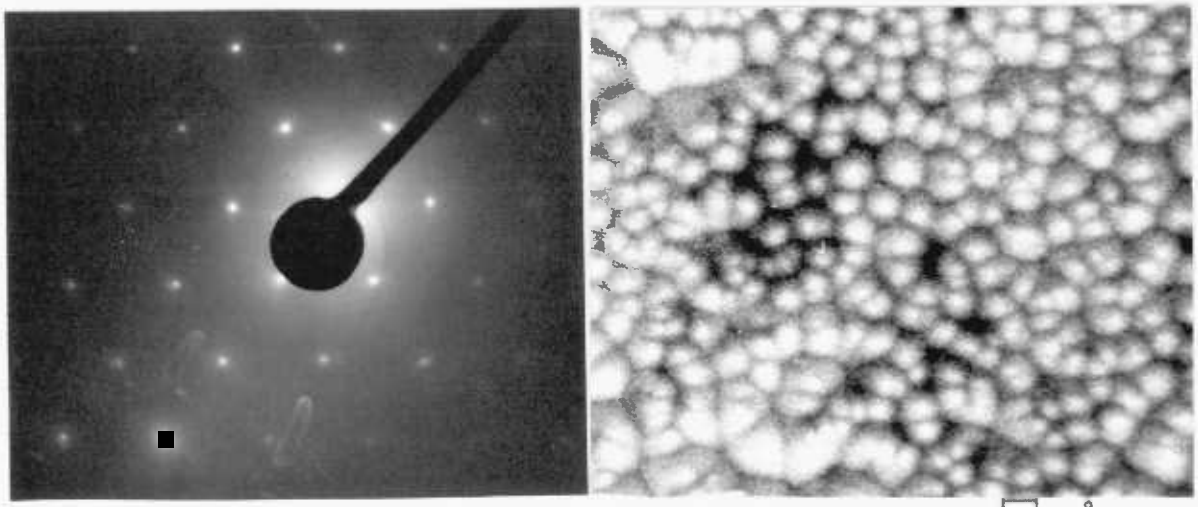
(ii) Poorly crystalline at 200°C on mica but obtaining better (hexagonal) crystalline properties as the temperature was raised to 250°C (Fig. 3.2 b) and further to 320°C (Fig. 3.2 c). Micrographs (Fig. 3.2 d) show small crystallites of CdSe on mica of approximate size of 500 Å when the substrate temperature was 300°C. The crystallites increase to nearly 600 Å when the temperature is increased to 350°C.



(a) Soda-glass at 200 C° (SADP) (b) Mica at 250°C (SADP)



(c) Mica at 320° C (SADP) (d) Mica at 300° C ~500Å



(e) CdS at 350° C (SADP) (f) CdS at 350° C ~8000Å

Fig 3.2 Crystallographic Properties of Sputtered CdSe Films.

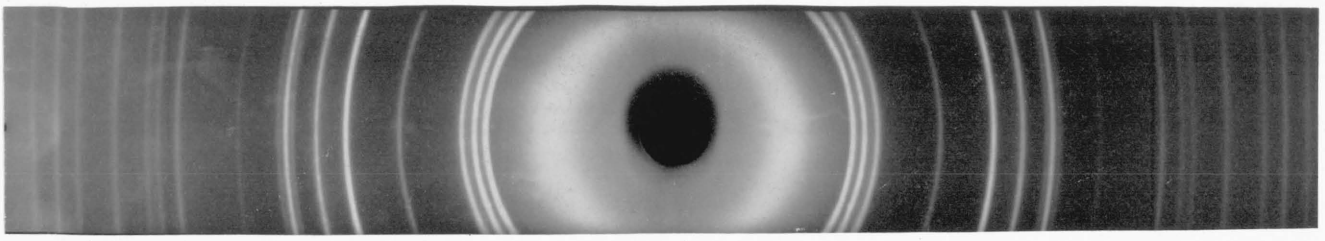


Fig. 3.3 X-Ray Diffraction of a Powdered $CdS_{0.1}Se_{0.9}$ Sample

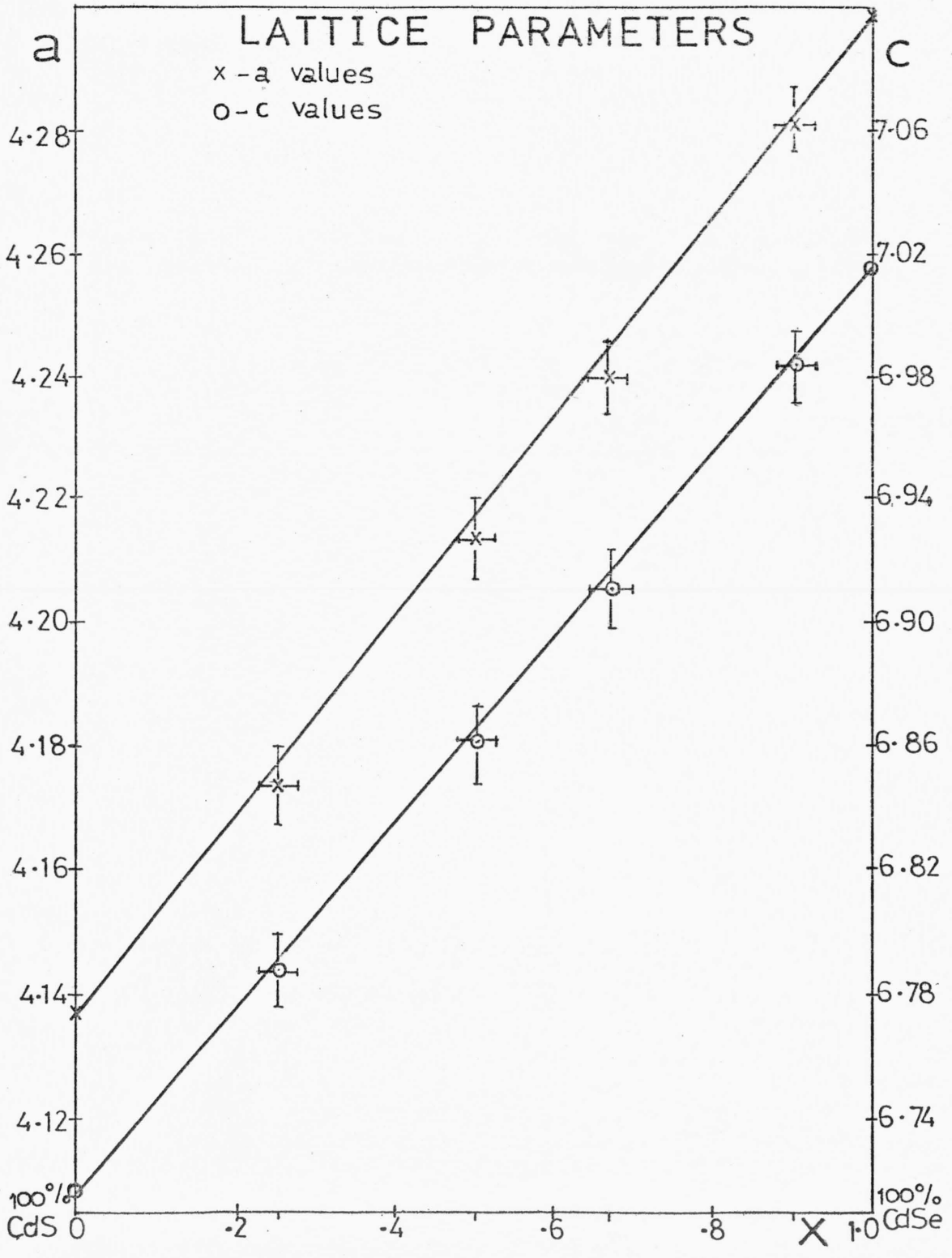


Fig. 3.4 Variation of Lattice Parameter a and c with Composition for CdS_xSe_{1-x} Crystals

(iii) Poorly crystalline (hexagonal) on the c-face of sapphire even up to 320°C due to a lattice mismatch ≃ 10%.

(iv) With fairly good cubic crystalline structure on (100) orientated KCl substrate with substrate temperature above 200°C.

(v) With good hexagonal crystalline structure of 1 μm CdSe on the c-face of CdS above ≃ 270°C as determined by the reflection method of electron diffraction. Fig. 3.2 (e) shows good crystalline orientation characterised by spot pattern at 350°C (showing perhaps better properties than at 300°C). The average size of these crystallites is ~ 8000 Å, as illustrated in the scanning electron microscope photograph of Fig. 3.2 (f). The study of CdSe grown on CdS at 350°C indicated fairly good epitaxy.

The lattice parameters, a and c, of the monocrystalline CdS, CdSe and their alloys, grown by the vapour transport method, have been measured by the Debye - Sherrer method. An example of powder diffraction film for $CdS_{0.1}Se_{0.9}$ is shown in Fig. 3.3. The d-spacings in the hexagonal lattice is related to the various lattice planes by

$$d = \frac{1}{\left[\frac{4}{3}\left(\frac{h^2 + hk + k^2}{a^2}\right) + \frac{l^2}{c^2}\right]^{\frac{1}{2}}} \qquad (3.1)$$

The results of a and c parameters illustrated in Fig. 3.4, indicate an approximate linear variation of lattice parameter with composition i.e. CdS_xSe_{1-x} crystals approximately obey Vegard's law.

3.3 Energy Band Structure in Wurtzite CdS_xSe_{1-x}

The electronic band structure depends on the type of structure, chemical bonding and the electronic configuration. The band structure is derived from the Brillouin zone in k-space (in this case, a right hexagonal prism), which in turn is a function of the crystal lattice and the wave quantum mechanics associated with the charge carriers. The magnitudes of elements in the band structure has, however, been determined from

experimental e.g. reflectivity and photo-emission experiments, together with theoretical methods.

The conduction band in CdS, CdSe and their alloys are virtually singular and parabolic in shape so that effective mass and mobility can be treated as isotropic. The valence band structure is, however, more complex due to anisotropic properties in these crystals resulting in spin orbital splitting. This has received considerable attention in the past decade. A simplified model of the band structure for CdS is illustrated in Fig. 3.5. It shows only three uppermost valence sub-bands around its principle symmetry point with the conduction and valence band extrema occuring at k = 0. The shape of the band structures for CdSe and the CdS_xSe_{1-x} alloy crystals are similar to that of CdS. Pedrotti and Reynolds (1962) have suggested that both the spin orbital splitting parameter and crystal field of the valence band of CdS_xSe_{1-x} vary approximately linearly between values of its composites.

Detailed analysis of the band structure of CdS and CdSe have been offered by Bergestresser and Cohen (1967) and Cohen (1967) using an emperical pseudo-potential method (EPM) together with optical data, in particular, refelctivity and photoemission. The method involves an approximation to the orthogonalized plane wave (OPW) technique (Herman and Shillman; 1960) in which the Schrodinger's equation contains an effective crystal potential represented by a number of terms of a Fourier expansion in the wave vectors.

The self-consistent OPW method has been applied by Collins et al (1966) to CdS to determine the six symmetry points of the wurtzite Brillouin zone. The band structure was also determined by another pseudo-potential method but the results were different from OPW calculations and from the EPM of Bergestresser and Cohen.

De Witt et al (1967) first used the EPM method to obtain a simplified solution, then the self-consistent OPW method to obtain a more accurate

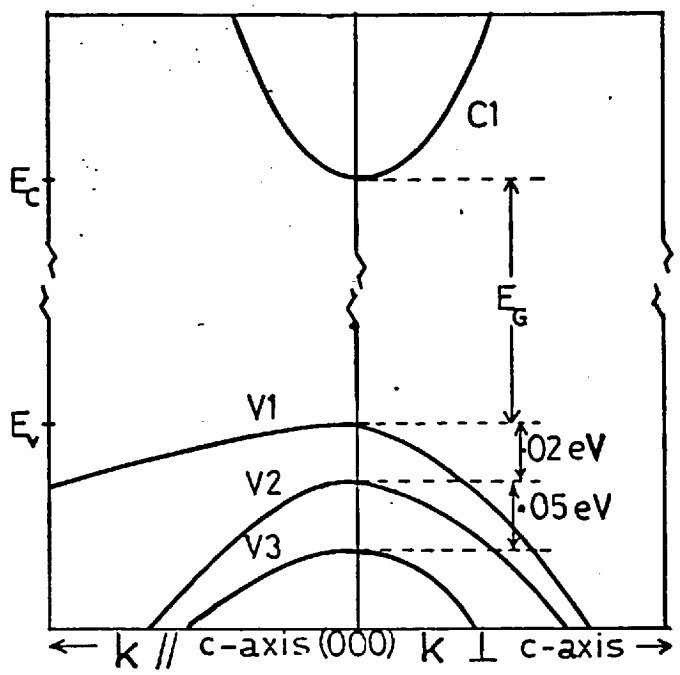


Fig. 3.5 Simplified Band Structure of CdS (After Blakemore, 1969)

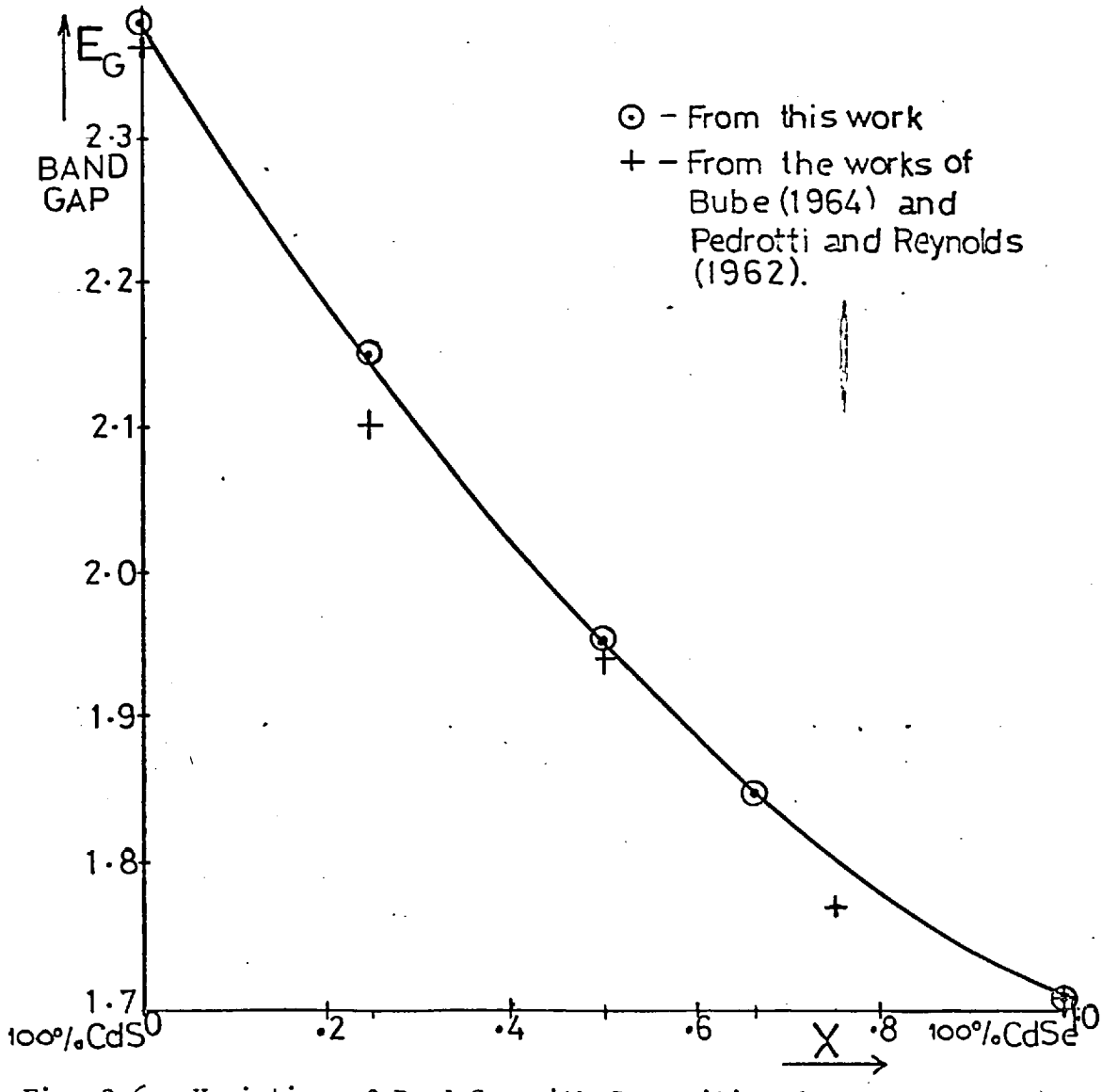


Fig. 3.6 Variation of Band-Gap with Composition for CdS_xSe_{1-x}

band structure of CdS_xSe_{1-x} crystals, assuming a linear variation in lattice parameter with composition. Their results showed similarities to the already closely related CdS and CdSe structures.

The **k·p** interaction method (Segall, 1967) has also been used to determine the band structure of wurtzite type crystals (Cardona, 1963) in the vicinity k = 0. Jahne and Gutsche (1967 a, b) applied a generalised 2nd order **k·p** pertubation method (as discussed by Fawcett and McLean (1965)), to CdS and CdSe and used a cubic secular equation obtained from a (6 x 6) Hamiltonian matrix, to derive the E(k) dependence of the three uppermost sub-valence bands for a general direction of k. In doing so they neglected k-dependent spin-orbital interaction. The sub-valence bands are strongly non-parabolic even in the vicinity k = 0.

The valence band consists of four separate bands, but when spin-orbital splitting is included, these increase to six. Note that the above derivation of band structures is strictly valid only for ordered systems such as intrinsic elemental semiconductors (Bonch-Bruevich, 1967).

The energy gaps of CdS, CdSe and their alloys have been determined by Pedrotti and Reynolds (1962) and Bube (1964) from experiments on photoconductivity spectra. The energy gaps were also measured from the fundamental absorption edge. The results for the band gap at room temperature as a function of composition, is shown in Fig. 3.6, and suggests an approximate linear variation. These results are in fair agreement with those of the above experimentalists. The band gap has a linear variation with temperature (Bube, 1964) and is normally expressed as

$$E_G\ (T) = E_G - A10^{-4}\ eV/^oK \qquad (3.2)$$

The value of A for all the CdS_xSe_{1-x} as determined by some works is $\sim$ 5-7.

It is therefore seen that the two constituent materials used here in the heterojunction fabrication have very similar band structures. These similarities should lead to the production of heterojunctions with satisfactory electrical and optical properties.

3.4 Some Transport Properties of CdS_xSe_{1-x}

3.4.1 Effective Mass

The effective mass is defined in terms of the second derivative of E with $\underline{k}$, or the acceleration of the wave packet under an external applied field. It has been suggested that the energy surfaces in the conduction band are approximately spherical (Dimmock and Wheeler, 1961) and Hopfield (1961), Zook and Dexter (1963) and Fujita et al (1966), so that the effective mass at the bottom of the conduction band is singular. The energy surfaces in the valence band are far from being spherical so that the hole effective mass is direction dependent for both the light and heavy holes.

The effective mass for CdS and CdSe have been determined by a number of methods, both electrical and optical. For CdS, values of the electron effective mass vary from one investigator to another. Values of $(0.22 \pm .02)\ m_e$ have been determined from free-carrier absorption (Piper and Marple (1961), $(0.20 \pm .01)\ m_e$ from Faraday rotation, $(0.20 \pm .01)\ m_e$ from exciton Zeeman studies (Hopfield and Thomas,1961), $m_\perp = 0.171\ m_e$ and $m_{//} = 0.153\ m_e$ from cyclotron resonance (Baer and Dexter,(1964)) (this difference between $m_\perp$ and $m_{//}$ has been attributed to piezoelectric polaron effects) $m_\perp = 0.18\ m_e, m_{//} = 0.19$ from magnetic splitting (Nassau et al 1970). The value of the effective mass for CdSe is, however, more consistant, being $0.13\ m_e$ (Wheeler and Dimmock 1962), Dimmock and Wheeler (1961). Kubo and Onuki (1965) obtained a value of $(0.15 \pm .01)m_e$ from free carrier absorption.

A more direct experimental method by Valakh et al (1968) based

on reflection spectra of low resistivity CdS_xSe_{1-x} crystals have shown a linear variation of effective mass with composition, varying from 0.21 m_e for CdS to 0.13 m_e for CdSe.

The hole effective mass, too, has been measured though not many results are available. For CdS values of 0.7 m_e ($m_\perp$) and 5 m_e ($m_{//}$) have been determined by Stradling (1967) Hopfield and Thomas (1961) whilst for CdSe, the value is 0.45 m_e ($m_\perp$) and 1 m_e ($m_{//}$) determined by Whitsett (1965) and Wheeler and Dimmock (1962)

3.4.2 Carrier Mobility

The electrical conductivity of a semiconductor under an applied electric field, F, is

$$\sigma = e(n\mu_n + p\mu_p) \tag{3.3}$$

where μ_n and μ_p are electron and hole mobilities respectively. Since both CdS and CdSe are n-type, then the contribution of holes can be ignored, giving $\sigma = ne\mu_n$.

If the electrons are subjected to a combined electric field and magnetic field then as a result the conductivity is obtained as

$$\sigma R_H \ (= ne\mu_n R_H) = r_H \mu_n = \mu_H \tag{3.4}$$

where μ_H is the Hall mobility, R_H the Hall coefficient, and r_H the Hall factor. Note that $r_H = \frac{\langle \tau^2 \rangle}{\langle \tau \rangle^2}$ from transport theory, and assumes a value of 1 for degenerate material and is not far from unity for moderately doped CdS (Li and Huang, 1971) . However, for non-degenerate materials with spherical equal energy surfaces,

$$r = \frac{\Gamma(5/2 - s)\Gamma(5/2)}{[\Gamma(5/2 - s)]^2} \tag{3.5}$$

if $\tau \propto E^{-S}$ (Kwok and Bube, 1973).

There are, however, various scattering mechanisms in these crystals which effectively reduce the carrier mobility. These mechanisms can be catagorised as charged impurity mode, acoustic mode, polar optical mode and piezoelectric mode scattering (ref. Ray, 1969) and Kobayashi, 1967). The first mechanism results from impurity or lattice defects and is important if impurities are deliberately included in the lattice to increase conductivity or if the crystal grows non-stoichiometrically as a result of native defects (e.g. CdS and CdSe grow with excess Cd in the crystal). The mechanism is important at low temperatures when lattice vibration is small. The second mechanism occurs because the atoms vibrate, deforming the potential energy configuration of the lattice, and as a result causes small vibrations in the band gap. This type of scattering gives rise to a $T^{-3/2}$ dependence of mobility. The third mechanism results from polar interactions between charge carriers and longitudinal optical phonons in ionic crystals. This mechanism is therefore important in II-VI compounds because of their partial ionic bonding (Suchet, 1965). The fourth mechanism is due to the interaction of carriers (electrons and the acoustical lattice vibrations as a result of the piezoelectric polarisation field created by mechanical stress, (this occurs for hexagonal semiconductors with no inversion symmetry like CdS and CdSe). Electrons and phonons can only interact when they possess similar wave vectors and this only occurs at low temperatures.

The values of S in equation (3.5) has been given numerical values of $-\frac{1}{2}$ and $-\frac{3}{2}$ (r_H = 1.10 and 1.93) for piezoelectric and charged impurity scatterings, respectively. For optical mode scattering r takes values between 1.05 and 1.25 for temperatures between 80°K and 400°K (Kwoki and Bube, 1973).

If more than one scattering mechanism occurs in the crystal, the resultant mobility is complex. It is, however, a good approximation

to add the reciprocal of mobilities. Suhan et al (1971) give expressions for the individual components of mobility for non-degenerate semiconductors in terms of their effective mass and temperature dependencies.

The intrinsic scattering mechanisms with regards to the transport properties in CdS has been well studied. When considering 'pure' CdS crystals, it is expected that the optical mode and the acoustic mode scatterings dominate at high temperature (above 150°K) while at lower temperatures (0-25°K) piezoelectric scattering dominates (Fujita, 1965). Above 150°K an exponential variation of mobility with temperature is observed, while below 25°K a $T^{-\frac{1}{2}}$ variation occurs. At temperature between 25°K and 150°K, the three mechanisms contribute equally to scattering (Kabayashi, 1967).

The electron mobilities in high purity CdS and CdSe crystals have been measured and their room temperature values are 350 and 650 cm^2/V-sec respectively (Ray, 1969), though values as high as 5×10^4 cm^2/V-sec at 1.8°K (Fujita, 1965) in CdS and up to 900 cm^2/V-sec at room temperature in CdSe (Devlin, 1967) have been reported. High photo-Hall effects in CdS and CdSe can increase Hall mobility many-fold, from 100 to 200 cm^2/V-sec for CdS (Bube et al, 1961) and from 100 to 900 cm^2/V-sec for CdSe by effectively increasing carrier concentration due to excitation of electron-hole pairs by the radiation.

The minority carrier drift mobility is very difficult to determine; average values of 15 cm^2/V-sec in CdS have been measured by Spear and Mort (1963), and in CdSe the value was 50 cm^2/V-sec, measured by Itakura and Toyoda (1965).

The effect of high electric field on the Hall mobility has also been studies. As the electric field strength is increased, the probability of piezoelectric scattering is decreased while the acoustic mode scattering is increased (since thermal vibrations of the lattice are

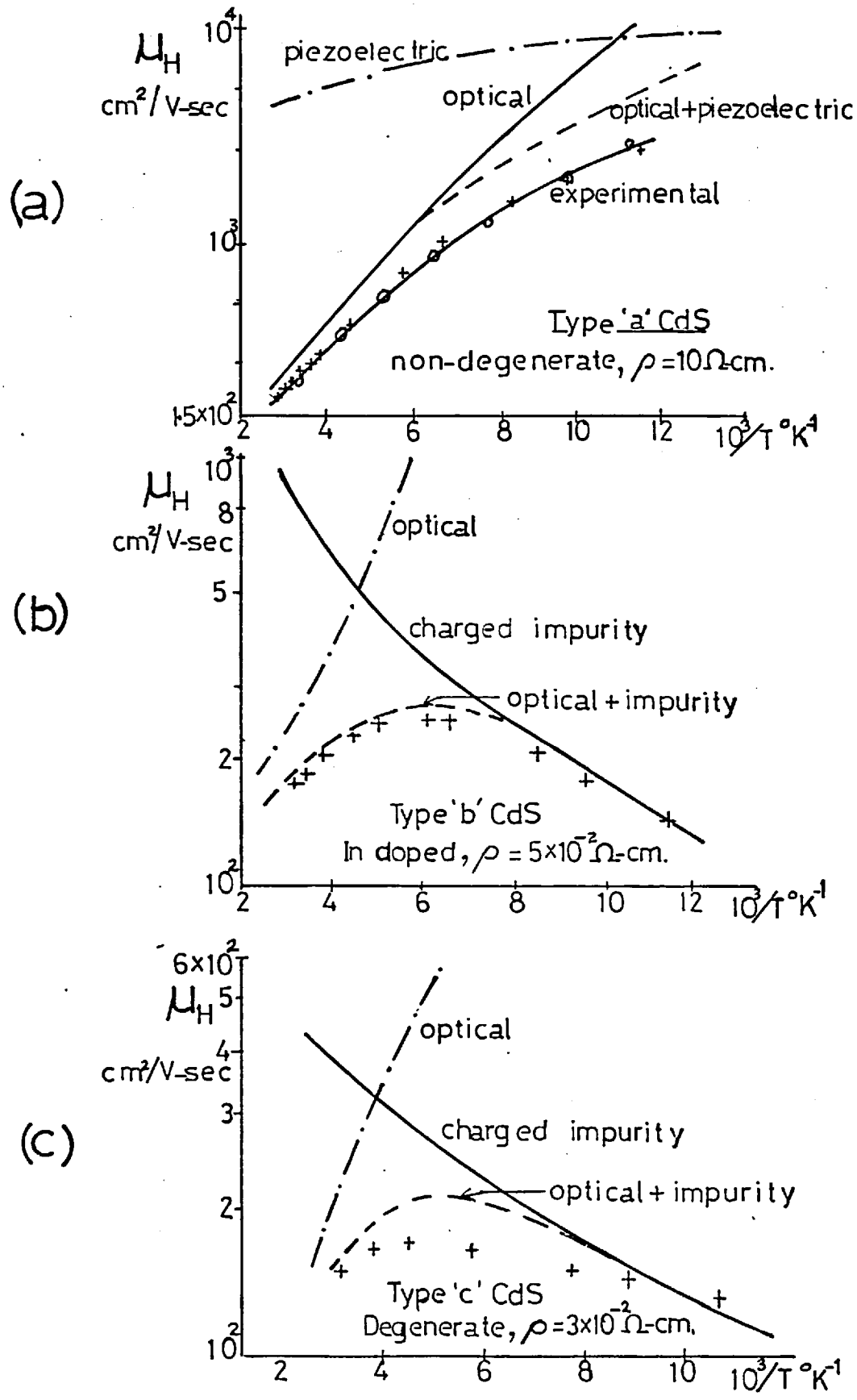


Fig. 3.7 Theoretical and Experimental Hall Mobility of Non-Stoichiometric Crystals as a Function of Temperature (After Kwok and Bube, 1973)

amplified), the collision times being $\propto F^{\frac{1}{2}}$ and $F^{-\frac{1}{2}}$ respectively. (Kobayashi, 1967). This means that the mobility should initially increase until a critical field strength is reached, after which it should decrease. This effect has been observed for CdS by Fujita et al (1965). However, results on doped CdS platlet at 230°K by Boer and Bogus (1968) show the mobility to be constant at 620 cm^2/V-sec for low fields but to decrease approximately as F^{-1} at fields higher than 30KV/cm.

Kwok and Bube (1973) studied non-stoichiometric CdS, ($\rho \sim$ 1-10 Ω-cm) in order to determine the main scattering mechanisms from temperature dependence of mobility studies, by measuring the Hall mobility. Three different CdS samples were used (a) ρ = 10Ω-cm, non-stoichiometric and non-degenerate over the whole temperature range, (b) $\rho = 5 \times 10^{-2}$ Ω-cm, doped with In and degenerate below 150°K, and (c) $\rho = 3 \times 10^{-2}$ Ω-cm, non-stoichiometric and degenerate over the whole temperature range. Type (a) was similar in resistivity and mobility to the CdS crystals grown as discussed in Chapter 2. The results of Kwok and Bube for type (a) crystals are illustrated in Fig. 3.7 (a), showing optical mode scattering as the dominant mechanism, while below 150°K piezo-electric scattering contributes. Type (b) (Fig. 3.7 (b)) shows optical mode scattering dominant above 210°K while impurity mode scattering dominant below 210°K. For type (c) crystals (Fig. 3.7 (c)) again optical mode scattering dominates at high temperature and charged impurity scattering at low temperatures.

Subhan et al (1971) obtained a theoretical fit to their temperature dependence of mobility for a model in which all the scattering mechanisms are present (m^* is a fitting parameter and assumes a value of 0.19 m_e).

Similar results have been obtained for CdSe mono-crystals showing the effect of impurities on the scattering mechanisms (Devlin, 1967).

Very little work has been done on the Hall effect in thin films of CdS and CdSe. The properties of these films vary considerably with the method of growth, substrate structure temperature etc. CdS and CdSe films grown by r.f. sputtering or evaporation are known to have a large number of grain boundaries. The mobilities are thus a few orders of magnitude lower than for single crystals. The Hall mobility has been measured by Gloede (1967) and Berger et al (1969) on evaporated polycrystalline CdSe films as used in thin film devices. At low temperatures, the mobility values are typical of those for polycrystalline films

$$\text{i.e. } \mu_H = \mu_{HO} \exp\left(-\Delta E/kT\right) \qquad (3.6)$$

This region can be attributed to impurity conduction due to excitation of electrons from impurity centres. At higher temperatures the mobility increases strongly reaching values ~ 100 cm^2/V-sec. Annealing of samples greatly increase the mobility.

The mobility of CdS_xSe_{1-x} monocrystals have been reported by Devlin and Shiozawa (1960) to pass through a minimum value of 250 cm^2/V-sec for x near $\frac{1}{2}$.

3.4.3 Dielectric Constant

Because of the ionocovalent nature of bonds in II-VI compounds, both the ionic and the electrostatic polarisation contribute to the dielectric properties. In CdS and CdSe where the ionicity is large 74 and 64% respectively, the static and optical dielectric constants are different (Ray, 1969).

The anisotropic properties of CdS and CdSe (and other hexagonal semiconductors) give rise to a direction dependent dielectric constants, ϵ_s & ϵ_∞. The dielectric constants have been measured by Berlincourt

et al (1963) and by Reynolds et al (1965) from refractive index measurements. The value of the static dielectric constant for CdS is ϵ_s ($\parallel$ c) between 8.64 and 9.35, ϵ_s ($\perp$ c) between 8.28 and 10.33 while for CdSe ϵ_s ($\parallel$ c) is between 9.25 and 10.20, ϵ_s ($\perp$ c) between 8.75 and 10.65. The optical values for CdS ϵ_∞ are between 5.17 and 5.23 and for CdSe between 5.96 and 6.4.

3.5 Imperfections in CdS and CdSe

Imperfections are lattice defects and can be either planar e.g. stacking faults and grain boundaries; line e.g. dislocations; or point defects e.g. vacancies or interstitial atoms caused by inclusion of impurities or non-stoichiometry. These imperfections give rise to energey levels in the forbidden gap. The shallow levels near the conduction band are donor levels, while deep lying levels are likely to be filled by capturing free carriers and are trapping levels. Acceptor levels and hole traps also exist in these compounds.

The energies of donor and acceptor levels have been determined for a variety of CdS and CdSe crystals by using the Hall effect, optical methods and the thermoelectric power method (from Seebeck coefficient measurements). Tables 3.1 and 3.2 give a fair selection of these levels in both materials together with the elemental impurities which are believed to give rise to these levels. (Most of these results were determined by Hall effect measurements). The shallow donor levels in both materials have been reported to be hydrogen-like (Piper and Halsted, 1960). It is well known that materials possess native defects due to tendency to grow with excess cadmium in the lattice. The levels associated with this type of imperfection are shown in the tables; they are important in undoped non-stoichiometric crystals.

Other native defects not only produce trapping levels but also sensitizing centres. Compensated donors give rise to electron traps and compensated acceptors to sensitizing centres. One of the most

useful techniques to determine trapping depths and densities is the thermally stimulated current (TSC) (Dussel and Bube 1967; Bube et al 1966; Bube 1967; Kindleyside and Woods, 1970) and space-charge-limited currents (STLC) (Manfredotti et al 1972; Markus et al 1970; Marakhonov and Seisyan 1973). Other methods include optically stimulated conductivity, photoconductivity and electric field ionization of traps.

The most used technique is certainly the TSC and as Dussel and Bube (1967) write: "TSC offers the advantage of experimental simplicity and potentially a high yield of information per unit time expended". Bube has however, favoured analysis of TSC data by a quasi-Fermi level approach. It is felt, however, Ibrikian (1974) that the best method of analysis of this data is by the method based on Shockley-Read statistics developed by Simmons and co-workers.

Although enormous amounts of data on the trapping parameters are available in the literature there are differences in the reported values of trapping energy. One explanation could be that the various crystals studied have inherent trapping properties different from each other, however, some investigators have used different techniques on the same samples (Dussel and Bube, 1966) and found discrepancies. Contrary to this, Manfredotti et al (1973 a, b) obtained fairly good agreement for trapping levels in CdSe crystals using different techniques.

There are indeed many trapping levels in CdS extending from 0.16eV below the conduction band determined by Bradbury (1964) and attributed to sulphur vacancies to 0.59 eV from Woods (1958) attributed to a vacancy complex. From a collection of TSC data by Bube (1964), Woods, Haine and Carley-Read (1968), the common levels in eV units are 0.19, 0.21, 0.23,0.30, 0.32 (cadmium vacancies),0.38, 0.45 (sulphur vacancies) 0.50, 0.59. A type of sensitizing centre in both CdS and CdSe has been attributed to Cd vacancies.

Recent trapping level data in CdSe has been obtained by Kindleyside and Woods (1970) Robinson and Bube (1971), Mackus et al (1970), Manfredotti (1973 a, b). The results show a series of levels ranging from 0.1 eV to 0.64 eV, but the levels in eV at 0.15, 0.18, 0.3, 0.35 and 0.5 are common with trapping densities 10^{12} and 10^{15} cm^{-3} as determined by Kindleyside and Woods (1970) or between 5×10^{10} and 10^{13} cm^{-3} as determined by Manfredotti et al (1973). Hole centres at 0.24 eV and 0.55 to 0.7 eV above the valence band possess a weak thermal quenching above 100°K and a high thermal quenching of conductivity above room temperature respectively. The density of traps obtained at these levels vary considerably from one investigator to another. A diffused trapping level at about 0.35 eV (or levels between 0.24 eV and 0.45 eV) with a total density $\sim 2 \times 10^{12}$ cm^{-3} has been attributed to cadmium interstitials acting as compensated donors (Manfredotti et al, 1973).

Manfredotti et al suggested that "these traps are probably correlated with compensated donors, which form clusters and behave as giant traps, strongly reducing the mobility". Faeth (1968) suggested that there may be a continuous trapping spectrum at levels close to the bottom of the conduction band and based his idea on the results of Bryant and Cox (1965) from luminescent emission showing very fine structures for these levels.

Faeth suggested a correlation between the trapping level energies in CdS and the number of levels above the valence band, represented by an emperical formula

$$E_i = a - (bi - ci^2) \qquad (3.7)$$

where a, b, c are constants and i an integer ranging from 0 at the top of the valence band to values of ten or more near the conduction band. Kindleyside and Woods applied this formula to their TSC data for CdSe and found good agreement. But the equation has only been applied to two materials and needs further verification.

Bube et al (1966) have reported trapping levels in CdS_xSe_{1-x} common to CdS lying 0.43 eV. below the conduction band and surrounded by a repulsive barrier of ~ 0.30 eV. Manfredotti et al 1973 (b) have observed trap distribution similarities between CdSe and $CdS_{.73}Se_{.27}$.

3.6 Surface Properties of CdS , CdSe and CdS_xSe_{1-x}

The surface of a covalent semiconductor has associated with it dangling bonds which normally give rise to trapping centres lying inside the band gap. The trapped charge leads to the formation of space-charge layers which can cause band bending in the surface layers. On real semiconductor surfaces, there exists, chemisorbed gases and other impurities which make the analysis of the surface state distribution complex. (For a comprehensive study of real semiconductor surfaces, the reader is refered to the text of Many, Goldstein and Grover (1965).

The surfaces of CdS and CdSe are partially depleted of electrons due to the acceptor-like properties of the surface states, being greater for CdSe than CdS. It is also known that the orientation of the free surface is important in determining the density and distribution of the dangling bond.

Studies on the 'clean' surface of CdS mono-crystals have been made by several investigators who include Mead (1965), Many and Katzir (1967) Many et al (1969) and Shappir and Many (1969). Work by Mead on the surface barrier height several metals on the basal plane (0001) and cleavage plane (1010) on CdS_xSe_{1-x} cleaved in vacuum are of considerable interest. He found that the barrier height for CdS varied as the work function of the metal, while for CdSe the barrier height was indpendent of metal. This result was attributed to the fact that CdS is more ionic than CdSe (being 74 and 64% respectively (Suchet, 1965). Thus the wave functions for CdS are more localized with smaller overlap than those of CdSe and hence its surface states lie near the band edges (from Shockley's theory, 1939). CdSe being more covalent, has larger overlap

or smaller atomic spacings and will possess surface states near the centre of the forbidden gap. The Fermi level at the surface of CdS can move up or down in energy without requiring surface charge to fill or empty these states, while due to the large density of states on the CdSe surface it is pinned at a given energy. The barrier height of a Schottky contact to CdSe will therefore be approximately independent of the metal.

Field effect and surface photo-voltage measurements have been made on the (0001) basal plane of CdS by Mark (1965) and Many and co-workers who found that the density of acceptor-like states is small $\sim 10^{11}$ cm^{-2}. These surface traps on CdS may arise from sulphur vacancies.

Adsorbed gases, in particular oxygen, play a significant role in the physical and chemical properties of wide gap semiconductors, affecting the electronic surface processes. Mark (1965) reported that oxygen-free CdS stores up to 10^5 times more trapped charge than when oxygen is photo-adsorbed.

Adsorbed oxygen ions act as deep lying donors at 0.9 eV below the conduction band (the donor level for adsorbed nitrogen or oxygen-free CdS is $\sim$ 0.54 eV). Adsorbed oxygen is believed to convert the surface traps into recombination centres, reducing the free electron lifetime, response time and photo-current.

Mark (1964) observed that the adsorbed negative ions of oxygen can be spontaneously desorbed by band-gap light incident on the CdS surface. The mechanism involved is migration of photo-generated holes to the CdS surface by the Schottky barrier field, thereby releasing the adsorbed oxygen. Desorption of oxygen ions can also be thermally induced in a slow-process involving transfer of electrons from the ions back to the conduction band. The minimum temperature for this process was $\sim 170^{\circ}C$ in vacuum. Desorption by electron bombardment where the

energy of electrons is sufficient to break oxygen bonding, has been studies by Novikov and Cherednichenko (1970), Palz and Ravelet (1970). The photoconductivity increases several orders of magnitude close to its 'clean' surface level.

Recent results have indicated that the chemisorption processes are more complex than earlier suggested. Schuber and Boer (1971) have reported that the type of crystal discussed above in which thermally stimulated current give a desorption maximum corresponding to the 0.9 eV trapping level can be transformed into a class of crystal if heated above 600^{o}K showing little change of conductance after desorption. This change has been attributed to Cd diffusion in the bulk and monatomic oxygen adsorption.

Room temperature chemisorption studies by Weber indicates both adsorption and photo-desorption occurs in step processes. Oxygen is first physically adsorbed as molecules, then captured by active surface centres, then chemisorbed as negatively charged oxygen molecules. In the desoprtion process the charged oxygen molecules are neutralised by photoexcited holes, then freed from the active surface centres.

Studies on this CdSe polycrystalline films (South and Hughes, 1974) suggests different surface structure than for single crystals, as results show no trapping centres for adsorption of oxygen (unless deliberately bombarded with argon ions).

Consigny and Madigan (1969) studies the properties of basal (0001) and cleavage (1010) planes of CdSe monocrystals (no. of atoms per unit area $\sim 7 \times 10^{14}$ cm^{-2}) and showed that the barriers were different for the two planes but independent of the metal used. Consigny and Madigan (1970) used MIS capacitor technique on CdSe/SiO structure to determine the surface states between chemically prepared CdSe and SiO on (0001) and (1010) planes. The density of the fast states on the basal plane was 10^{12} cm^{-2} approximately twice as large as on the cleavage plane being 0.6 eV and 0.7 eV below the bottom of the conduction band,

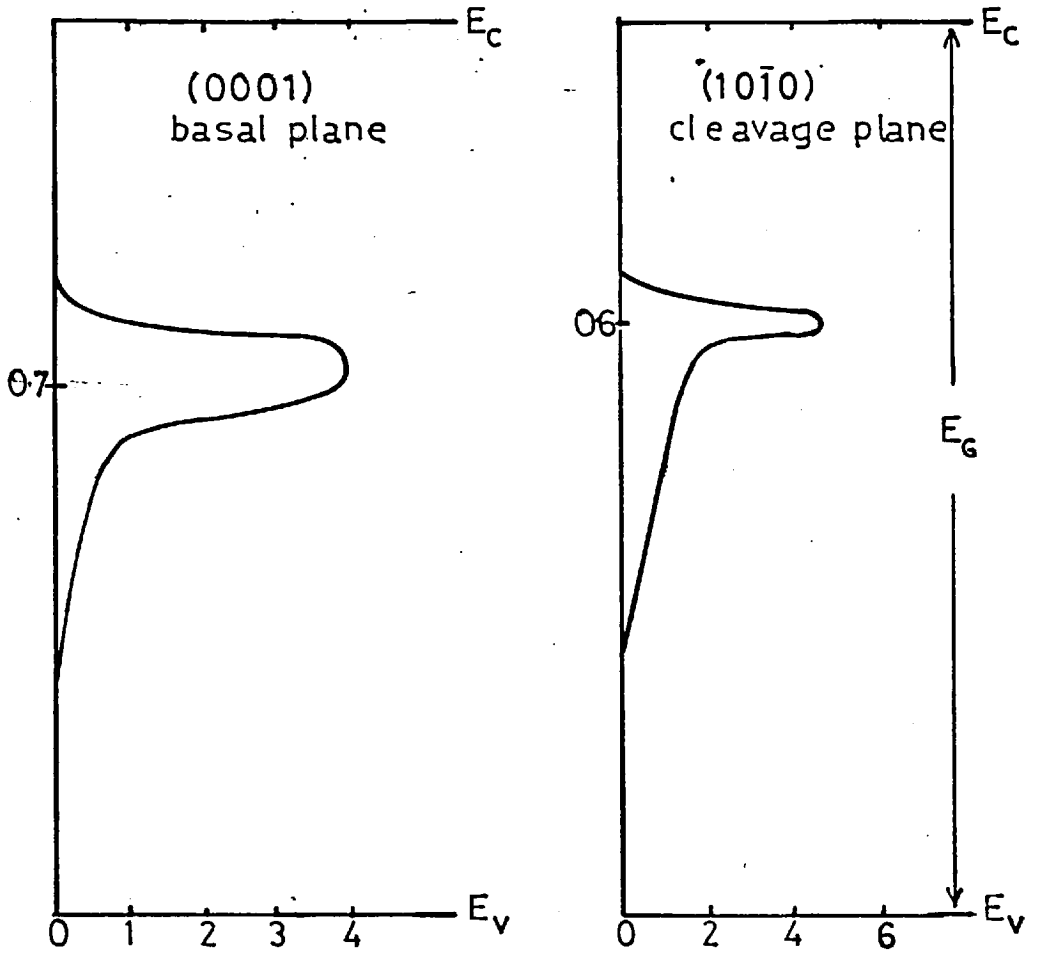


Fig. 3.8 Surface States on CdSe (after Consigny and Madigan, 1969)

respectively Fig. 3.8 illustrates the depth and distribution of these surface states for the two planes near the centre of the forbidden gap (after Consigny and Madigan) supporting Mead's model. They did not observe pinning of the Fermil level as surface density did not exceed 10^{13} cm^{-2}, the value suggested by Bardeen (1947) above which pinning of the Fermi Level is expected. Consigny and Madigan concluded that the density of surface states is reduced by the SiO as it does in the SiO_2:Si system.

3.7 Ohmic and Rectifying Contacts to CdS and CdSe

Metallic contacts as electrodes to semiconductors are of fundamental imprtance in analysing the electrical properties of the semiconductors. There are basically two types, ohmic and non-ohmic or rectifying contacts the difference being the potential barrier developed between metal and semiconductor as a result of Fermi level equalisation in the two materials. Ohmic contacts ideally have zero barrier potential providing a reservoir of electrons with easy access to the conduction band (in n-type materials) while rectifying contacts ideally have large barrier heights where carrier flow is caused by thermionic emission over the barrier for forward conduction but cannot surmount the barrier in reverse bias.

A contact is described as ohmic if it exhibits linear I-V characteristics in both directions of voltage. There are various steps in assuring that the metal chosen forms ohmic contact. First of all its work function, ϕ_W, has to be matched to the electron affinity, χ, of the semiconductor such that the contact barrier between metal and semiconductor is small enough for thermal excitation over any small barrier

i.e. $$\phi_W - \chi < kT \qquad (3.8)$$

The density of surface states of the semiconductor can influence the choice of ϕ_W. The method of metalisation is also important.

Vacuum deposition or sputtering is superior to other techniques, as contacts can be made to have intimate contact with the semiconductor. Contacts could also be well defined by deposition through a suitable stencil or photoresist. Finally the temperature of the semiconductor can be conveniently elevated to induce diffusion of the metal into the surface layer. Two further steps may be taken to produce good contacts. Firstly, there can be deliberate alloying of the metal with the semiconductor to form an N^{++} region in the vicinity of the metal electrode so that quantum mechanical tunnelling is increased many fold. Secondly, there can be creation of recombination centres at the metal semiconductor interface e.g. by lapping the back surface of the substrate before the contact is established.

A rectifying contact on the other had is obtained by the formation of a depletion layer in the semiconductor adjacent to the contact such that $\phi_W - \chi \gg kT$.

Ohmic contacts to CdS and CdSe are not really difficult to achieve. In, Ga and their alloys are normally chosen since they are low work function materials which are not chemically reactive. Such contacts have been used by numerous investigators e.g. Smith (1955). Other metals such as Al, have been reported to form ohmic contact to CdS and CdSe and are tabulated by Milnes and Feucht (1972). It should be noted that some of these metals also form rectifying contacts to the semiconductors. It is clear that ohmic contacts are more easily applied to highly conducting crystals . Low noise is a very important requirement in ohmic contacts. Little account is made of the noise properties associated with the ohmic contacts apart from In and Ga.

At temperatures of about $100^{\circ}C$ and above, In and Ga begin diffusing into the bulk of the semiconductors. Also, these metals are mechanically weak and can be erased from the semiconductor surface. Therefore these contacts have limited applications. In this work In-Au

alloys were applied to the CdS, CdSe and the alloy crystals and proved to give reliable ohmic contact with low noise properties (see Section 4.3).

Rectifying contacts of Au, Ag, Cu, Pt and Pd have been investigated by Goodman (1964), Spitzer and Mead (1963), Mead (1965), (Aven & Mead, 1965), Consigny and Madigan (1969, 1970). They form rectifying barriers of varying heights to CdS but the barrier height is independent of metal used on CdSe. The result has been attributed to the high surface state density of CdSe (Section 3.6).

Experiments have been performed by applying Ag rectifying contacts to one surface of wafers of CdS, CdSe and alloy crystals and In/Au to the other surface to estimate carrier concentration by the differential capacitance technique (Kennedy and O'Brien, 1969). Excellent I-V characteristics were obtained for the Ag/CdS diodes, but as x became $< \frac{1}{2}$, larger leakage currents were observed, especially for the Ag/CdSe diodes. The carrier concentration for these crystals are shown in Table 3.3 together with the estimated barrier height determined from $1/C^2$ versus V plots. Similar experiments were performed for Ag contacts on the CdSe layer of heterojunctions created by sputtering 1 μm CdSe layers on CdS_xSe_{1-x}. In/Au ohmic contacts were applied to the CdS_xSe_{1-x} 'back' surface. It was hoped to obtain (a) carrier concentration in the CdSe epi-layer (b) carrier profiles at the interface and (c) carrier concentration in the substrate by assuming all the voltage to be dropped in the Schottky barrier depletion layer. This was, however, not successful as the devices exhibited breakdown before sufficient voltage could be applied due to the high carrier concentration in the epitaxial layer near the interface. But data was obtained for the carrier concentration in the epi-layer depletion region before breakdown ocurred.

3.8 Space-Charge-Limited Currents

When good ohmic contacts are applied to very high resistivity wide-gap semiconductors such as CdS and CdSe, space-charge-limited

currents (SCLC) flow in the bulk of the semiconductor similar to those in insulators as described by Mott and Gurney (1940) with current magnitudes higher than for ohmic currents.

SCLC flow in high resistivity semiconductors because unnneutralized space-charge accumulates due to the dielectric relaxation time τ_D being greater than the transit time τ_t through the semiconductor. Space-charge will accumulate if

$$\frac{\tau_t}{\tau_D} = \frac{L^2}{\mu V \rho \epsilon} < 1 \qquad (3.9)$$

In the absence of trapping levels, the current is given by the solid-state equivalent of child's law, obtained by solving the Poisson's equation. Wright (1959) obtained

$$J = \frac{9}{8} \frac{\mu \epsilon V^2}{L^3} \qquad (3.10)$$

describing a square law variation with voltage and independent of resistivity and limited only by the space-charge.

At low voltages ohmic current behaviour is observed, $J = \frac{e\mu N_D V}{L}$, characterised by very high resistivity (Zuleeg and Muller, 1964; Zuleeg, 1963).

SCLC was first observed in insulating CdS crystals by Smith and Rose (1955), Rose (1955), Smith (1955). In order to observe these currents one electrode was ohmic (In) for injection while the other was of the blocking type.

In studying thin films of CdS or CdSe, the injected currents are observed to be limited by trapping centres capturing the charge carriers (Zuleeg, 1963; Zuleeg and Muller, 1964; Marakhonov and Rusyan, 1973; Pavlenko and Muzalevskri, 1971).

When the injected charge is captured by traps at level E_t and density N_t, then the current is expressed as

$$J = \frac{9}{8} \frac{\mu \epsilon \theta V^2}{L^3} \tag{3.11}$$

where θ is the ratio of free to trapped charge given by $\theta = \frac{N_c}{N_t} \exp - \frac{E_C - E_t}{kT}$ (Rose, 1955 ; Lampert, 1956, 1962; Bube, 1962).

Rose (1955) expressed the current during trap filling for an exponential trap distribution as

$$J = \text{const.} \ (V - V_o) \left(\frac{E_o}{kT} + 1 \right) \tag{3.12}$$

where V_o is a threshold voltage corresponding to the quasi Fermi level being at the trapping level.

The current varies at a power greater than two. When all the traps are filled all further injected charge remain as free carriers in the conduction band and the current returns to a square law of voltage dependence as

$$J = \frac{9}{8} \frac{\mu \epsilon V^2}{L^3}$$

At the voltage corresponding to all traps being filled V_{TFL} the total traps density is given by

$$N_t = \frac{\epsilon V_{TFL}}{qL^2} \tag{3.13}$$

For the CdSe film, if $t \sim 1 \mu m$, $\rho \sim 10^3 \Omega$-cm, $\mu \sim 10$ cm^3/V-sec, then SCLC just becomes important at ~ 1 volt. For analysis of the CdSe film under SCLC conditions, Section 6.2.

The electrical properties of CdS and CdSe can be summarised in the form of a table giving values from the Literature and from the values determined by measurements here (Table 2.4). The variation of the electrical properties with composition is also indicated.

3.9 Optical Properties

Optical data has been used to determine electrical properties of II-VI compounds (see sections 3.3 to 3.5). Spectrographic techniques have provided valuable information on the fundamental properties of the material e.g. optical absorption spectra to determine the energy band-gap and the valence sub-band structures. In this section these techniques are briefly applied to the optical properties of CdS and CdSe. For further information for II-VI compounds, especially CdS, see Dunod (1964), Segall and Marple (1967), Bube (1960, 1964, 1965, 1967), Reynolds (1965, 1969), Ray (1969), and Thomas (1967). However, a great deal is owed to Thomas, Hopfield and co-workers for their outstanding work in understanding the opto-electronic structure in CdS and other II-VI compounds.

The observed reflection spectra for CdS at $4.2^{\circ}K$ shows in addition to peaks corresponding to transitions from the three uppermost valence sub-bands, weaker transitions associated with exciton transition (Thomas and Hopfield, 1959). They also observed exciton splitting under an applied magnetic field which was dependent on crystal orientation. Hopfield (1961) showed that in the fundamental absorption band edge for intrinsic CdS, fine structure appeared at low temperatures. This structure was explained in terms of the formation of ground state excitons. The absorption of photons results in the transference of electrons from a filled valence band to an excited state very close to the conduction band. The holes left behind in the valence band interact with these electrons to form bound electron-hole pairs (the excitons) by coulombic attraction (as in the hydrogen atom).

Each valence sub-band gives rise to a series of exciton states, the peaks result from splitting of valence band by spin orbital interactions, for instance three non-overlapping exiton series for CdSe (Wheeler and Dimmock, 1962). The peaks on the long wavelength side of the absorption spectra gives a measure of the binding energy of the exciton state and

the intensity is proportional to the probability of finding two carriers together in the bound state. The splitting between the top two valence sub-bands is less than the binding energy of the exciton. On the application of an electric field, electrons and holes will move through the crystal giving rise to photoconductivity.

In CdS and CdSe, the transmission (where photon energies are just greater than the band-gap) and reflection spectra corresponding to the absorption edge involves direct electronic transmission i.e. K constant at (000). The absorption edge is sharper for such transitions compared with indirect transitions and the absorption coefficient is high ($\sim 10^4$ cm^{-1} for CdS and CdSe). The magnitude of the absorption coefficient determines the energy level pairs available for optical transitions (i.e. number which interact with the radiation).

Isotropic stress gives rise to variation of the energy levels shifting the absorption edge and reflectivity peaks. The pressure coefficients for CdS and CdSe are relatively small (Ray, 1969).

The fine structure maxima in the photoconductivity spectra for CdS and CdSe and their alloys, have been observed to coincide with the absorption maxima. For CdS, six photoconduction peaks are observed at $77^{o}K$ but at $4.2^{o}K$ even more peaks occur. The photoconductivity spectra in CdSe is more complex due to impurity peaks. Oscillatory photoconductivity are observed at higher energies due to oscillatory values of the electron lifetime in the conduction band as a function of energy. Oscillatory photoconductivity has also been observed in CdS_xSe_{1-x} by Larger et al (1966).

Radiative recombination is the inverse of the photoexcitation processes, i.e. conduction band electrons recombining with valence band holes emitting radiation corresponding to the band-gap. In extrinsic material, radiative recombination may take place via impurity or defect

levels (with radiative energy $< E_G$). The recombination may either be spontaneous or with emission of radiation via impurity/defect states or an Auger process.

Edge emission spectra associated with the recombination of conduction band electrons and valence band holes have been observed in CdS and CdSe (Halsted, 1967). In CdS, the zero photon peak of spectrum at 77°K is shifted to a shorter wave length to that at 4.2°K. Pedrotti and Reynolds (1960) explained this as recombination between two bound states at 4.2°K which are separated by a smaller energy than between the free electrons and trapped holes (which provide the emission) at 77°K, the bound electron states being ionized. Similar spectra has been observed in CdS_xSe_{1-x} and CdSe. Bound exciton complexes have been observed and are created by optical excitation in the crystal. Four exciton complexes have been postulated for CdS by Thomas and Hopfield (1962) where the excitons are bound to neutral and ionized donors and acceptor states.

Photoemission at room temperature has been observed in the CdS_xSe_{1-x} crystals grown by the vapour-phase method (Chaper 2) when the samples were irradiated with an electron beam. The wavelength of the emission corresponded closely to the band-gaps of the CdS_xSe_{1-x} samples, as measured by the absorption edge method discussed in section 3.3. This can be explained in terms of radiative recombination creating by the electron beam excitation, producing stimulated emission.

On the application of large forward bias on p-n junctions of degenerate direct transition material irradiation can result from the injection of carriers. Thomas and Hopfield (1962) discussed the inversion population in CdS by electrical pumping. Laser action has been observed in CdS by utilizing electron beam excitation at low temperatures, (Benoit a La Guillaume et al 1965, 1967; Litton and Reynolds, 1967). Laser action has also been observed in CdS_xSe_{1-x} and CdSe by Hurwitz, (1966) by optical pumping,

a method in which the radiation, having photon energy just greater than the band-gap, is used to excite the semiconductor.

Semiconductors are not expected to exhibit pronounced photoconductivity gain unless certain defect centres are included in the crystal. In the case of n-type material, the defect has to behave as an acceptor-like recombination centre and for CdS and CdSe, higher photosensitivity can be achieved by doping with halogen or Cu. (The CdS_xSe_{1-x} crystals grown by the vapour-phase technique exhibited very little photoconductivity properties since they were grown 'pure' not including such impurity centres).

When the carriers are photogenerated, the capture cross-section for holes, being increased, allows free electrons to exist in the conduction band for longer periods i.e. the free carrier lifetime is improved (by a factor of 10^4 for CdS and CdSe (Bube, 1967)) so that their transit time in the crystal is increased, leading to photoconductivity gain (the capture cross-section ratio of electrons to holes being as high as $\sim 10^8$).

The increase in conductivity, $\Delta\sigma$, with illumination is described by the equation

$$\Delta\sigma = \Delta n e \mu_n + n e \Delta \mu_n \qquad (3\text{-}14)$$

and will therefore depend on the excitation rate and on mobility changes e.g. effective increase in ionized impurity scattering centres or transition from lower to higher mobility states.

Higher photosensitivity has been observed in CdS by introducing both donor and acceptor impurities.

The inclusion of a donor impurity e.g. I , generates acceptor-like cation vacancies of negative charge and having high capture cross-section for holes but not electrons. Acceptor impurities e.g. Cu creates negatively charged sensitizing centres (Bube, 1967).

Photoconductivity can be thermally and optically quenched in a process involving high enough energies to excite electrons from the valence band into sensitizing centres, converting them from recombination centres into hole traps.

TABLE 3.1 - IMPURITY LEVELS IN CdS

DONOR LEVELS	IMPURITY IDENTITY	REFERENCES
.007		Li and Huang (1971)
0.024	Hydrogenic Donor	Woodbury (1965), Morikawa (1965)
0.029	Cl,Br,I, Substitute S	Devlin (1967)
0.033	Al,Ga, In, Substitute Cd	Li and Huang (1971), Thomas and Hopfield (1962), Nassau et al (1970)
.035	F	Nassau et al (1970)
.175		Li and Huang (1971)

ACCEPTOR LEVELS		
0.6	Cu substitute Cd	Bube (1960)
1.0	Ag substitute Cd Cd Vacancy	Bube (1960)

TABLE 3.2 - IMPURITY LEVELS IN CdSe

DONOR LEVELS	IMPURITY IDENTITY	REFERENCES
0.014	Hydrogenic Donor	Burimeister (1965)
0.016	Cl,Br,I, Substitute Se	
0.03	In,Ga Al	Shiozawa et al (1962)
0.14	Se Vacancy	

ACCEPTOR LEVELS		
0.1		Reynolds et al (1965)
.64	Cu Substitute Cd	Bube (196)
1.0	Cd Vacancy	Bube (196)

TABLE 3.3 - CARRIER CONCENTRATION AND BARRIER HEIGHT OF CdS, CdSe AND ALLOYS

SUBSTRATE	CARRIER CONC.	BARRIER HEIGHT
CdS	$(5 \pm 1) \times 10^{15}$ cm^{-3}	$.75 \pm .05$
$CdS_{.75}Se_{.25}$	$(7 \pm 1) \times 10^{15}$	$.75 \pm .05$
$CdS_{.5}Se_{.5}$	$(8 \pm 1) \times 10^{15}$	$.65 \pm .05$
$CdS_{.33}Se_{.67}$	$(1.4 \pm 0.3) \times 10^{16}$	$.6 \pm .1$
CdSe	$(2.3 \pm 0.5) \times 10^{16}$	$.5 \pm .1$
CdSe (epi-layer)	$(5 \pm 1) \times 10^{14}$	$.45 \pm .1$

TABLE 3.4 SOME EXPERIMENTAL PROPERTIES OF CdS, CdSe AND THEIR ALLOY CRYSTALS AT 300°K

	CdS	CdS_xSe_{1-x}	CdSe
Band Gap, E_G (eV)	2.38	*	1.71
$\frac{dE_G}{dT}$ (10^{-4} eV/°C)	~ 5		~ 5
Lattice Constant, c (Å)	4.1368	*	4.2985
Lattice Constant, a (Å)	6.7163	*	7.0150
Electron Affinity, χ (eV)	4.79	‡	4.95
Electron effective Mass, m_e (m_o)	0.20	*	0.13
Hole effetive Mass $m_{//c}$ (m_o)	5		1
Hole effective mass $m_{\perp c}$ (m_o)	0.7		0.45
Electron Mobility, μ_e (cm^2/V-sec)	350	280 ($x = \frac{1}{2}$)	650
Hole Mobility, μ_n (cm^2/V-sec)	15		50
Relative Dielectric Constant, $\epsilon_{s//c}$	9.5	‡	9.3
Relative Dielectric Constant, $\epsilon_{s\perp c}$	9	‡	10.2
Optical Dielectric Constant, ϵ_∞	5.2		6
Refractive Index	2.3		2.6
Temperature Coeff. of expansion (10^{-6} $°C^{-1}$)	4.0		4.8
Surface State Density, N_S	$\sim 10^{10} - 10^{11}$		$\sim 10^{13}$
(Dangling Bond Density, N_{DB} ($\times 10^{14}$ cm^{-2})	6.75		6.25

* Experimental linear (approximate) variation with composition.

‡ Assumed linear variation in calculations (Chapter 6).

REFERENCES - CHAPTER 3

Aven, M., Mead, C. A. (1965) Appl. Phys. Letts. 7, 8.

Baer, W. S., Dexter, R. N. (1964) Phys. Rev. 135, A1388.

Bardeen, J. (1947) Phys. Rev. 71, 717.

Benoit A La Guillaume, C., Debever, J. M. (1965) C. R. Acad. Sci. 261, 5428

Benoit A La Guillaume, C., Debever, J. M., Salvan, F. (1967) Int. Conf. II-VI Semiconducting Compounds (D. G. Thomas Ed.) p.669.

Bergstresser, T. K., Cohen, M. L. (1967) Phys. Rev. 164, 1069.

Berlincourt, D. A., Jaffe, H., Shiozawa, L. R. (1963) Phys. Rev. 129, 1009.

Berger, H., Janiche, G., Grachovskaya, N. (1969) Phys. Stat. Solidi 33, 417.

Blakemore, J. S. (1969) Solid State Physics p.309., Saunders Co. Publ.

Boer, K. W., Bogus, K. (1968) Phys. Rev. 176, 899.

Bonch-Bruevich, V.L. (1967) Int. Conf. II-VI Semiconducting Compounds (D. G. Thomas Ed.) p.623.

Bradbery, G. W., Spear, W. E. (1964) Brit. J. Appl. Phys. 15, 1127.

Bryant, F. J., Cox, A. F. L. (1965) Brit. J. Appl. Phys. 16, 1065.

Bube, R. H. (1960) Photoconductivity in Solids, Wiley & Sons, N.Y.

Bube, R. H. (1962) J. Appl. Phys. 33, 1733.

Bube, R. H. (1964) J. Appl. Phys. 35, 586.

Bube, R. H. (1967) Phys. & Chem. of II-VI Compounds, Ch.13 (M. Aven and J. S. Prener Eds.), North-Holland, Amsterdam.

Bube, R. H., Macdonald, H. E., Blanc, J. (1961) T. Phys. Chem. Soldis 22, 173.

Bube, R. H., Dussel, G. A., HO, C., Miller, L. D. (1966) J. Appl. Phys. 37, 21.

Cardona, M. (1963) J. Phys. Chem. Solids 24, 1543.

Chopra, K. L., Khan, I. H. (1967) Surface Science 6, 33.

Cohen, M. L. (1967) Int. Conf. II-VI Semiconducting Compounds (D. G. Thomas Ed.) p.462.

Collins, T. C., Euwena, R. N., De Witt, J. S. (1966) J. Phys. Soc. Japan S21, 15

Consigny III, R. L., Madigan, J. R. (1969) Sol St. Com. 7, 189.

Consigny III, R. L., Madigan, J. R. (1970) Sol. St. Electron 13, 113.

Devlin, S. S. (1967) Phys. & Chem. of II-IV Compounds, Ch. 11, (M. Aven & J. S. Prener Eds.) North-Holland, Amsterdam.

DeWitt, J. S., Euwema, R. N., Collins, T. C. (1967) Int. Conf. II-VI Semiconducting Compounds (D. G. Thomas. Ed.) p.611.

Devlin, S., Shiozawa, L. R. (1960) Bull. Am. Phys. Soc. 5, 151.

Dimmock, J. O., Wheeler, R. F. (1961) J. Appl. Phys. 325, 2271.

Dunod. (1964) Ed., Proc. 7th Int. Conf. Physics Semicond. Paris, 1964.

Dussel, G. A., Bube, R. H. (1966) J. Appl. Phys. 37, 13.

Dussel, G. A., Bube, R. H. (1967) Phys. Rev. 155, 764.

Faeth, P. A. (1968) J. Electrochem Soc. 115, 440.

Fawcett, W., McLean, T. P. (1965) Proc. Phys. Soc. 85, 1315.

Fujita, H., Kobayashi, K., Kawai, T., Shiga, K. (1965) J. Phys. Soc. Japan 20, 109.

Gloede, W. (1970) Proc. Int. Conf. Phys. Chem. Semicond. Heterojunctions Layer Structures, Budapest, 1970, 3, 95.

Goodman, A. M. (1964) J. Appl. Phys. 35, 537.

Haine, M. E., Carley-Read (1968) Brit. J. Appl. Phys. 1, 1257.

Halsted, R. E. (1967) Physics & Chemistry of II-VI Compounds Ch. 8 (M. Aven, J. S. Prener Eds.) North-Holland Publishing Co. - Amsterdam.

Herman, F., Skillman, S. (1960) Proc. Int. Conf. on Semicond. Phys. Prague (Publ. House Checz. Acad. Sci., Prague, 1961) p.20.

Hopfield, J. J. (1961) J. Appl. Phys. 32, 2277.

Hopfield, J. J., Thomas, D. G. (1961) Phys. Rev. 122, 35.

Hurwitz. C. E. (1966) Appl. Phys. Letts. 8, 121.

Hurwitz, C. E. (1966) Appl. Phys. Letts. 8, 243.

Ibrikian, K. (1974) Private Communication.

Itakura, M., Toyoda, H. (1965) Jap. J. Appl. Phys. 4, 560.

Jahne, E., Gutsche, E. (1967) Phys. Status Solidi 21, 57. (Also Int. Conf. II-VI Semiconducting Compounds 1967). (D. G. Thomas Ed.) p.825.

Kennedy, D. P., O'Brien, R. R. (1969) I.B.M. J. Res. Dev. p.212.

Kindleyside, L., Woods, J. (1970) J. Phys. D: Appl. Phys. 3, 451.

Kobayashi, K.(1967) Int. Conf. II-VI Semiconducting Compounds (D. G. Thomas Ed.) p.755.

Kubo, S., Onuki, M. (1965) J. Phys. Soc. Japan 20, 1280.

Kwok, H. B., Bube, R. H. (1973) J. Appl. Phys. 44, 138.

Lampert, M. A. (1956) Phys. Rev. 103, 1648.

Lampert, M. A. (1962) Proc. IRE 50, 1781.

Langer, D. W., Park, Y. S., Euqena, R. N. (1966) Phys. Rev. 152, 788.

Litton, C. W., Reynolds, D. C. (1967) Int. Conf. II-VI Semiconducting Compounds (D. G. Thomas Ed.) p.694.

Li, S.S., Huang, C.I. (1971) Phys. Rev. B3, 3266.

Manfredotti, C., Rizzo, A., Santorsola, G. (1972) Phys. Status. Solidi A 12, 163.

Manfredotti, C., Rizzo, A., Vasanelli, L. (1973) J. Appl. Phys. 44, 5463.

Manfredotti, C., Semisa, D., Depe, E. (1973) Phys. Status Solidi 20, 477.

Many, A., Goldstein, Y., Grover, N. B. (1965) Semiconductors Surfaces Ch.4, North-Holland Publ. Co.

Many, A., Katzir, A. (1967) Surface Science 6, 279.

Many, A., Shappir, J., Shaked, U. (1969) Surface Science 14, 156.

Marakhonov, V. M., Seisyan, R. P. (1973) Soviet Physics - Semiconductors 7, 769

Mark, P. (1964) J. Phys. Chem. Sol. 25, 911.

Mark, P. (1965) J. Phys. Chem. Sol. 26, 959.

Mavkus, P., Sakalas, A., Smilga, A., Vivvakas, J. (1970) Phys. Status Solidi A2, 171.

Mead, C. A. (1965) App. Phys. Letts. 6, 103.

Mott, N. F., Gurney, R. W. (1940) Elec. Processes in Ionic Cryls. Oxford p.168

Nassau, K., Henry, C. H., Shiever, J. W. (1970) 10th Int. Conf. Phys. Semicond. p.209, Cambridge Mass.

Novikov, B. V., Cherednichenko, A. E. (1970) Phys. Letts. 32A, 205.

Palz, W., Ravelet, S.(1970) Sol. St. Electron. 13, 1241.

Pavlenko, A. A., Muzalevskii, E. A. (1971) Sov. Phys.-Semicond. 4, 1373.

Pedrotti, L. S., Reynolds, D. C. (1960) Phys. Rev. 120, 1664.

Pedrotti, F. L., Reynolds, D. C. (1962) Phys. Rev. 127, 1584.

Piper, W. W., Halsted, R. E. (1961) Proc. Int. Conf. Semicond. Phys. Prague, 1960, p.1046.

Piper, W. W., Marple, D. T. E. (1961) J. Appl. Phys. 32, 2237.

Ray, B. (1969) II-VI Compounds, Pergamon Press.

Reynolds, D. C., Litton, C. W., Collins, T. C. (1965) Phys. Status Solidi 9, 645

Robinson, A. L., Bube, R. H. (1971) J. Appl. Phys. 42, 5280.

Rose, A. (1955) Phys. Rev. 97, 1538.

Schubert, R., Boer, K. W. (1971) J. Phys. & Chem. Solids 32, 77.

Segall, B. (1967) Physics & Chemistry of II-VI Compounds (M. Aven and J. S. Prener Eds.) p.20. North-Holland Publ Co. Amsterdam.

Segall, B., Marple, D. T. F. (1967) Physics & Chemistry of II-VI Compounds (M. Aven & J. S. Prener Eds.) Ch.7, North -Holland Publ. Co. - Amsterdam.

Shamilova, K. V., Andrushko, A. F., Duna. I. (1966) Sov. Phys.-Crys. 10, 414.

Shappir, J., Many, A. (1969) Surface Science 14, 169.

Smith, R. W. (1955) Phys. Rev. 97, 1525.

Smith, R. W., Rose, A. (1955) Phys. Rev. 97, 1531.

South, G., Hughes, D. M. (1974) Thin Solid Films 20, 135.

Spear, W. E., Mort, J. (1963) Proc. Phys. Soc. 81, 130.

Spitzer, W. G., Mead, C. A. (1963) J. Appl. Phys. 34, 3061.

Stradling, R. A. (1967) Proc. Phys. Soc. 90, 175.

Thomas, D. G., Hopfield, J. J. (1959) Phys. Rev. 116, 573.

Subhan, M. A., Islam, M. N., Woods, J. (1972) J. Phys. Chem. Solids 33, 229.

Suchet, J. P. (1965) Chemical Physics of Semiconductors Van Nostrand Co.

Valakh, M. Ya., Vitrikhovskii, N. I., Lisitsa M. P. (1968) Phys. Status Solidi 27, K81.

Wheeler, R. G., Dimmock, J. O. (1962) Phys. Rev. 125, 1805.

Whitsett, C. R. (1965) Phys. Rev. 138A, 829.

Woods, J. (1958) J. Electron. Cont. 5, 417.

Wright, G. T. (1959) Proc. Instr. Elect. Engrs. B106, Suppl. 17.

Zook, D., Dexter, R. N. (1963) Phys. Rev. 129, 1980.

Zuleeg, R. (1963) Sol. St. Electron. 6, 193.

Zuleeg, R., Muller, R. S. (1964) Sol. St. Electron 7, 575.

CHAPTER 4 - EXPERIMENTAL DETAILS

4.1 Introduction

High quality single crystal boules of CdS, CdSe and their alloy crystals were grown by the modified Piper-Polich technique described in Section 2.3. Wafers cut from these boules were polished parallel to the basal plane. Their electrical properties, e.g. band gap, resistivity, mobility and carrier concentration were studied by the methods discussed in Chapter 3. The values of these quantities are important in the construction of the energy band profile of the heterojunction. CdSe was r.f. sputtered under optimum conditions (see later) to form an expitaxial layer without significant grading of the junction. CdSe films were also made on other substrates to study crystallographic and electrical properties of the film (Section 3.2).

To complete the fabrication of the heterojunction devices, ohmic contacts were applied to both 'top' and 'back' surfaces of the structure and the samples were scribed, diced and encapsulated using a reproducible method to enable reliable electrical assessments to be made on the devices (see later). The important electrical properties, which include I-V and C-V characteristics, from which very important information of the device behaviour can be obtained will be discussed in this chapter, together with the fabrication technique.

4.2 Substrate Preparation and Electrical Assessment

Cutting and Polishing

The crystal boule was mounted with wax on a cutting jig having goniometer movements as illustrated in Fig. 4.1 A back reflection Laue X-ray photograph was taken to determine the orientation. The crystal was rotated until the basal plane was perpendicular to the X-ray beam. A reference plate was fixed to the jig, perpendicular to the x-ray beam so that the crystal could be cut parallel to this plate and hence to the basal plane.

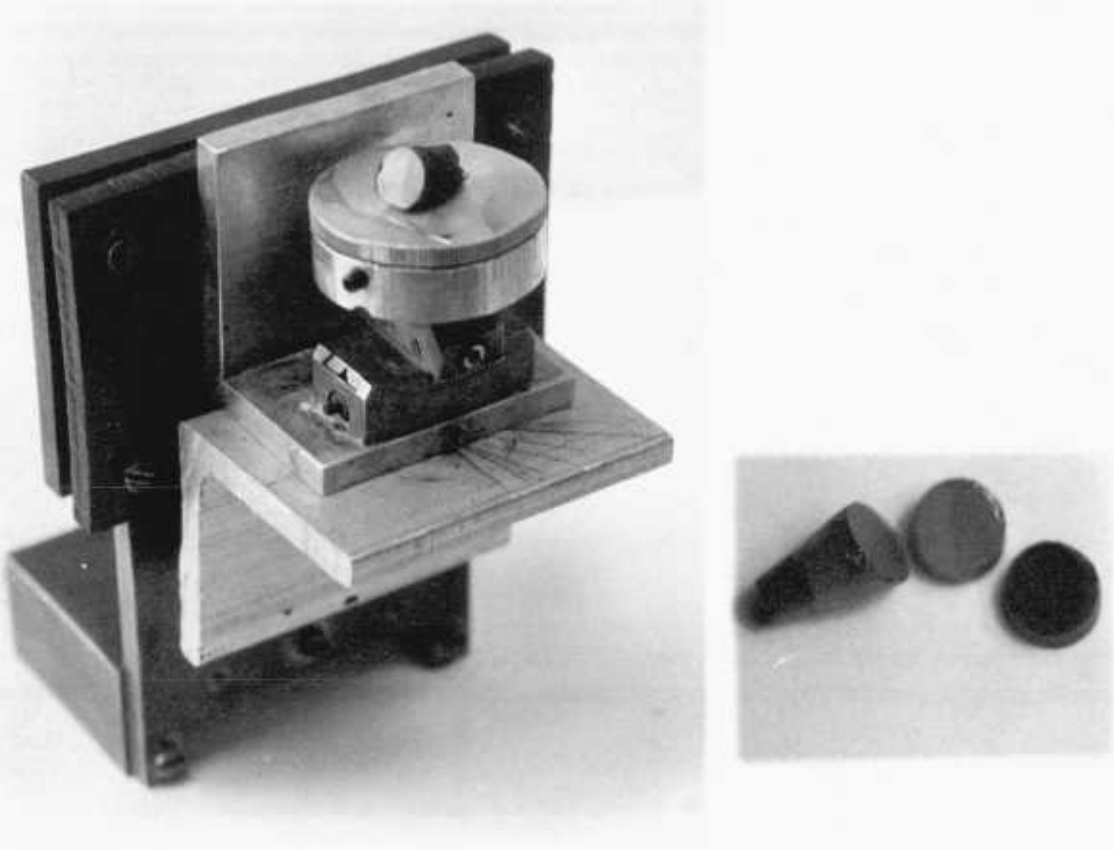


Fig. 4.1 Jig for Cutting Highly Orientated (0001) CdS_xSe_{1-x} Wafers

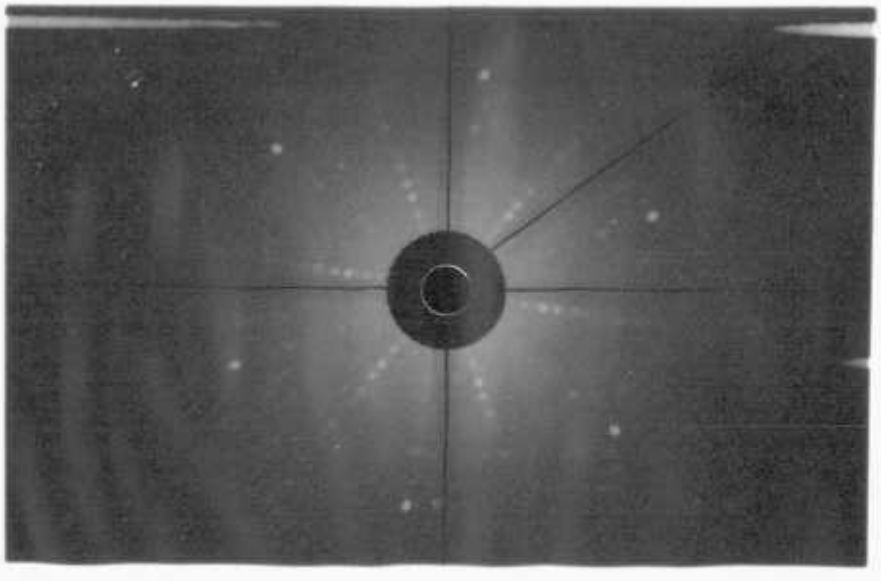


Fig. 4.2 Laue X-Ray Photograph of a CdS_xSe_{1-x} Sample Cut Parallel to Basal Plane

Convenient sized substrates, of area ~ 1 cm^2, and thickness $\simeq$ 2mm were then cut with a silicon carbide disc. The substrates were waxed to a polishing block and further X-ray photographs were taken to determine if any minor adjustments were necessary ($\lesssim 1^\circ$) to re-orientate the substrate into the basal plane. A Laue X-ray photograph of a sample in this orientation is given in Fig. 4.2. Adjustable screws on the polishing jig were used to re-orientate those samples which were off the basal plane.

The substrates were subsequently mechanically lapped and polished with diamond paste to give a $\frac{1}{4}$ micron mirror-like surface.

The samples were then chemically polished to remove surface damage and impurities. Two chemical polishes are normally used for CdS but the one preferred comprised of 4 grams of $K_2 Cr_2 O_7$ dissolved in 50 m.l. orthophosphoric acid at 180°C (Maeda et al, 1967). The chemical polish for the CdSe substrate consisted of 0.5% bromine in methanol at room temperature (Strehlow, 1969). If either of these polishes are used on the alloy crystals, sulphur is precipitated in small lumps over the crystal, leaving a very uneven matt finish on the substrates. These 'polishes' were therefore not suitable for the alloy crystals. A large number of other II-VI and III-V chemical polishes were tried on the alloy crystals and it was seen that the best available chemical polish is a 5 minute treatment in a 50 cc 10% solution of H_2SO_4 with 4 gm. $K_2Cr_2O_7$ at about 90°C, followed by a 15 minute boil in 50% orthophosphoric acid in methanol.

A number of etches are available for identification of the Cd and S or Se faces of CdS and CdSe crystals (Sullivan and Bracht, 1967; Strehlow, 1969) but these etches were not suitable for the alloy crystals because of the sulphur deposited on the crystal by the etchants. It has been shown that heterojunction properties of CdSe grown on Cd or S faces were identical (Perez,1971) and hence it was not necessary to differentiate between the two types of faces when depositing CdSe.

Substrates of these crystals were prepared by the above methods for Hall-effect measurements, Schottky diode and heterojunction diode fabrication. After thorough rinsing in distilled water, they were stored for a very short time in ethyl alcohol before being blown dry with pure nitrogen gas and placed in the sputtering apparatus.

Before growing the CdSe layer, it was very important to remove adsorbed oxygen molecules (which acts as acceptor like surface states to these substrates (see section 3.6)), and other gaseous impurities. Many of the oxygen molecules will be desorbed if the substrate is heated in the vacuum at $\sim 10^{-5}$ torr, at 350°C for 2 hours (Green 1973). It is believed that not all the oxygen atoms were desorbed and it was not possible to remove them.

4.3 Preparation of the CdSe Layer

The sputtering apparatus, originally designed and built by Leveson (1973), was modified to sputter material from a compressed powder CdSe target onto a substrate which could be held at elevated temperatures. The apparatus of Fig. 4.3, shows a Q.V.F. 6/9 Pyrex chamber, consisting of a 9" internal diameter pipe section with two pairs of 6" side-arms projecting orthogornally, which was connected to the high vacuum line via one pipe section, while the top section housed the target assembly. Two orthogonal Helmholtz coils were mounted externally around these pipe sections. The side arms were used to house shutter controls the gas-bleed valve, the gauge units and to load the apparatus with the substrates. The target assembly, illustrated in Fig. 4.4 has a dark-space shield which surrounded the target and which was held at earth potential during sputtering.

The CdSe target 3" in diameter, was obtained from Nordiko. Its purity was better than 5N and its analysis is shown in the Appendix B. It was mounted on a 6" dural backing electrode by means of silver-loaded Araldite. A Eurotherm control unit was used to maintain the substrate

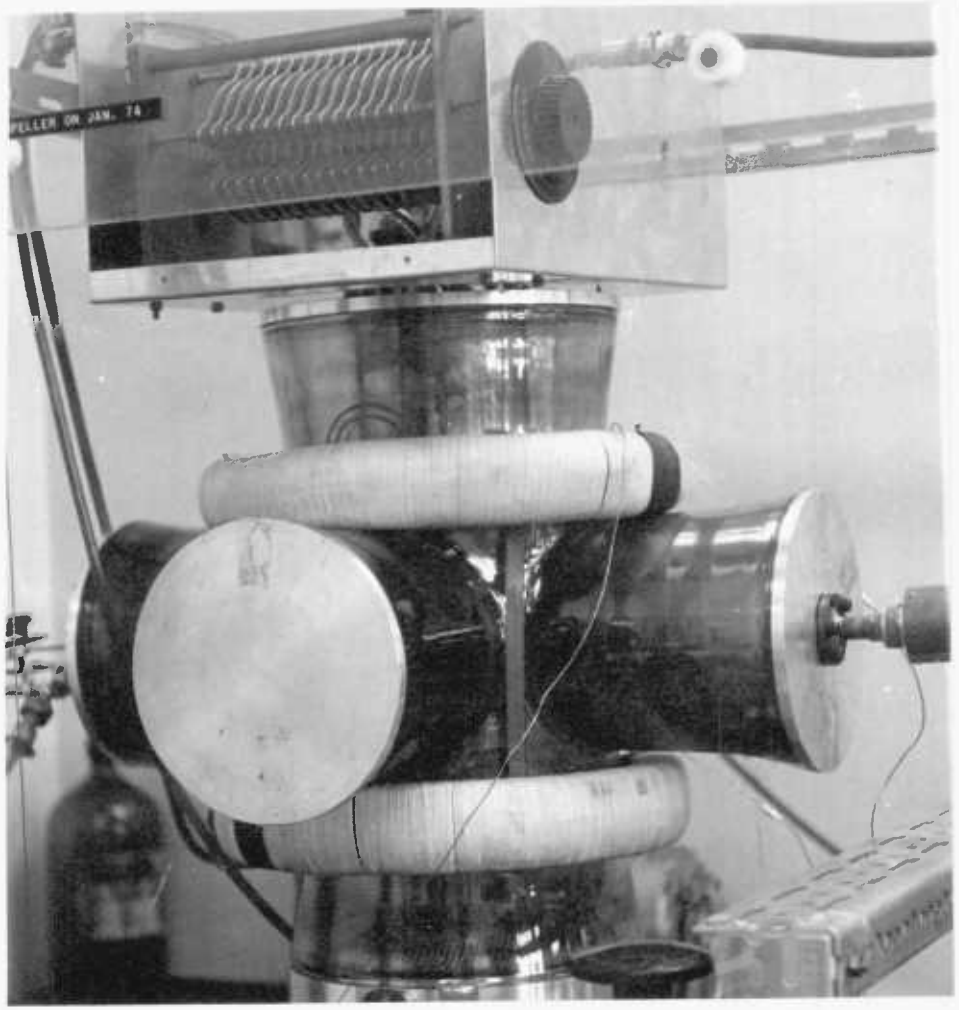


Fig. 4.3 Photograph of Sputtering Equipment

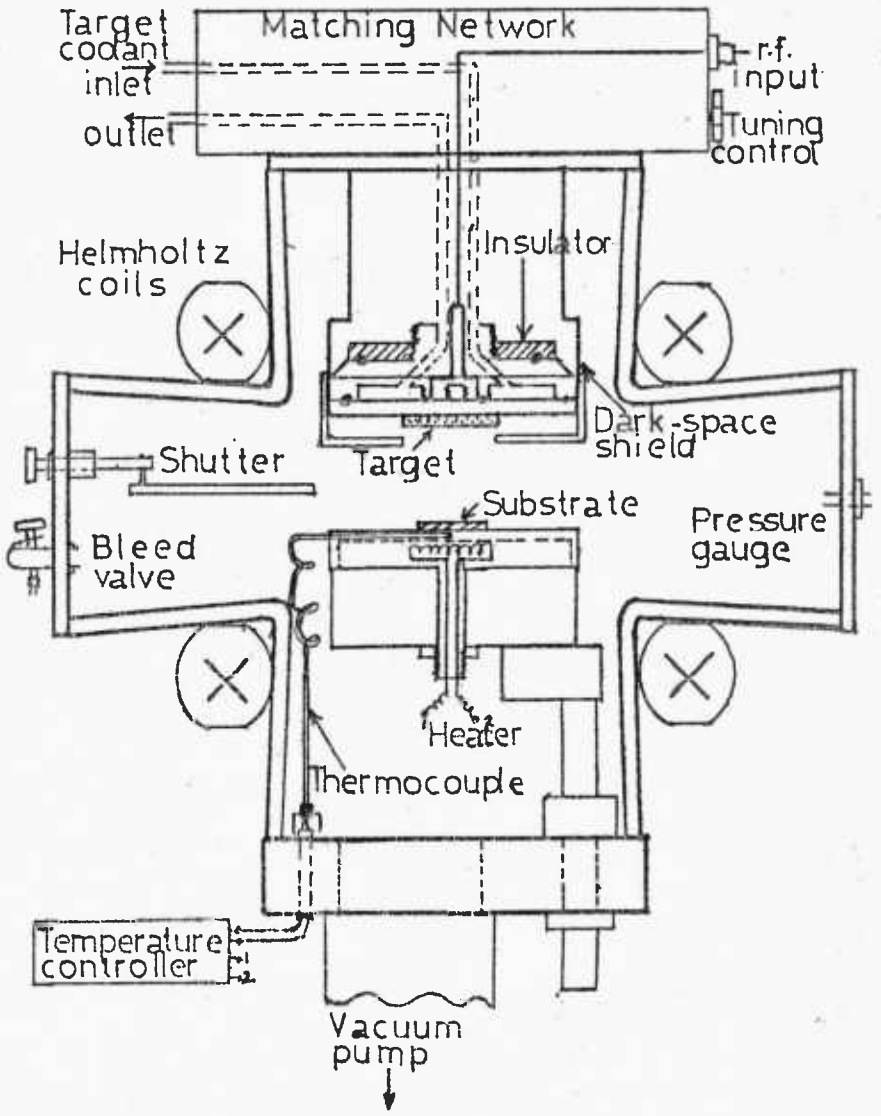


Fig. 4.4 Cross-Section of Sputtering Equipment

table which was heated with a molybdenum heater at the required temperature.

The sputtering gas used in the apparatus was argon; bled into the chanber through a needle valve until the argon pressure was maintained at about 4 microns.

R.F. power at 13.16 MHz produced by an MRC sputtering supply unit was fed to the target electrode through a suitable matching network, to produce the plasma. The matching network illustrated in fig. 4.5 reduces or eliminates the reflected r.f. power. A parallel magnetic field, produced by the Helmholtz coils, enhances the sputtering rate and enables sputtering to be carried out at low pressures. The physical processes occuring in sputtering and application of the method to the production of semiconducting films have been discussed by several workers (e.g. Maissel and Glang, 1970; Davidse, 1967; Davidse and Maissel 1966; Holland and Prestland, 1972; Wosky, 1963). We shall not discuss these matters further here.

The energy distribution of sputtered materials are approximately Maxwellian for bombardment energies of the magnitude 150 - 200 eV. The high energy tail of the distribution does not have sufficient energy to implant ions of Cd, S or Se into the substrate lattice. In fact, the depth of penetration would be less than 500 Å at these voltages.

The variables which affect the overall quality and properties of the sputtered films were optimised so that the grown films were 'sufficiently crystalline' without causing a loss in diode rectification due to grading of the junction. Efforts were made to produce films as stoichiometric as possible with the exclusion of impurities present in the vacuum chamber e.g. water vapour and other residual gases as these are known to alter the electrical properties of semiconducting films. The inclusion of argon atoms in the films is small and does not alter electrical properties of the materials.

The optimum conditions for the sputtering of CdSe layers on CdS and CdS_xSe_{1-x} substrates are as follows:-

Argon gas pressure	=	3 - 5 μm
r.f. power delivered	=	120 watts
substrate temperature	=	350°C
substrate distance from target	=	10 cm

The expected sputtering rate under these conditions was ~ 0.2 - 0.3 um/hr. To reduce the amount of mechanical strain during the cooling cycle (caused by differences in the coefficient of expansion) the initial cooling rate was 20°C/hr. These conditions gave films with average crystallite size 8000 Å (Fig. 3.2 (f)).

Since the work involves the comparison of the different $CdSe/CdS_xSe_{1-x}$ diodes, it was necessary to grow the epi-layer under similar conditions during the production of different types of devices.

Initially CdSe films of ~500 Å thickness were sputtered onto different substrates at various temperatures so that the election microscope could be used to determine the crystalline properties of the film as a function of the fabrication method as discussed previously in paragraph 3.2.1. The films showed good adhesion to the different substrates. However, they could be removed from the various substrates by subjecting the samples to hydroflouric acid fumes followed by immersion in water (the films then floated on the surface of the water).

4.4 The Fabrication of the Heterojunction Device

CdSe layers were sputtered onto the chemically polished CdS_xSe_{1-x} substrates under the conditions described in Section 4.3. A highly reproducible method (a modified form of that used by the author in producing GaAs Gunn Effect Devices, AEI DC 1201/2) was used to fabricate the $CdSe/CdS_xSe_{1-x}$ heterodiodes.

4.4.1 Ohmic Contact to the CdSe Layer and CdS_xSe_{1-x} Substrate

Only a few metals, essentially those with low work-function, form ohmic contacts to CdS and CdSe, as discussed in Section 3.7 Most investigators have used In (m.p. 155°C), Ga (m.p. 29.8°C) or In-Ga alloys to form their ohmic contacts to CdSe. These contacts are indeed ohmic, but they are not mechanically stable and can be wiped off. Also, they melt at low temperatures thereby limiting its role to the low current range to avoid contacts going through the epi-layer. In addition, gold wire cannot be bonded easily to this type of contact.

In the work on ohmic contacts to GaAs tin forms an ohmic contact, Ag, a rectifying contact, but the Sn/Ag alloy, in which Ag acts as support metal, produces an ohmic contact by applying the alloy to the GaAs at a suitable temperature in a hydrogen atmosphere. A similar procedure was used with CdSe and CdS, again with In as the ohmic metal and Au as the support metal. A mixture of approximately 15% In (by wt.) and Au were placed in close proximity in a molybdenum boat and evaporated in an Edward 12E vacuum plant at $\sim 10^{-5}$ torr onto the device. The In/Au mixture melts as the temperature is increased to form an alloy which then slowly evaporates onto the CdSe or CdS substrate. After complete evaporation, the temperature of the boat is increased to heat the contact to make it ohmic. It was not found necessary to use a hydrogen atmosphere during this process. The contacts were initially tested on bulk CdS and CdSe and proved to be ohmic and of low noise.

4.4.2 Top Metallization

A high quality mask (stencil) in which circular windows 0.02" in diameter with a mark to space ratio of 2:1 was used to evaporate a 'top' contact of Au/In of thickness 2000-3000 Å to the CdSe layer.

4.4.3 Back Metallization

The samples with the top contact downwards were mounted by means

of wax onto a 2" square glass plate with 150 μm thick cover glass discs mounted at its corners. The back surfaces were then lapped with 1200 mesh SiC powder until the sample thickness were that of the cover glass discs. After removal from the lapping plate and being thoroughly degreased, In-Au alloy was evaporated over the whole lapped surface to form the back ohmic contact.

4.4.4 Scribing and Dicing

The samples were waxed to cover glass discs which were held on the vacuum chuck of a diamond scriber. After alignment, very fine scribe lines were made with a diamond tool between the circular contacts on the CdSe layer. The samples were removed from the cover glass and waxed to a spring steel plate and were then cleaved on a curved block. Good square chips were obtained, especially when the top contact pattern was made to coincide with a cleaving edge. Damage was confined to the edge of the chips.

4.4.5 Encapsulation

The heterodiode chips were probed with a spring loaded molybdenum whisker held in a micromanipulator making contact to the top Au-In dot while the back surface of the chip was in contact with a gold plated copper plate held at opposite potential to the top contact and the I-V characteristic displayed on a Tektronix 575 curve tracer. An indium preform was placed on the stud of a gold plated diode capsule (ref. No. HA/1228 P Mitronics) held in the heated chuck of a Slee Chip Mounter. When the preform melted, in the presence of forming gas, a heterodiode chip held by suction on a pick-up tube was placed on top of the preform and the capsule was quickly cooled and suction broken. Under the right conditions the chip became rigidly mounted to the capsule. The diodes were again probed to ensure that no degradation occured during this step. The capsule was next placed in the chuck of another Slee equipment for hot wedge wire bonding. 0.001" gold wire was bonded from

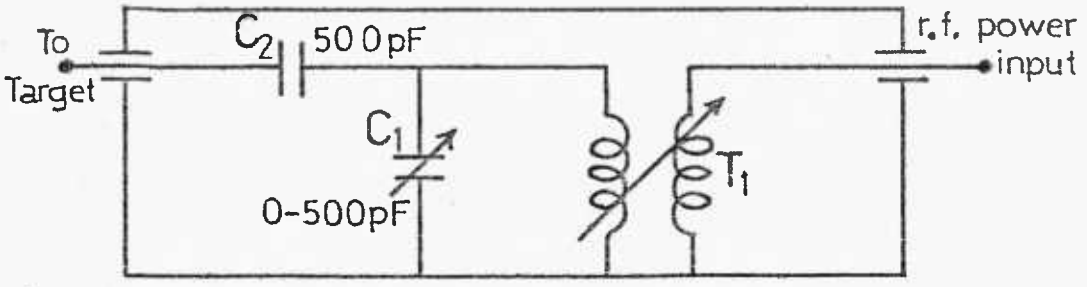


Fig. 4.5 Circuit Diagram of the Matching Network

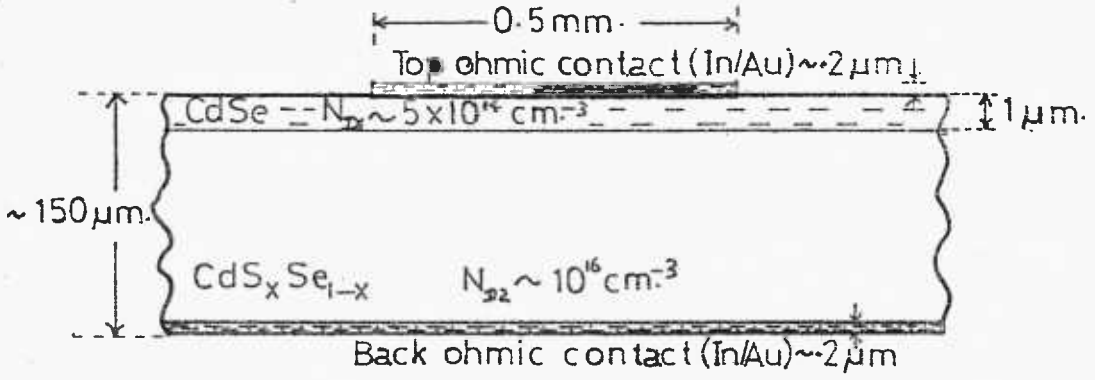


Fig. 4.6(a) Cross-Section of a $CdSe/CdS_xSe_{1-x}$ Diode Chip

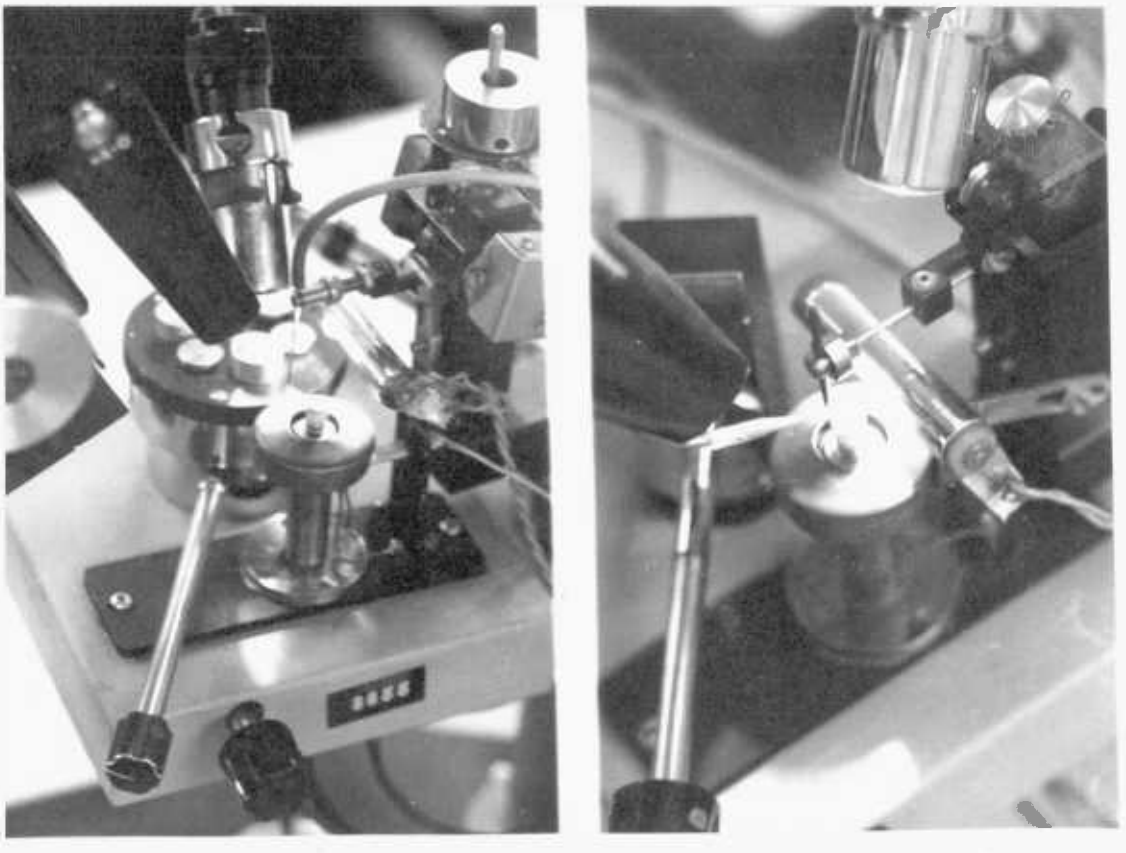


Fig. 4.6 (b) Chip Mounter (c) Wire Bonder

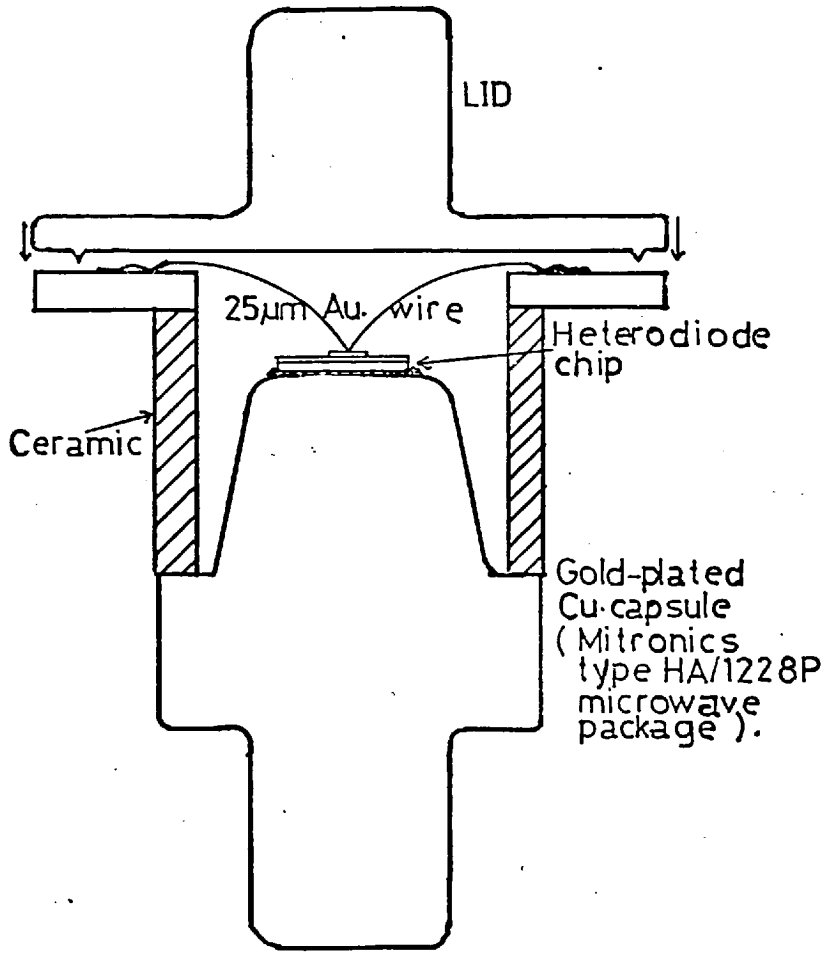


Fig. 4.6(d) The Encapsulated Heterodiode

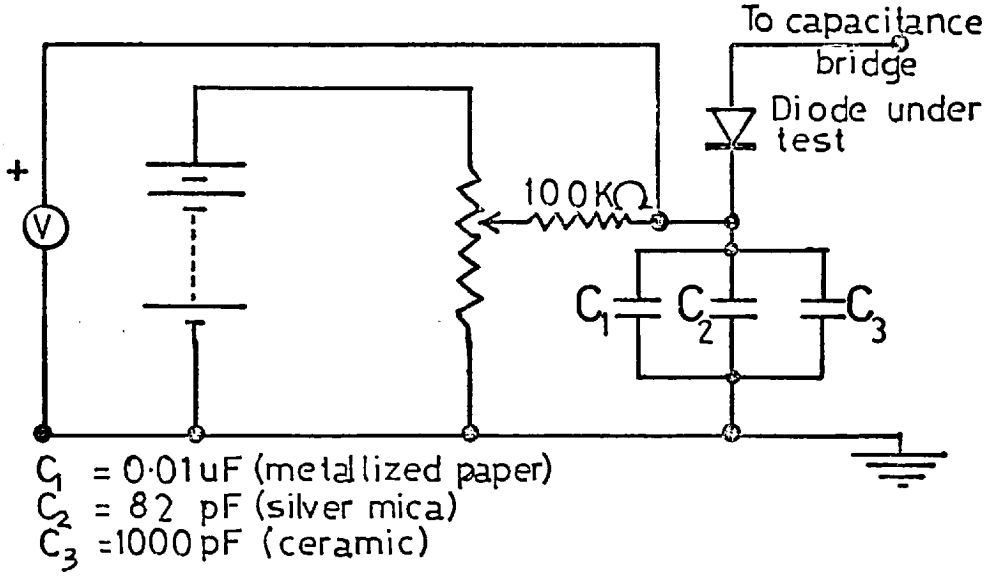


Fig. 4.7 Biasing Circuit for C-V Measurements

the flange of the capsule to the top contact and back to the flange at opposite side as illustrated in Fig. 4.6. (Test probes were initially made after this step to ensure that the thermal compression did not degrade the device). A lid was then spot welded to complete the diode encapsulation.

There were certain advantages to be gained by using the above fabrication technique. Firstly, the In-Au contacts were well defined by evaporating through a mask and diode area were of different devices to within 5% of each other. The alloy does not melt below about 430°C so that diodes could be run at relatively higher temperatures (than devices with In contacts) without fear of destruction of the epi-layer. By thinning the substrate, series resistance could be greatly reduced together with the mounting provides an adequate heat sink to enable higher currents to be used since the heated region is close to the stud.

4.5 Electrical Measurements

The current-voltage characteristics of all $CdSe/CdS_xSe_{1-x}$ heterodiodes were measured in the dark for temperatures in the range 185°K to 330°K using a digital voltmeter and a Keithley instrument 601 B electrometer to measure voltage and current respectively. (The forward conductance was only slightly increased under illumination with a 6V/30W tungsten lamp) (times 6 at low bias and times 2 at high bias).

The junction capacitance of the heterodiodes as a function of reverse bias voltage (and very small positive bias) was measured at frequencies in the range 1.6 KHz to 1 MHz on Wayne Kerr capacitance bridges B221 and B601 and on a Boonton capacitance bridge (75B - S8) (with interial bias for 1 MHz measurements). The biasing circuit used for measurements on the Wayne Kerr bridges is illustrated in fig. 4.7. The level of the a.c. signals on the Wayne Kerr bridges was $\simeq$ 15 mV while that on the Boonton bridge was 12mV.

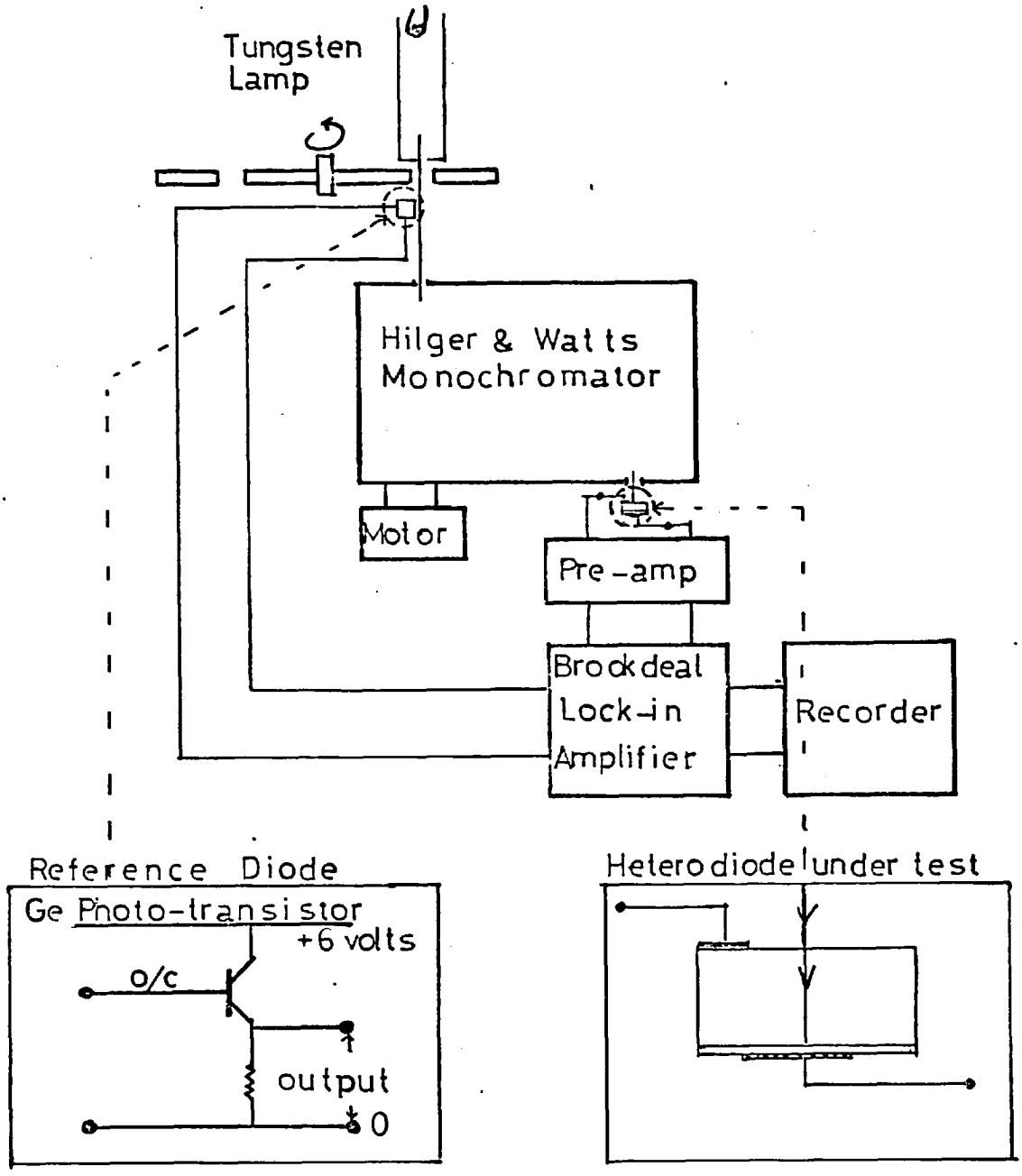


Fig. 4.8 Arrangement Used in PhotoVoltaic Spectral Response Measurements of Heterodiodes

The photovoltaic spectral photoresponse was obtained in the following way:-

White light from a tungsten lamp was chopped at 20 Hz before being fed into the Hilger and Watts Monochromator and also a photo-transistor using the experimental arrangement shown in Fig. 4.8. The chopped mono-chromatic light was focused onto the polished surface of the wide-gap material (substrate) and the photovoltage produced was amplified by the Brookdeal phase lock amplifier FL355 using the photo-transistor signal as reference. The Brookdeal meter unit MS 320 was used to provide a d.c. output which was recorded on a chart recorder. The monochromator could be driven over the required wave length range.

REFERENCES - CHAPTER 4

Davidse, P. D. (1967) Vacuum 17, 139

Davidse, P. D., Maissel, L. I. (1966) J. Appl. Phys. 37, 574

Green, M. (1973) Private Communication, Imperial College, Univ. of London.

Holland, L., Priestland, C. R. D. (1972) Vacuum, 22, 133.

Leveson, R. (1973) Ph.D. Thesis, Univ. of London.

Maissel, L. I., Glang, R. (1970) Handbook of Thin Film Technology, McGraw-Hill

Maeda, M., Dorken, M., Fukui, H. (1967) Jap. J. Appl. Phys. 6, 652.

Perez, E. J. (1972) Ph.D. Thesis, Univ. of London.

Strehlow, W. H. (1969) J. Appl. Phys. 40, 2928.

Sullivan, M. V., Bracht, W. R. (1967) J. Electrochem. Soc. 114, 295

Wolsky, S. P. (1963) Trans. 10th Nat. Vac. Symp., p-309, Macmillan Co. N.Y.

CHAPTER 5 - THEORY OF ISOTYPE HETEROJUNCTION

5.1 Introduction

The heterojunction has been defined as the electrical contact between two different mono-crystalline semiconductor crystals having different band profiles and their properties arise solely from the interaction of charge carriers at the interface because of discontinuities in the material parameters.

A survey on the development of the heterojunction theory has been presented in Chapter 1 and it was seen that the simple models could not explain all experimental characteristics. As a result, a number of hypotheses have been made in order to remove the discrepancies between observed and predicted heterojunction properties. Theory has been divided into abrupt and graded heterojunctions, the former dealing with instantaneous transition (including transitions over a few atomic distances) in traversing the interface and the latter concerns transport through the junction of continuously varying compositions of the two constituent. Interface states, arising mainly from lattice and thermal mismatches between the two bulk materials modify these theories as they act as recombination centres of large cross-section, thus greatly affecting the transport of carriers across the junction. A study of these theories will be offered in this chapter dealing with n-n structures although it can be transfered to p-p structures.

The most important charge carrier transport mechanisms especially those applying to the CdSe/CdS_xSe_{1-x} structures will be dealt with, as well as energy-band profiles and capacitive effects. A brief mention will be made of the photo-response behaviour.

5.2 Theoretical Band Profile and Junction Capacitance

The band profiles are important in heterojunction studies as they describe the electronic properties of the discontinuities at the interface

resulting from intimate contact. The charge and potential distributions at the interface relate to the diode capacitance and built-in voltage and may suggest possible transport mechanisms of the charge carriers across this region.

The relevant parameters in constructing the band profiles are the band-gap, E_G, dielectric constant, ϵ, electron affinity, χ (defined as the energy required to remove an electron from the bottom of the conduction band, E_C, to the vacuum level), the work-function, ϕ_W (defined as the difference between Fermi level and vacuum level, which unlike χ, depends on the semiconductor resistivity).

For heterojunction pairs in which lattice mismatch is small ($< 1\%$), the band profile can easily be constructed from a knowledge of the quantities listed above. However, for pairs in which lattice mismatch is $> 1\%$, or the junction is graded, the band profile deviates from this idealized situation and becomes difficult to construct accurately. In the case of large lattice mismatches, monopoles, dipoles or both may arise at the interface due to ionized states, the magnitude of these charge layers determining the degree of deviation from the idealized case. The effect of grading on the junction will affect the shape of the band profiles since the discontinuous variables of the abrupt case become continuous functions of distance and, as a result, the height of the rectifying barrier is diminished.

The exact shape of the band profile, hence the expression for junction capacitance, is obtained by solving Poisson's equation for the space-charge regions near the junction. It should be noted, however, that this equation cannot be solved analytically though numerical solutions have been obtained. Both Czerveny (1968) and Kumar (1968) have solved the Poisson's equation for the abrupt case and Oldham and Milnes (1963) for the graded case. The theory will be

presented along the lines of their work.

5.2.1 Abrupt Model Without Interface States

Fig. 1.2 (a) shows the flat band structures of the two isolated semiconductors without surface states prior to being brought together into intimate contact. When contact is established, the Fermi level, E_F, is constant through the whole system and the vacuum level is no longer common to both materials. A typical equilibrum band profile of an abrupt n-n heterojunction without interface states is illustrated in fig. 1.2 (b). In this ideal model, the lattices are so similar that no charge is developed at the interface and the lattice is continuous. The electric displacement, D, and the electrostatic potential, ϕ, are continuous across the interface, but conduction and valence band edges are discontinuous. These discontinuities may be smeared out over a few atomic distances, but transitions are still considered instantaneous.

Because of the work function difference, the equalization of the Fermi level results in a flow of electrons from the lower work-function material, S2, to the other S1, to establish equilibrum. This electron displacement at the interface corresponds to the formation of an accumulation region in S1, characterised by a bending down of band edges by an amount $q V_{D1}$, and a depletion region in S2 with a bending up of the bands by an amount qV_{D2}.

The total built-in voltage, V_D, is hence given by the difference in the work function of the two materials and equals the sum of the partial built in voltages supported by each material. From the diagram, it is given by the sum of the electron affinity, χ, and the difference between the Fermi level and the bottom of the conduction band = δ

i.e.

$$\phi_W = \chi + \delta \tag{5.1}$$

hence the built-in voltage is

$$V_D = V_{D1} + V_{D2} = \frac{1}{q} (\phi_{W1} - \phi_{W2}) = \frac{1}{q} (\Delta E_C - \Delta\delta) \tag{5.2}$$

where ϕ_{W1} and ϕ_{W2} are the work functions of S1 and S2 respectively.

The conduction band and valence band are discontinuous by amounts ΔE_C and ΔE_V, respectively. ΔE_C is simply the difference in the electron affinities of the two materials.

i.e.

$$\Delta E_C = \chi_1 - \chi_2 \tag{5.3}$$

and
$$\Delta E_V = (E_{G1} - E_{G2}) + (\chi_1 - \chi_2)$$
$$= \Delta E_G - \Delta E_C \tag{5.4}$$

where

$$\Delta E_G = (E_{G1} - E_{G2})$$

$$\therefore \quad \Delta E_C + \Delta E_V = \Delta E_G \tag{5.4b}$$

Also, by making use of Boltzmann statistics

$n = N_C \exp \frac{E_C - E_F}{kT}$ and assuming complete ionization, $n = N_D$, the diffusion potential may be expressed as

$$qV_D = \Delta E_C - kT \ln \left(\frac{N_{C2} \ N_{D1}}{N_{C1} \ N_{D2}} \right) \tag{5.5}$$

where N_{D1} and N_{D2} are the donor concentration and N_{C1} and N_{C2} are the effective density of states in the conduction band in materials S1 and S2 respectively.

Having obtained the fundamental parameters at the interface, some knowledge of the variation of the electrostatic potentials away from the interface is desirable. This can be obtained from the solution of the Poisson's equation, making use of the above variables for boundary conditions.

The most general form of the 1-D Poisson's equation is

$$\epsilon(x)\frac{d^2\psi}{dx^2} + \frac{d\psi}{dx}\quad\frac{d\epsilon(x)}{dx} + \rho(x) = 0 \qquad (5.6)$$

where ψ is the normalized electrostatic potential, ρ is the space-charge and is given by

$$\rho = q\left(N_D^+ - n^- - N_A^- + p^+\right)$$

N_D^+ , N_A^- are the ionized donors and acceptors and n^- and p^+ are the carrier concentrations.

At this point it is necessary to make simplifying assumptions in order to solve Poisson's equation. These are:

(a) Acceptor and hole concentrations are negligible in an n-n system.

(b) The impurities are fully ionized i.e. $N_D^+ = N_D$

(c) Non-degenerate statistics i.e. Boltzmann statistics are applicable.

Equation (5.6) is now simplified as

$$\epsilon\frac{d^2\psi}{dx^2} = -\rho(x) \qquad (5.7)$$

and $$\rho(x) = -q\,(N_D - n) \qquad (5.8$$

is the space charge existing in an accumulation layer in S1 and a depletion layer in S2.

In this abrupt model, the parameter χ, N_D, E_G, ϵ and m^* are assumed constant in one material and then charge over instantaneously to the values in the other material at the interface.

Solutions will be attempted first for the accumulation layer. Here, the electron distribution is

$$n = N_C \exp \frac{E_F - E_C}{kT} \tag{5.9}$$

Equation (5.8) now becomes

$$\rho = q \left(N_D - N_C \exp \frac{E_F - E_C}{RT} \right) \tag{5.10}$$

substituting this expression in the Poisson's equation

$$\frac{d^2\psi}{dx^2} = \frac{qN_D}{\epsilon} \left(\frac{N_C}{N_D} \exp \frac{E_F - E_C}{kT} - 1 \right) \cdot \tag{5.11}$$

$$\text{Let} \quad \xi = \frac{E_F - E_C}{kT} - \ln \frac{N_{D1}}{N_{C1}} \tag{5.12}$$

where ξ therefore represents the departure of E_C from the bulk level of S1 i.e. $\xi = 0$ in the bulk and equals ξ_t in the bulk of S2, as in fig. 5.1.

Equation (5.11) is therefore

$$\frac{d^2\psi}{dx^2} = \frac{qN_D}{\epsilon} (1 - e^{\xi}) \tag{5.13}$$

relating E_C to ψ by the expression

$$E_C = -q\psi - \chi$$

and normalizing electron affinity, distance and differences in conduction band as

$$X = \frac{\chi}{KT} \quad , \quad Z = \frac{x}{L_D} \quad , \quad \Delta\xi_C = \frac{\Delta E_C}{kT}$$

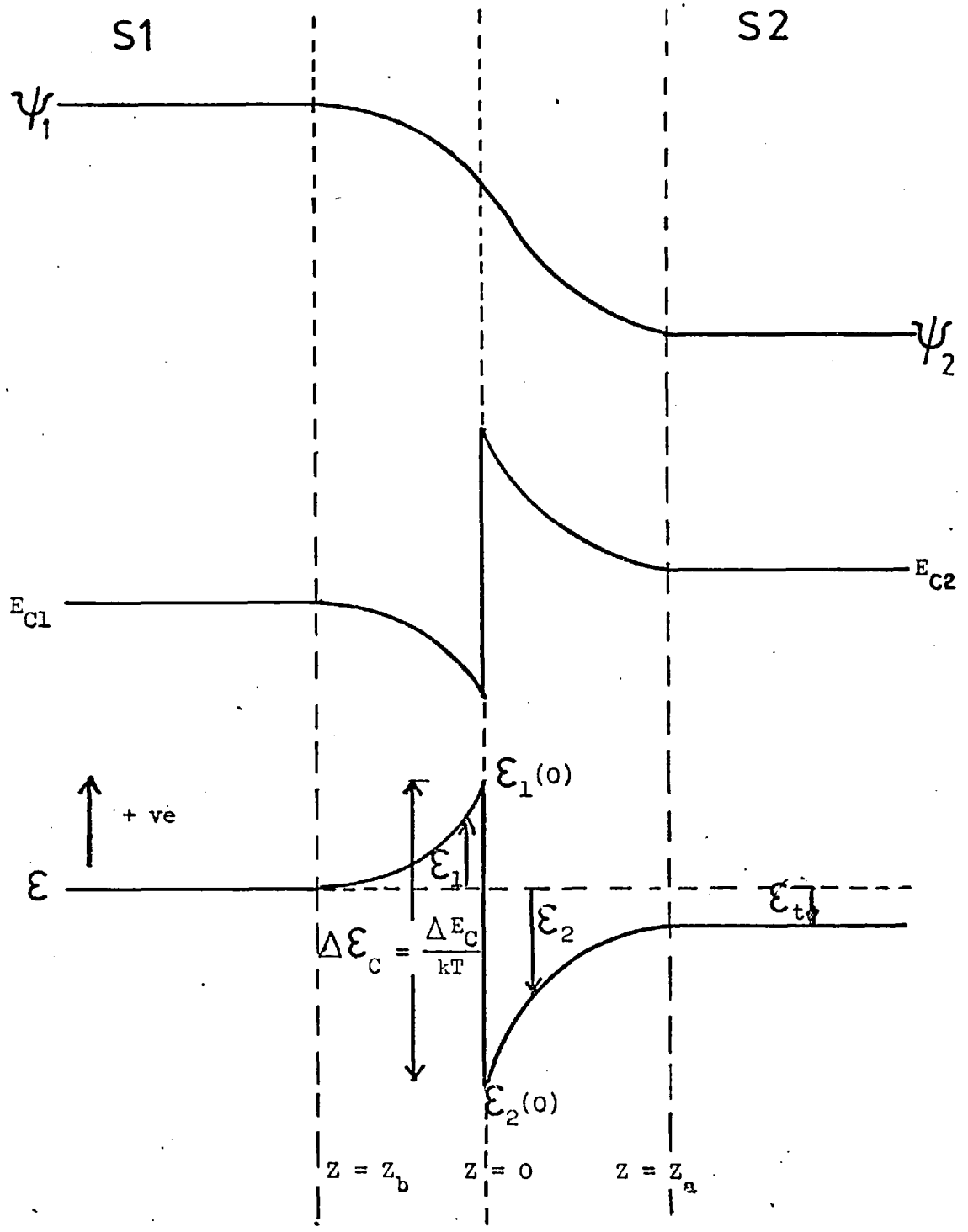


Fig. 5.1 Variation of ψ, E_C and $\mathcal{E}$ across the Heterojunction Interface.

where L_D is the Debye length given by $L_D = \left(\frac{kT\epsilon}{q^2 N_D}\right)^{\frac{1}{2}}$

One obtains $\frac{d^2\mathcal{E}}{dx^2} = \frac{dp}{dz} = \frac{dp}{d\mathcal{E}} \frac{d\mathcal{E}}{dz} = p \frac{dp}{d\mathcal{E}}$

where $p = \frac{d\mathcal{E}}{dz}$

From equation (5.13), $p \frac{dp}{d\mathcal{E}} = 1 - e^{\mathcal{E}}$

or $pdp = (1 - e^{\mathcal{E}})\, d\mathcal{E}$

Integrating $\frac{1}{2}p^2 = (\mathcal{E} - e^{\mathcal{E}}) + C$

Now for S1 at $Z = -\infty$ (i.e. in the bulk), $\mathcal{E} = 0$, $p = 0$

$C = 1$

$$\therefore \quad p^2 = 2\,(e^{\mathcal{E}} - \mathcal{E} - 1)$$

i.e for S1 $$\frac{d\mathcal{E}_1}{dz} = \sqrt{2\,(e^{\mathcal{E}_1} - \mathcal{E}_1 - 1)} \qquad (5.14a)$$

or $$\int_{\mathcal{E}_1}^{\mathcal{E}_1(0)} (e^{\mathcal{E}_1} - \mathcal{E}_1 - 1)^{-\frac{1}{2}}\, d\mathcal{E} = Zo - Z \qquad (5.14b)$$

This integral can only be evaluated numerically e.g. for a given value of $\mathcal{E}_1(0)\left(\equiv\frac{qV_{D1}}{kT}\right)$, the part of the potential appearing acorss S1 at Z = 0 (fig. 5.1).

Applying a similar treatment to the depletion layer of S2, where $Z>0$ and puting $\mathcal{E}_2 = \mathcal{E}_t$ in the bulk gives

$$\frac{d\mathcal{E}_2}{dz} = \sqrt{2\left(e^{(\mathcal{E}_2 - \mathcal{E}_t)} - (\mathcal{E}_2 - \mathcal{E}_t) - 1\right)} \qquad (5.15)$$

where ξ_t represents the difference in the bulk value of E_C of the two materials at thermal equilibrum. $\xi_2(0) - \xi_t$ is the potential appearing across the depletion layer of S2 at $z = 0$. Note $V_{D1} + V_{D2} = V_D = \frac{kT}{q}(\xi_t(0) - \Delta\xi_C)$ is the total built in potential of the heterodiode.

The variation of potential in S1 with distance from the interface is shown in fig. 5.2 after Kumar where $\xi_1(0)$ is given a typical value of 3. The width of the transition layer should be obtained by setting $\xi_1 = 0$ in equation (5.14b), but the integral diverges indicating there is no sharp edge. However, Kumar has shown that most of the space-charge is confined to within $3L_D$ of the interface (see later).

Introducing boundary conditions in order to solve the integral (5.14b), that the conduction band edge is discontinuous by amount ΔE_C, and the normal component of dielectric displacement, D_1 is continuous across the interface.

i.e.
$$\xi_1(0) = \xi_2(0) + \Delta\xi_C$$
$$\epsilon_1 \left.\frac{d\xi_1}{dz}\right|_{z=0} = \epsilon_2 \left.\frac{d\xi_2}{dz}\right|_{z=0} \qquad (5.16)$$

then
$$\frac{e^{\xi_1(0)} - \xi_1(0) - 1}{e^{(\xi_2(0) - \xi_t)} - (\xi_2(0) - \xi_t) - 1} = \frac{\epsilon_2 N_{D2}}{\epsilon_1 N_{D1}} = K \qquad (5.17)$$

The parameter K represents different doping ratios.

On the application of an external voltage, V, let V_1 be supported by S1 while V_2 is supported by S2 such that $V = V_1 + V_2$. Under these quasi-equilibrum conditions, $\xi_1(0)$ and $\xi_2(0)$ in equation (5.17) now represent the contact potential plus external voltage supported by S1 and S2 respectively.

It is possible to obtain a value for V_{D1} and since V_D is given by the expression (5.5) rearranged as

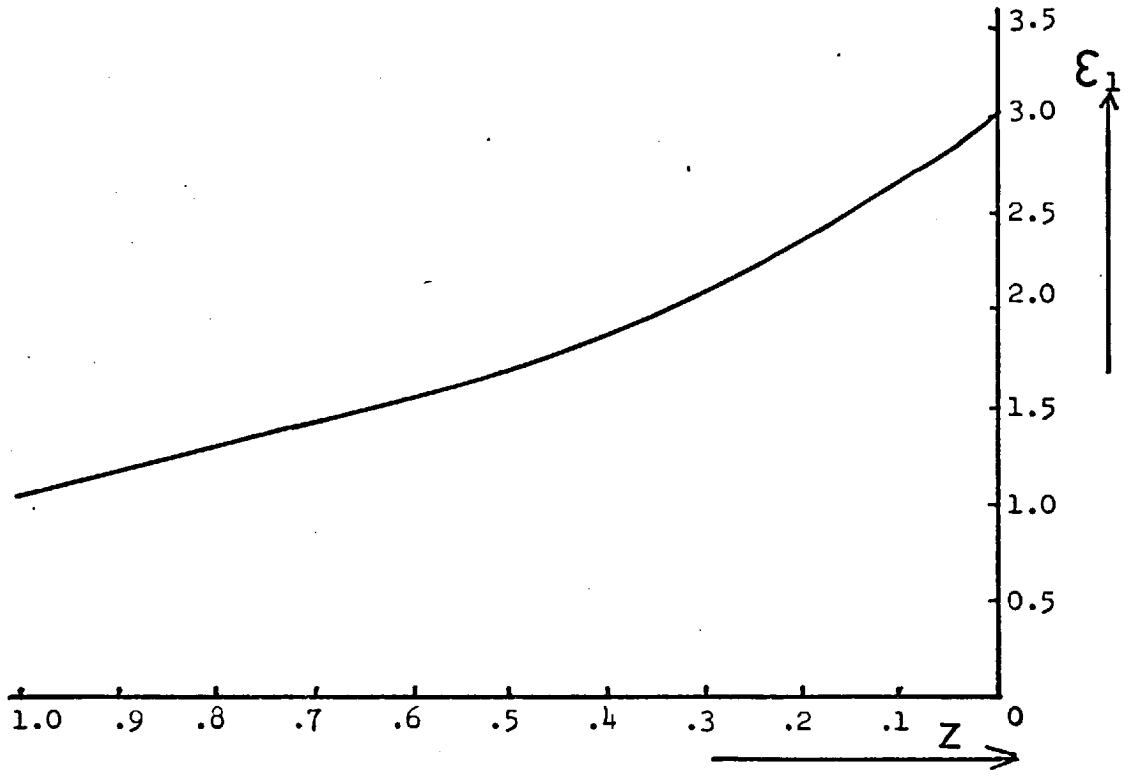


Fig. 5.2 Variation of Potential $\mathcal{E}_1$ in S1 with distance from the Interface (After Kumar,1968).

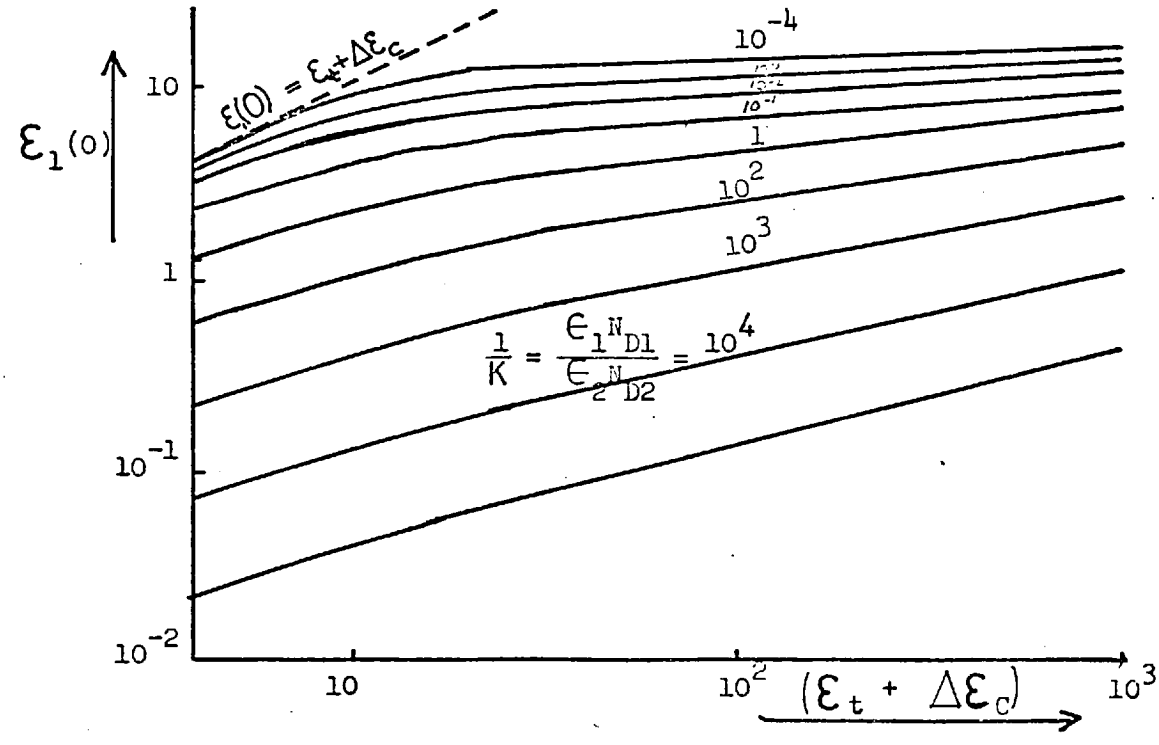


Fig. 5.3 Variation of Potential $\mathcal{E}_1(0)$ Across the Accumulation Region with Total Potential Drop $(\mathcal{E}_t + \Delta\mathcal{E}_c)$, $\frac{1}{K}$ being Parameter (Solution of Equation 5-19, after Czerveny, 1968)

$$\frac{qV_D}{kT} = \Delta\mathcal{E}_C + \ln\left[\frac{N_{D2}}{N_{D1}}\left(\frac{m_1^*}{m_2^*}\right)^{\frac{3}{2}}\right] \qquad (5.18)$$

then V_{D2} can also be determined.

At thermal equilibrum if $\epsilon_1 N_{D1} \gg \epsilon_2 N_{D2}$, then most of the electrostatic potential appears across S2 i.e. $\mathcal{E}_1(0) = 0$; this is identical to the case of a rectifying metal-semiconductor or Schottky contact. If however, $\epsilon_1 N_{D1} \ll \epsilon_2 N_{D2}$, then the value of V_{D1} $(\mathcal{E}_1(0))$ approaches that of V_D $(\equiv \mathcal{E}_t)$ except for large reverse bias when the value $\mathcal{E}_t - \mathcal{E}_1(0) + \Delta\mathcal{E}_C$ becomes much larger than $\mathcal{E}_1(0)$, across the accumulation layer. Fig. 5.3 represents the temperature independent solutions of Czerveny for equation (5.17) for $\mathcal{E}_1(0)$ across the potential represented by $(\mathcal{E}_t + \Delta\mathcal{E}_C)$ for different doping ratios, K . $(\mathcal{E}_t + \Delta\mathcal{E}_C)$ ranges from a thermal equilibrum value of -0.1 to -10^3, corresponding to a reverse bias of 25 volts, while K ranges from 10^4 to 10^{-4}. For a given heterojunction pair, the parameter K is fixed, thereby fixing a value of $\mathcal{E}_t$.

$$\text{The total space-charge} = \int_{-\infty}^{0} q\left[N_{D1} - n(z)\right] dz \qquad (5.19)$$

$$= q N_{D1} \left(e^{\mathcal{E}_1(0)} - \mathcal{E}_1(0) - 1\right)^{\frac{1}{2}}$$

$$\text{Now, } \frac{\text{total space charge between } Z=0 \text{ and } Z}{\text{total space charge}} = 1 - \left(\frac{e^{\mathcal{E}_1} - \mathcal{E}_1 - 1}{e^{\mathcal{E}_1(0)} - \mathcal{E}_1(0) - 1}\right)^{\frac{1}{2}}$$

$$\simeq \left(1 - \frac{\mathcal{E}_1}{\mathcal{E}_1(0)}\right) \quad \text{for small } \mathcal{E}_o$$

$$\simeq \quad 1 - e^{+\sqrt{2}z} \qquad (5.20)$$

where the integral (5.14b) has been evaluated by Kumar as $\frac{1}{\sqrt{2}} \frac{\varepsilon_1(0)}{\varepsilon_1}$

A plot of equation (5.20) shows that 98% of the space-charge is confined to within $3L_D$ of the interface, illustrated in fig. 5.4 after Kumar. Hence, a measure of the accumulation width can be found. The depletion width is found by a method similar to homojunctions i.e. $N_{D2} \cdot X_{dep.}$ = total space-charge.

A useful computer technique for obtaining numerical solutions of the transition layers for semiconductors with doping levels of 10^{14} - 10^{16} cm^{-3} has been proposed by Hampshire et al (1968), who started with the Poisson's equation (considering Fermi statistics) in terms of the energy of the bottom of the Conduction band, E_C.

$$\epsilon \frac{d^2E_C}{dx^2} = q^2 n_D - \int_{E_C}^{\infty} \frac{q^2 N(E)dE}{\exp\left(\frac{E-E_F}{kT}\right) + 1} \qquad (5.21)$$

where n_D is the density of ionized donors, given by

$$n_D = \frac{N_D}{1 + \frac{1}{2}\exp\left(\frac{E_D - E_F}{kT}\right)}$$

E_D being the ionization energy of the donor level. In the depletion layer, for the doping levels in consideration, n_D is accurate to 0.05% of N_D; in the accumulation layer, although n_D varies slightly more with x near the interface, the electron density at that point is very high.

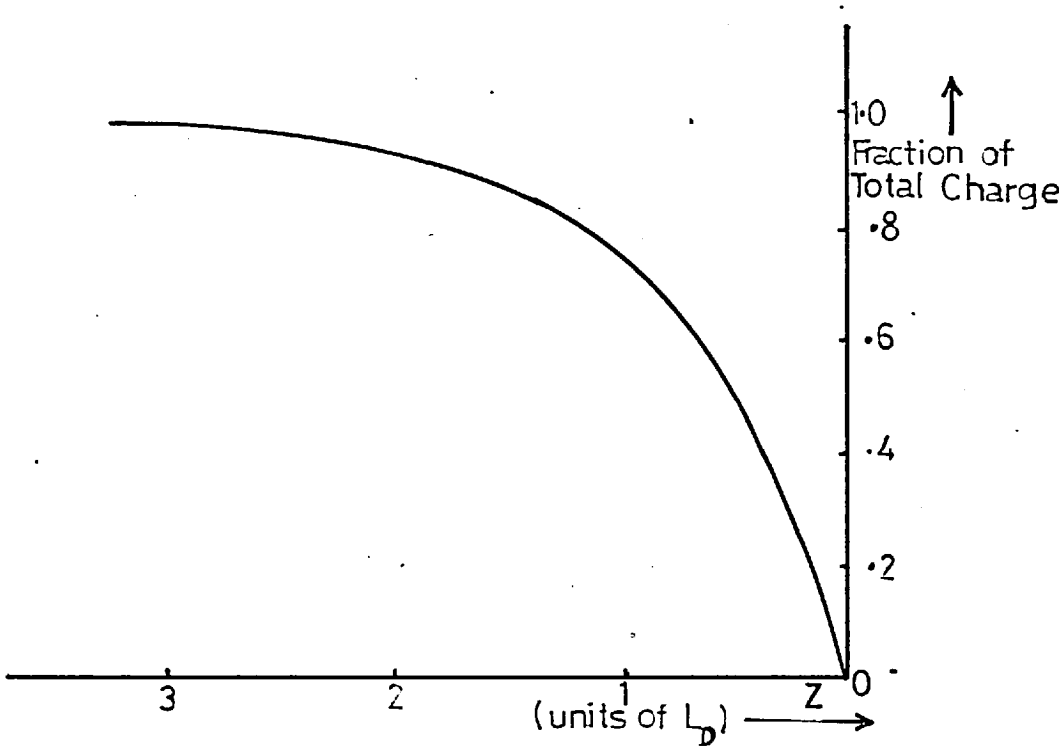


Fig. 5.4 Space-Charge Distribution in S1 (After Kumar, 1968)

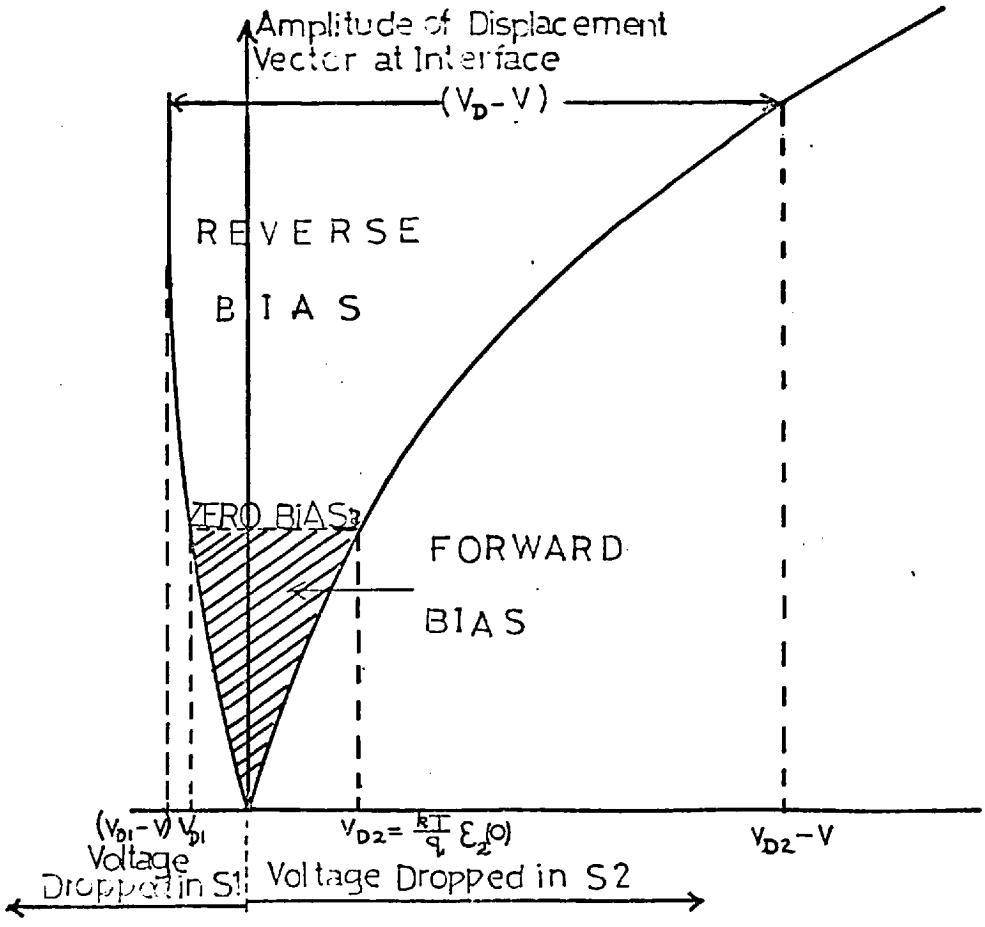


Fig. 5.5 Computer Solution for the Voltage Variation Across Heterojunction (After Hampshire, 1968)

Hence it can be assumed again that $n_D = N_D$ under these conditions. The integral term in equation (5.21) is the product of density of state and Fermi occupation function, and so represents the number of free carrier present.

Using the Ehrenberg approximation (Blakemore, 1962) for the Fermi function integral, the equation is reduced to

$$\frac{d^2E_C}{dx^2} = A - \frac{B}{1 - C \exp \xi_C} \qquad (5.22)$$

where E_C is defined as zero in the bulk of both S1 and S2, $\xi_C =$

$$\frac{E_C}{kT}, \quad A = \frac{q^2N_D}{kT\epsilon} = \frac{1}{L_D^2}, \quad B = \frac{4N_Cq^2}{kT\epsilon} \quad C = \frac{4N_C}{N_D}$$

In solving this equation, a numerical method is applied with boundary conditions of the continuity of the normal component of displacement Vector, D. The result is illustrated in fig. 5.5, where D is plotted against the electrostatic potential variation in the transition layers. At zero bias, a horizontal line of length, V_D, is drawn between the two curves, and the shaded area between these curves and this line represents forward bias, while that above the line represents reverse vias. Any horizontal line bisects the curves, whose separation is V_D-V, where V is the applied voltage, gives the fraction of total voltage supported on either side of the interface. The diagram shows that almost all of the negative applied voltage occurs in the depletion layer of S2. These results were obtained under quasi-equilibrum conditions, but in forward bias, a considerable number of carriers may be injected, thereby changing the concentration in the transition layers. The solution then

is not strictly valid under forward bias greater than a few tenths of a volt.

The Junction Capacitance

The current flow through the transition layers is normally considered as comprising of a conduction and a displacement or capacitive component. At increasing reverse bias, electrons accumulate near Z = 0 in S1 and are depleted further from the space charge layer in S2, thereby increasing its width. Since in the depletion layer there are few carriers to cause conduction, the change of space-charge is due solely to the displacement component.

The charge per unit area in the depletion layer is

$$Q = \epsilon_2 \frac{dV_2}{dx} = \frac{\epsilon_2}{q} \frac{d(E_C - E_F)}{dx}$$

$$= \frac{\epsilon_2}{L_{D2}} \frac{kT}{q} \frac{d\mathcal{E}_z}{dz}\Big|_{Z=0} \qquad (5.23)$$

$$\text{from equation (5.15)} = \frac{\epsilon_2}{L_{D2}} \frac{kT}{q} \sqrt{2e^{(\mathcal{E}_2(0)-\mathcal{E}_t)} - (\mathcal{E}_2(0)-\mathcal{E}_t) - 1}$$

However, the exponential term may be neglected as being small compared with $(\mathcal{E}_t - \mathcal{E}_2(0) - 1)$

$$Q = \frac{\sqrt{2}\,\epsilon_2}{L_D} (\mathcal{E}_t - \mathcal{E}_2(0) - 1)^{\frac{1}{2}}$$

The junction capacitance, C, per unit area is defined as

$$C = \frac{dQ}{dV} = \frac{dQ}{d\mathcal{E}_t} \cdot \frac{q}{kT}$$

$$= \frac{\sqrt{2}\,\epsilon}{2\,L_{D2}} \qquad \frac{\left(1 - \frac{d\mathcal{E}_2(0)}{d\mathcal{E}_t}\right)}{\left(\mathcal{E}_t - \mathcal{E}_2(0) - 1\right)^{\frac{1}{2}}}$$

$$= \frac{\epsilon_2}{\sqrt{2}\,L_{D2}} \qquad \frac{\left(1 - \sqrt{\frac{1}{\mathcal{E}_t - \mathcal{E}_2(0)\left(1 - \frac{\epsilon_2 N_{D1}}{\epsilon_2 N_{D2}}\right)}}\right)}{\left(\mathcal{E}_t - \mathcal{E}_2(0) - 1\right)^{\frac{1}{2}}}$$

rearranging, $$C^{-2} = \frac{2\,L_{D2}^2}{\epsilon_2^2} \frac{\left(\mathcal{E}_t - \mathcal{E}_2(0) - 1\right)}{\left[1 - \frac{1}{\mathcal{E}_t - \mathcal{E}_2(0)\left(1 - \frac{1^{N_{D1}}}{2^{N_{D2}}}\right)}\right]^2} \qquad (5.24)$$

The above equation has been solved graphically by Czerveny (fig. 5.6) for C^{-2} as a function of the total normalized potential $(\mathcal{E}_t + \Delta\mathcal{E}_C)$ with K as parameter. (Note that $\mathcal{E}_t$ has already been defined to include the amount, $\Delta\mathcal{E}_C$, so the quantity $(\mathcal{E}_t - \Delta\mathcal{E}_C)$ is equivalent to Czerveny's ψ_t (for solution of the electrostatic potential).

In the case of strong assymmetry for $\epsilon_1 N_{D1} \gg \epsilon_2 N_{D2}$, the results are straight lines almost identical to the line $(\mathcal{E}_t + \Delta\mathcal{E}_C - 1)$, representing the case of a Schottky contact, where $(\mathcal{E}_2(0) + \Delta\mathcal{E}_C)$ is negligible.

For $\epsilon_1 N_{D1} \sim \epsilon_2 N_{D2}$, the results are still straight lines close and almost parallel to the Schottky contact line, but the intercept on the $(\mathcal{E}_t + \Delta\mathcal{E}_C)$ axis, by extrapolation, gives a cut-off voltage different from the diffusion voltage, V_D. In this case $(\mathcal{E}_2(0) + \Delta\mathcal{E}_C)$ is small but not negligible. The slopes of the lines, $\frac{\partial(C^{-2})}{\partial\mathcal{E}} = \frac{2\,L_{D2}^2}{\epsilon_2^2}$ $= \frac{2}{qN_{D2}\,\epsilon_2}$, gives a measure of the donor concentration in the material S2.

In the case of the other high assymmetry, $\epsilon_1 N_{D1} \ll \epsilon_2 N_{D2}$, the expression for C^{-2} is no longer represented by the straight line $C^{-2} \propto (\mathcal{E}_t - \mathcal{E}_2(0) - 1)$, and the potential drop in the narrow gap material S1,

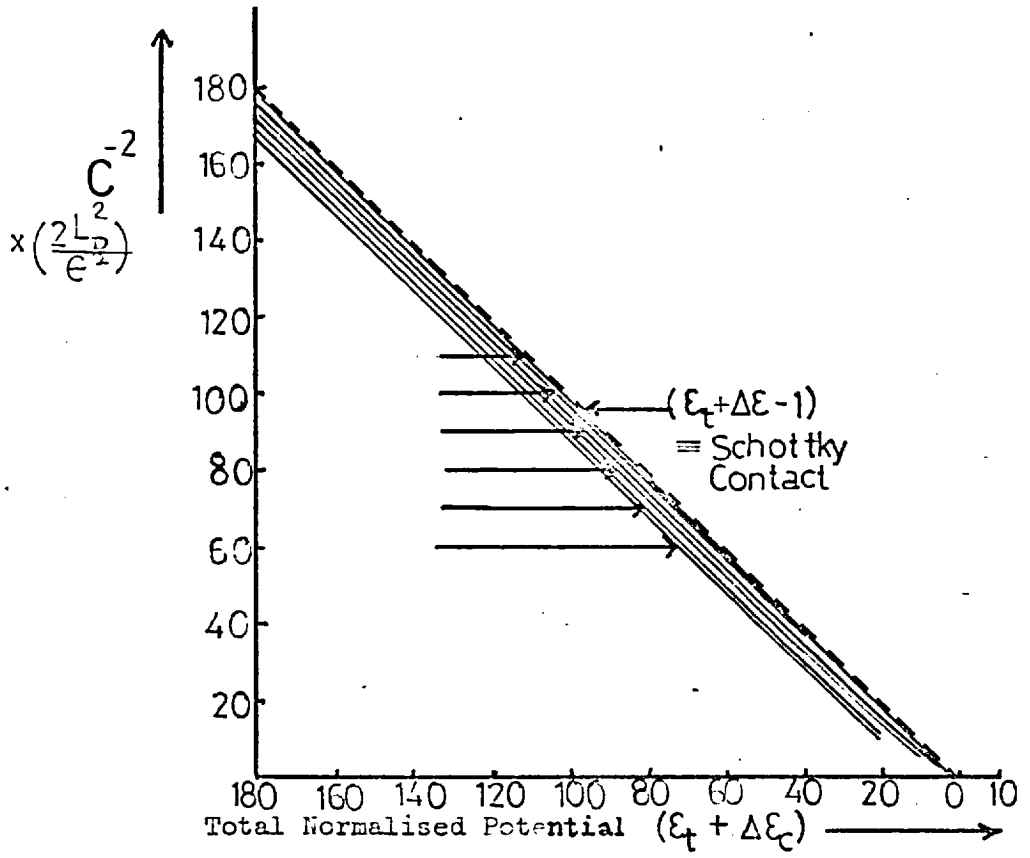


Fig. 5.6 C^{-2} - Potential Variations for Different Doping Assymmetries (After Czerveny, 1968)

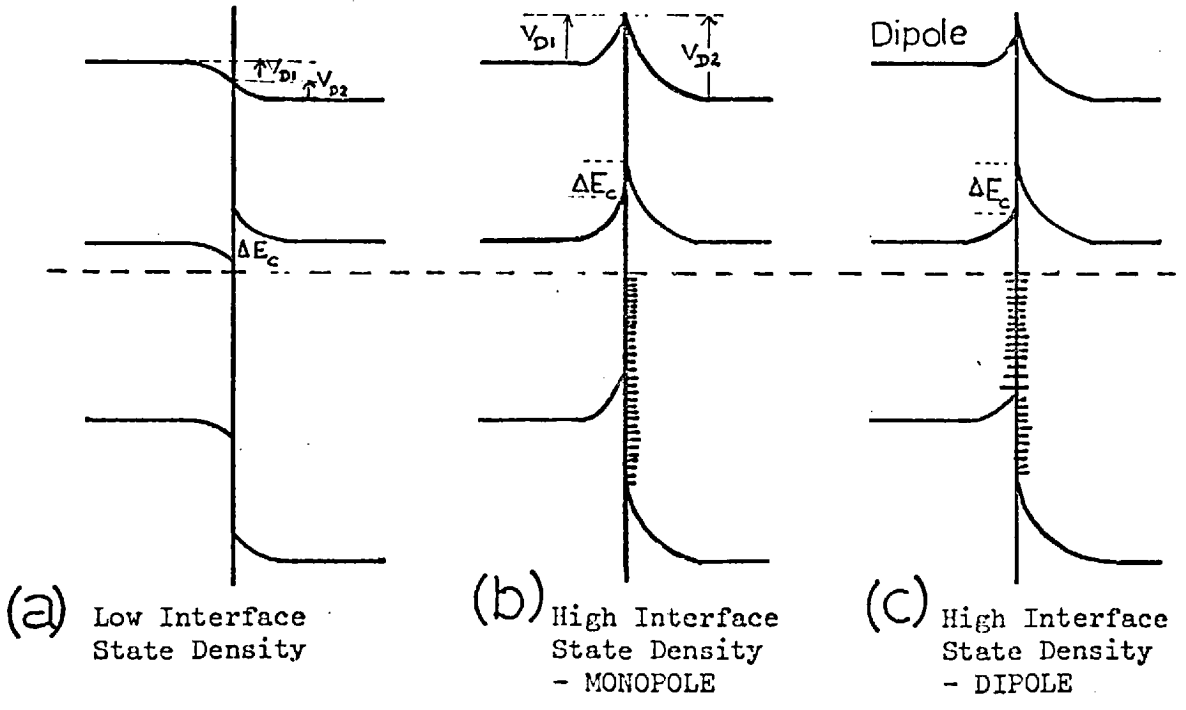


Fig. 5.7 Band Profile of Abrupt n-n Heterodiodes (a) Anderson's Model, (b) Oldham and Milne's Model (Monopole), (c) Van Ruyven's Model (Dipole).

becomes significant. The line deviates even further from the Schottky contact line, and the intercept voltage becomes quite different from V_D. The slope of the line will incorrectly predict N_{D2}. Hampshire (1968) calculated the percentage error of N_{D2} as being 6.5% in the worst case for N_{D2} (depletion) $\simeq 10^{16}$ cm^{-3}, N_{D1} (accumulation) $\simeq 10^{14}$ cm^{-3}, and only 0.5% for $N_{D2} \simeq 10^{14}$ cm^{-2}, $N_{D1} \simeq 10^{16}$ cm^{-3}. In his calculation for V_D, the errors were 3% for the best case but 38% for the worst case.

Similar expressions for the capacitance C, of equation (5.24) have been derived by Zased (1969) and Kumar (1968), and if the same simplifying assumptions are made for the different doping assymmetries, the capacitance as expressed by their equations, will be the same.

5.2.2 The Model with Interface States

Interface states, arising from dislocations caused by lattice and thermal mismatches, play an important role in the equilibrum band profile. These states produce a net interfacial charge to form either a monopole layer, dipole layer or both. Consider a negative interfacial charge in an n-n system, the band bending of the accumulation region decreases to maintain charge neutrality. The amount by which the band at the interface moves up depends directly on the magnitude of the interfacial charge, and if more and more states are generated, the band bending moves through the region of being flat and eventually forms a depletion layer. Such a model, equivalent to two Schottky diodes back-to-back, was proposed by Oldham and Milnes (1964), to explain the peculiar characteristics of Si-Ge diodes for current saturation with both polarity of voltages.

For a semiconductor with hexagonal structure (and oriented to the basal plane), the surface bond density N_{BD} is given by

$$N_{BD} = \frac{2}{\sqrt{3}\, a^2}$$

where a is the lattice constant.

Hence the minimum number dangling-bond density resulting from abrupt contact (or number of unpaired atoms) is the difference between N_{BD} for the two materials, N_{DB}

i.e. $$N_{DB} = \frac{2}{\sqrt{3}}\left(\frac{1}{a_2^2} - \frac{1}{a_1^2}\right) \qquad (5.25)$$

and is(the total length of dislocations per unit area) X(no. of dangling bonds per unit length), e.g. for $CdSe/CdS_xSe_{1-x}$ when $x = 1$, $N_{DB} = 5 \times 10^{13}$ cm^{-3} and when $x = \frac{1}{2}$, $= 2.6 \times 10^{13}$ cm^{-3}.

It can be considered that when contact is made, the material with the higher dangling-bond density saturates the dangling bonds of the other material, and determines the interface state distribution. The fraction of unsaturated bonds is 2m, say

i.e. $$2m = \frac{N_{DB}}{N_{DB2}}$$

where $N_{DB2} > N_{DB1}$

$$= \frac{a_1^2 - a_2^2}{a_1^2} = 4\left(\frac{a_1 - a_2}{a_1 + a_2}\right)$$

$m = 2\left(\frac{a_1 - a_2}{a_1 + a_2}\right) \times 100\%$ is defined as the percentage lattice mismatch. For the CdSe/CdS structure m is $\simeq$ 3.8% and the value will decrease as the selenium content in the alloy stubstrate is increased. Note that if the lattice mismatch $>$ 8%, it becomes almost impossible to produce epitaxy.

In studying nGe-nSi heterodiodes Oldham and Milnes (1964) found that the density of electrically active interface state large enough to greatly influence the band bending and electrical properties. Fig

5.7 (a) shows the band profile of the abrupt junction with low interface state density (approximately Anderson's Model). The discontinuity in the conduction band still equals the electron affinity difference but the amount of band bending of the conduction band edge is determined by the density of the interface states. D is no longer continuous at the interface. Fig. 5.7 (b) shows the band profile for diodes of Oldham and Milnes where lattice mismatch is large (4%) with a charge density of $\sim$ q x 10^{14} cm^{-2}. The interface state distribution is similar to that of the free silicon surface, such that both sides of the interface are depleted of electrons due to the acceptor-like nature of the interface states. They added that any dense set of interface states near or below the silicon band gap would produce double depletion.

The double depletion model is equivalent to two Schottky diodes back-to-back and is more important for materials of low doping concentrations, because if one or both materials are highly doped, tunnelling through one or both barriers is likely, reducing the tendency of the current to double saturate.

Before attempting to give a quantitative description of the interface states on the band diagram, a brief mention will be made of another model, - that due to Van Ruyven in which he assumes a dipole in addition to the monopole at the interface. In this model both the electrostatic potential ϕ and electric displacement D, are discontinuous, and the band diagram for this is illustrated in Fig. 5.7 (c).

Consider now interface states as lying in a sheet of infinitesimal thickness at the interface. Associated with these states is a constant charge density, Q_{IS}, in a monopole and a dipole voltage $\frac{kT}{q} P_I$, where P_I is the normalized dipole. It is necessary to solve the Poisson's equation as before and to include the effect of interface charge. The discontinuity in the conduction band is now $\Delta E_C = \Delta\chi - kT P_I$ and the total diffusion potential is $V_D = V_{D1} + V_{D2} + \frac{kT}{q} P_I$.

The boundary conditions are modified as follows:-

$$\mathcal{E}_1(0) = \mathcal{E}_2(0) + P_I + \Delta\mathcal{E}_C$$

$$\epsilon_1 \left.\frac{d\mathcal{E}_1}{dz}\right|_{z=o} = \epsilon_2 \left.\frac{d\mathcal{E}_2}{dz}\right|_{z=o} - \frac{q}{kT} \cdot qQ_{IS}$$

Applying these boundary conditions to the Poisson's equation of (5.16), the solution is

$$\frac{\left(e^{\mathcal{E}_1(0)} - \mathcal{E}_1(0) - 1\right)^{\frac{1}{2}} + \frac{Q_{IS}}{\sqrt{2}L_{D1}N_{D1}}}{\left[e^{\mathcal{E}_2(0) - \mathcal{E}_t + P_I} - (\mathcal{E}_2(0) - \mathcal{E}_t + P_I - 1\right]^{\frac{1}{2}}} = K^{\frac{1}{2}} \qquad (5.27)$$

Assuming that the dipole contribution is negligible, then the above equation is simplified to

$$\frac{\left(e^{\mathcal{E}_1(0)} - \mathcal{E}_1(0) - 1\right)^{\frac{1}{2}} + \frac{Q_{IS}}{\sqrt{2}\,L_{D1}N_{D1}}}{\left[e^{\mathcal{E}_2(0) - \mathcal{E}_t)} - (\mathcal{E}_2(0) - \mathcal{E}_t) - 1\right]^{\frac{1}{2}}} = K^{\frac{1}{2}} \qquad (5.28)$$

The equation predicts a decrease in the electric field in S1 as Q_{IS} increases resulting in a reduction in band bending of the accumulation layer with a simultaneous increase of the band bending in the depletion layer of S2. Fig. 5.8 shows a solution of this equation for $K = 1$ and $N_D = 10^{15}$ cm^{-3}. It is observed that Q_{IS} has to be of a sufficiently moderate magnitude ($\gtrsim q \times 10^{8}$ cm^{-2}), before any major changes can take place in the band bending of $\mathcal{E}_1$. As Q_{IS} increases beyond ($q \times 10^{9}$ cm^{-2}) the accumulation layer deminishes until it is transformed into a depletion layer at $Q_{IS} > (q \times 10^{10}$ cm^{-2}).

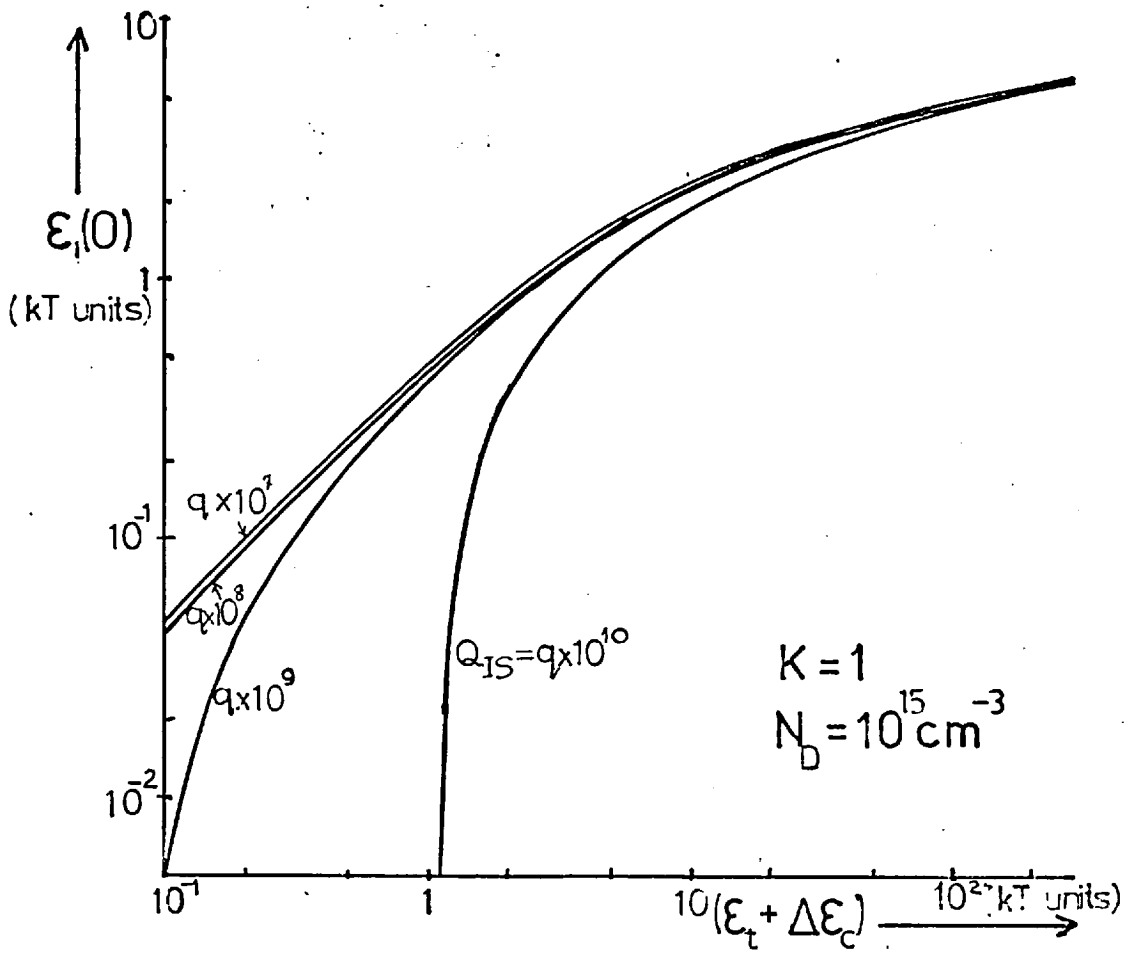


Fig. 5.8 Variation of $\mathcal{E}_1(0)$ with $(\mathcal{E}_t + \Delta\mathcal{E}_c)$ for Constant Monopole Q_{IS} (solution of Equation (5-28)

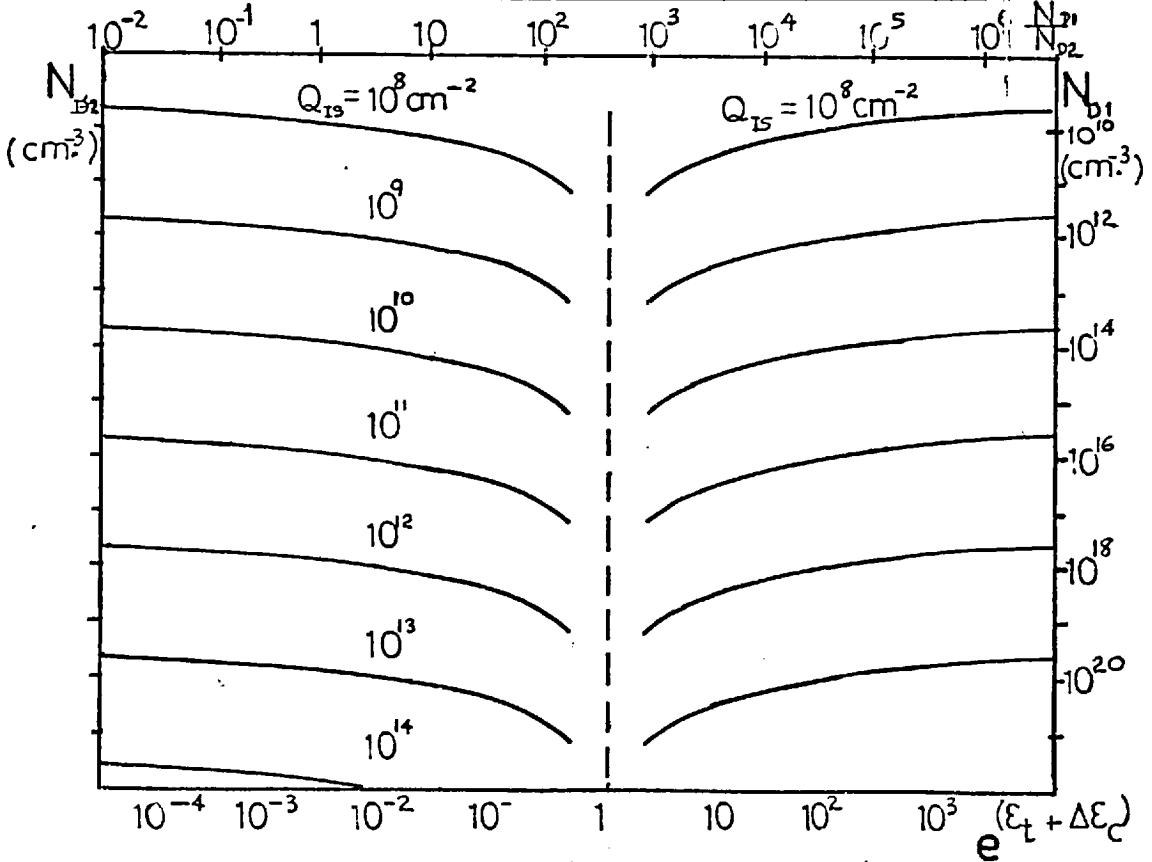


Fig. 5.9 Flat-Band Conduction for S1 and S2 (Solution of Equation (5.29)

Consider the case of the accumulation layer approaching that of the flat-band form i.e. at a critical value just before the transformation to depletion. Charge neutrality conditions imply that the depletion layer in S2 increases to a total positive charge equal in magnitude to the negative Q_{IS}. Here $\mathcal{E}_1(0) = 0$ and the equation (5.28) becomes

$$\frac{Q_{IS}^2}{e^{-\mathcal{E}_t} - \mathcal{E}_t - 1} = K L_{D1}^2 N_{D1}^2 = \frac{kT\epsilon_2}{q} N_{D2} \qquad (5.29)$$

A solution of this equation is illustrated in fig. 5.9 where N_D is plotted as a function of $\mathcal{E}_t + \Delta\mathcal{E}_c$ with Q_{IS} as parameter, ranging from 10^8 to 10^{14} cm^{-2}. If $Q_{IS} \simeq q \times 10^{12}$ cm^{-2} then N_{D2} must be $> 10^{18}$ cm^{-3} to just prevent a depletion region from forming in S1. In the limit, when Q_{IS} is large (i.e. $> q \times 10^{13}$ cm^{-2}), then the value of N_{D2} cannot be made larger and a depletion layer is formed in S1. It follows from equation (5.29) that the condition for double depletion is

$$Q_{IS} > L_{D2} N_{D2} \left(e^{\mathcal{E}_t} - \mathcal{E}_t - 1 \right)$$

In a similar treatment to deriving equation (5.29) for the accumulation - depletion case, a solution for a double-depletion model is

$$\frac{\frac{Q_{IS}}{L_{D1}N_{D1}} - \left(e^{\mathcal{E}_1(0)} - \mathcal{E}_1(0) - 1\right)^{\frac{1}{2}}}{\left[e^{\mathcal{E}_2(0) - \mathcal{E}_t} - (\mathcal{E}_2(0) - \mathcal{E}_t) - 1\right]^{\frac{1}{2}}} = K^{\frac{1}{2}} \qquad (5.30)$$

where $\mathcal{E}_1(0)$ now becomes a negative value and the solution of equation (5.30) is shown in fig. 5.10 (after Perez), where $\mathcal{E}_1(0)$ is plotted as

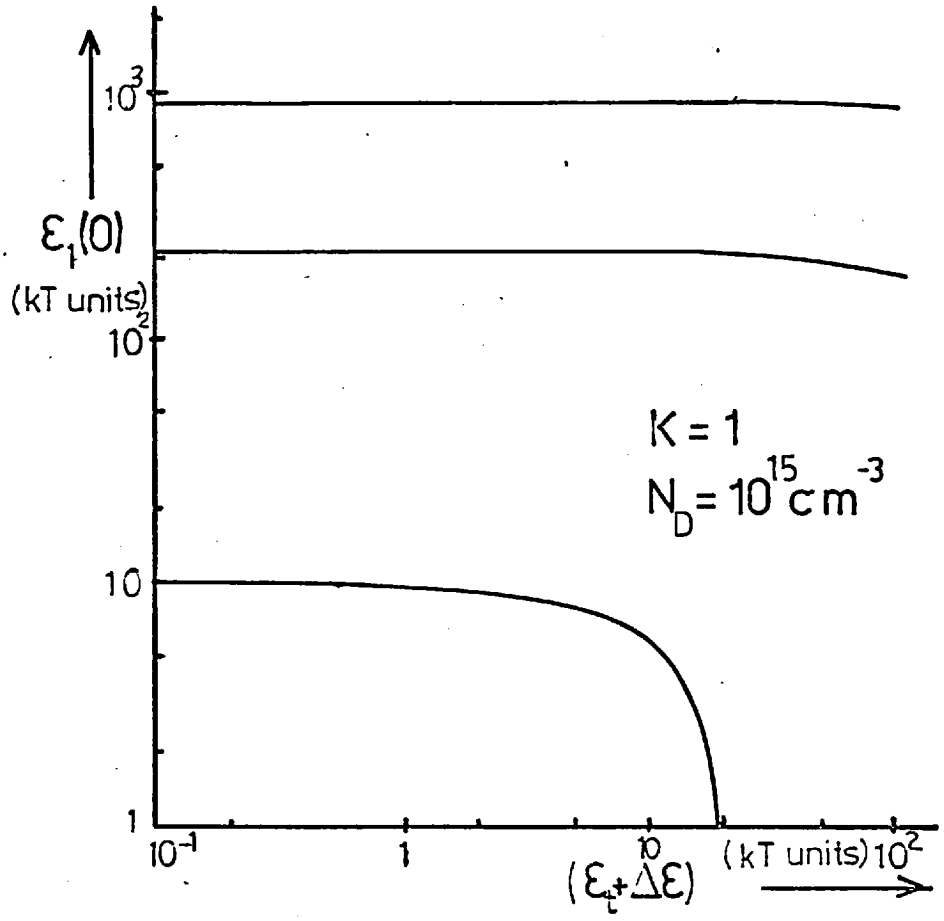


Fig. 5.10 Variation of Potential in Si as a Function of Total Applied Potential for a Double-Depleted Diode (Solution of Equation 5-30)

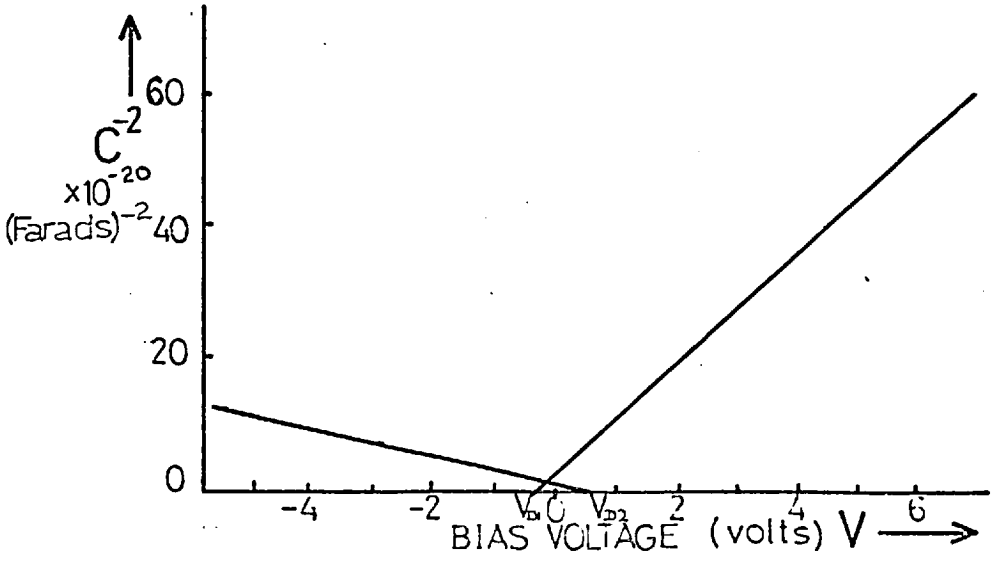


Fig. 5.11 Capacitance-Voltage Variations of an nGe-n Si Heterodiode (After Donnelly and Milnes, 1965)

a function of $(\mathcal{E}_t + \Delta\mathcal{E}_c)$ for $N_{D1} \simeq 10^{15}$ cm^{-3} and doping parameter K = 1. The diagram shows that if Q_{IS} is just above its critical value, then on the application of reverse bias, all the voltage drop occurs in S2 and the depletion region is reduced and may even be retransformed into an accumulation layer at higher biases. If Q_{IS} is high, the effect of bias of either polarity is to increase the depletion with the positively biased material leaving the other virtually unaltered, and Q_{IS} is almost independent of this bias.

Junction Capacitance of Heterojunction with Interface States

The effect of interface states on the junction capacitance of an abrupt junction has been studied by Donnelly and Milnes (1965, 1966), Van Opdorp (1969) because of discrepancies between observed and predicted (from the Anderson's model) values of C^{-2} versus applied voltage intercepts, being a few tenths of a volt lower for the observed cases.

If the constant monopole, Q_{IS} of interface charge - qQ_{IS} is less that its critical value (i.e that which determines flat-band conduction), then the capacitance can be approximately estimated by the method as in the case with no interface states (section 5.2.1). If however, Q_{IS} is larger than this critical value corresponding to double depletion, then the capacitance will be modified as suggested by Donnelly and Milnes to be similar to those observed in grain boundary structures.

On the application of a biasing voltage of either polarity, the net negative charge on the interface states increases so that the forward bias side remains virtually uncharged. Hence the capacitance is given by

$$\left.\begin{aligned} C_1 &\simeq \left(\frac{q}{2\epsilon_1 N_{D1}}\right)^{\frac{1}{2}} (V_{D1} + V)^{-\frac{1}{2}} \text{ for } V>0 \\ C_2 &\simeq \left(\frac{q}{2\epsilon_2 N_{D2}}\right)^{\frac{1}{2}} (V_{D2} - V)^{-\frac{1}{2}} \text{ for } V<0 \end{aligned}\right\} \qquad (5.31)$$

In terms of the normalizing potentials $(V_{D1} + V) = \frac{kT}{q} \times (\mathcal{E}_t - \mathcal{E}_1(0) + \Delta\mathcal{E}_c)$ and $(V_{D2} - V) = \frac{kT}{q} (\mathcal{E}_t - \mathcal{E}_2(0) + \Delta\mathcal{E}_c)$

A typical double saturation plot of C^{-2} versus biasing voltage for an nGe-nSi diode of Donnelly and Milnes is shown in Fig. 5.11 and are straight lines for the two biases giving voltage intercepts of V_{D1} and V_{D2}.

This method has been used to evaluate the interface state density.

$$Q_{IS} \simeq - (2q\ {}_1N_{D1})^{\frac{1}{2}} + (2q\ {}_2N_{D2})^{\frac{1}{2}}$$

so that the density of interface states N_{IS} is therefore

$$N_{IS} \geqslant - \frac{Q_{IS}}{q}$$

Donnelly and Milnes (1967) suggested that each interface state may show a different degree of filling at different biases with a quasi-Fermi level of its own, bearing no relations to the adjacent materials. Such a quasi-Fermi level may not even exist and each level may have its own occupation statistics which may not follow Fermi-Dirac statistics, determined by the rate of interstate and band-to-state transitions. Also, capacitance may be frequency dependent because of the time constants involved in the filling and emptying of the states.

Van Opdorp and Kenerva (1967) and Van Opdorp (1969) mathematically analysed the voltage and frequency dependence capacitance of two Schottky diodes back-to-back, corresponding to a double saturation heterojunction. Their low-frequency C-V curves predicts a sharp minimum at a constant C_{min} for the low frequencies, higher frequencies, instead of the sharp minimum, a broad maximum appears. But at high bias, all the curves

follow the C^{-2} versus V relationship, the bias required being greater as the frequency is increased.

Van Opdorp and Kenerva suggested that the dipole generation from interface states is negligible since ΔE_c appears to be constant over a number of diodes. If a dipole were present, it would be represented in the magnitude of ΔE_c, but as dipoles are not constant over a number of devices, and ΔE_c is constant, then they are assumed absent.

The Equivalent Circuit

The equivalent circuit of a heterodiode in which the interface state density is relatively low i.e. one in which the current does not saturate for both boltage polarities may be approximately represented by that of a Schottky diode (fig. 5.12a) where R_S is the bulk resistance, X, the true junction capacitance and Y, the true parallel conductance. If, however, the capacitance and conductance of the heterodiode are measured on a capacitance bridge (e.g. Boonton, type 75B-58), the bridge meausres a capacitance, C, in parallel with a conductance, G (illustrated in fig. 5.12b). It therefore follows that

$$\frac{1}{G + j\omega C} = R_S + \frac{1}{Y + j\omega X} \tag{5.32}$$

Equating real and imaginary parts, the true capacitance and parallel conductance are

$$X = \frac{C}{(1 - RG)^2 + \omega^2 R^2 C^2} \tag{5.33a}$$

$$Y = \frac{G(1 - RG) - \omega^2 RC^2}{(1 - RG)^2 + \omega^2 R^2 C^2} \tag{5.33b}$$

If, however, the interface state density is high enough to cause current saturation for both boltage polarities, the equivalent circuit can be

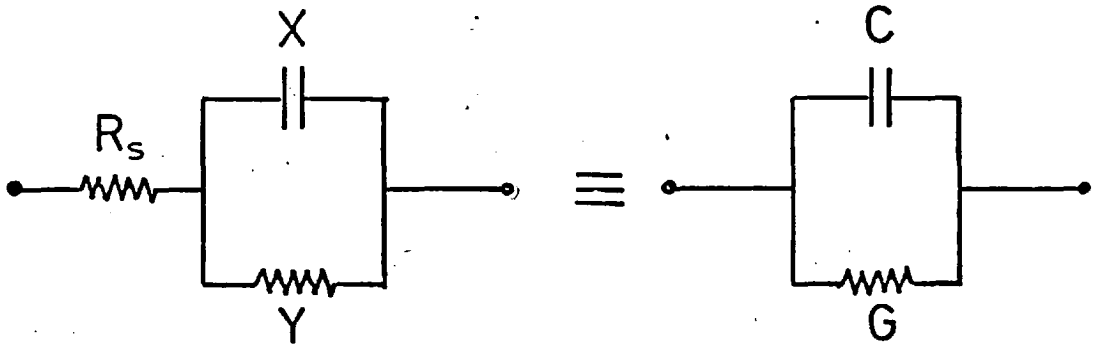


Fig. 5.12 (a) Equivalent Circuit of a Heterodiode with Low Interface State Density

(b) Circuit as Measured by a Capacitance Bridge

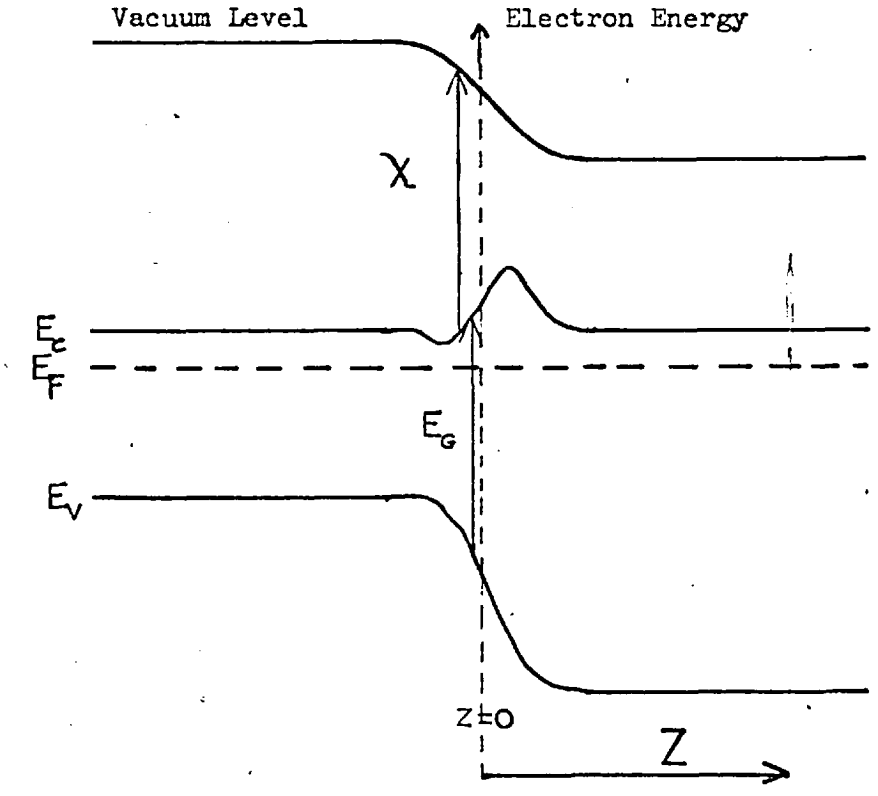


Fig. 5.13 Band Profile of a Graded n-n Heterojunction

represented by two Schottky diodes back-to-back (Van Opdorp, 1969; Hampshire and Tomlinson 1970a, b)

5.2.3 The Graded Junction Model

In real heterojunction devices, intermixing of the constituent materials occur at the interface, and if this intermixing is confined to within a few atomic dimensions adjacent to the plane of the junction, this junction is considered abrupt and section 5.2.2 describes its electrical behavious. If, however, intermixing is extended for more than a few atomic spacings giving an alloy of continuously varying composition, then the junction is considered graded and can no longer be treated by section 5.2.2, since many of the electronic properties of the junction become dependent upon position. Grading results in a reduction of the rectifying barrier.

It is extremely difficult to obtain a solution of the Poisson's equation if E_G, χ, N_{D1}, ϵ and m* are all dependent on position. Simplifying assumptions are needed and the equation is more readily solved for a specialised case. In the model, the doping concentration in the two wide-gap semiconductors are taken as of the same order so that the difference $(E_C - E_F)$ is almost identical. The materials possess similar dielectric constants and effective masses so that variations of these two quantities in the graded region will be neglected. This model can be applied to the case of CdSe/CdS_xSe_{1-x} diodes. As the electron affinity and band gap are continuous varying functions through the transition regions, as shown in fig. 5.13, new boundary conditions are needed to solve the Poisson's equation. In this treatment the effect of interface states will be neglected.

Starting with the Poisson's equation (5.6) to equation (5.13) of the abupt case, which are still valid for this model and remembering E_C is related to χ and ψ by the expression (from fig. 5.13)

$$E_C = -q\psi - \chi$$

Then $$\frac{d^2E_C}{dx^2} = q\frac{d^2\psi}{dx^2} - \frac{d^2\chi}{dx^2} \qquad (5.34)$$

from equations (5.12) and (5.13)

$$\frac{d^2\mathcal{E}}{dx^2} = -\frac{1}{kT}\cdot\frac{d^2E_C}{dx^2} = +\frac{1}{kT}\,q\left(\frac{d^2\psi}{dx^2} + \frac{d^2\chi}{dx^2}\right) \qquad (5.35)$$

Normalizing as before, $Z = \frac{x}{L_D}$, $\mathcal{X} = \frac{x}{kT}$, $\Psi = \frac{q\psi}{kT}$ and

substituting (5.35) in (5.13)

$$\frac{d^2\mathcal{E}}{dz^2} = \frac{q^2N_D}{kT\epsilon} \times L_D^2\,(e^{\mathcal{E}} - 1) + \frac{d^2\mathcal{X}}{dz^2}$$

i.e. $$\frac{d^2\mathcal{E}}{dz^2} = \left(e^{\mathcal{E}} + \frac{d^2\mathcal{X}}{dz^2} - 1\right) \qquad (5.36)$$

Note that this form of the Poisson's equation is similar to that in the abrupt case except for the term involving the normalized electron affinity (having a similar form to the normalized charge density). The requirement for rectification is that the energy barrier should be $>$ a few kT, implying $\mathcal{E} < -1$ i.e. $\frac{d^2\mathcal{E}}{dz^2} > 0$

or $$e^{\mathcal{E}} + \frac{d^2\mathcal{X}}{dz^2} - 1 > 0$$

However, $e^{\mathcal{E}}$ can be ignored as being small compared with $\frac{d^2\mathcal{X}}{dz^2}$

$$\therefore \quad \frac{d^2\chi}{dz^2} > 1 \qquad (5.37)$$

The value of the barrier height is determined at the point ξ being a minimum which implies $\frac{d^2\xi}{dz^2} > 0$.

This ties up with the equation derived by Oldham and Milnes (1963) except they obtained their equation by defining ξ as the negative of the value used here i.e. $-\left(\frac{E_C - E_F}{kT} + \ln \frac{N_D}{N_C}\right)$.

Before proceeding with the Poisson's equation it is necessary to assume a specific form of $\chi(x)$. Oldham and Milnes assumed a hyperbolic tangent as being a good compromise between the various solutions of the Fick's diffusion equation.

$$\text{i.e.} \quad \chi(x) = -\left(\frac{\Delta\chi}{2}\right) \tanh\left(\frac{x}{L}\right) + \text{constant.} \qquad (5.38)$$

where $\Delta\chi$ is the total change of χ over a characteristic length L.

Now differentiating equation (5.38) once, $\frac{d\chi}{dz} = -\frac{\Delta\chi}{2} \frac{L_D}{L}\left(1 - \tanh^2 Z \cdot \frac{L_D}{L}\right)$

Differentiating again $\frac{d^2\chi}{dz^2} = \Delta\chi\left(\frac{L_D}{L}\right)^2 \cdot (1 \tanh^2 Z \cdot \frac{L_D}{L})(\tanh Z \cdot \frac{L_D}{L})$

Differentiating once more to obtain the maximum value of $\frac{d^2\chi}{dz^2}$

$$\text{i.e.} \quad \frac{d^3\chi}{dz^3} = -\Delta\chi\left(\frac{L_D}{L}\right)^3 \left[1 - 4 \tanh^2 Z \cdot \frac{L_D}{L} + 3 \tanh^4 Z \cdot \frac{L_D}{L}\right]$$

which must be zero at the maximum i.e.

$$(1 \tanh^2 Z \cdot \frac{L_D}{L})\ (1 - 3 \tanh^2 Z \cdot \frac{L_D}{L}) = 0$$

$$\therefore \tanh Z \frac{L_D}{L} = -\sqrt{\frac{1}{3}} \text{ for a max.}$$

Applying this to equation (5.37)

$$\therefore L < \left(\frac{2\Delta\chi\epsilon}{3\sqrt{3}\, q^2 N_D}\right)^{\frac{1}{2}} \equiv L_c \tag{5.39}$$

This suggests that L can only vary over a small distance compared with L_c, defined in the above equation. The condition for rectification becomes $\frac{L_c}{L}$ must be large (>1)

Using the boundary condition that

$n = N_D$ at $x = \pm 10 L_D$

$(\Delta\chi = 20\ kT)$

Oldham and Milnes obtained numerical solutions to the Poisson's equation by means of a relaxation method to display the complete conduction band edge. The solution is illustrated in fig. 5.14 with the grading parameter $\frac{L_c}{L}$ varying from 0 to 30, where the large value approaches that for the abrupt case, and the value zero to the case where there is no rectifying barrier i.e. ohmic contact. Where $\frac{L_c}{L} \sim 1$, then the effective barrier height is low and rectification becomes poor due to thermal emission over the barriers in the absence of bias. In their studies on graded $Al_xGa_{1-x}As$-GaAs heterojunction Womac and Rediker (1972) stated that a structure with total band gap discontinuity 20 kT (at room temperature) degraded to give only 1 kT for grading over the space charge width.

The above analysis involves special electrical properties in the constituent semiconductors viz equal doping, effective mass and dielectric constants on both sides of the junction and a hyperbolic tangent variation

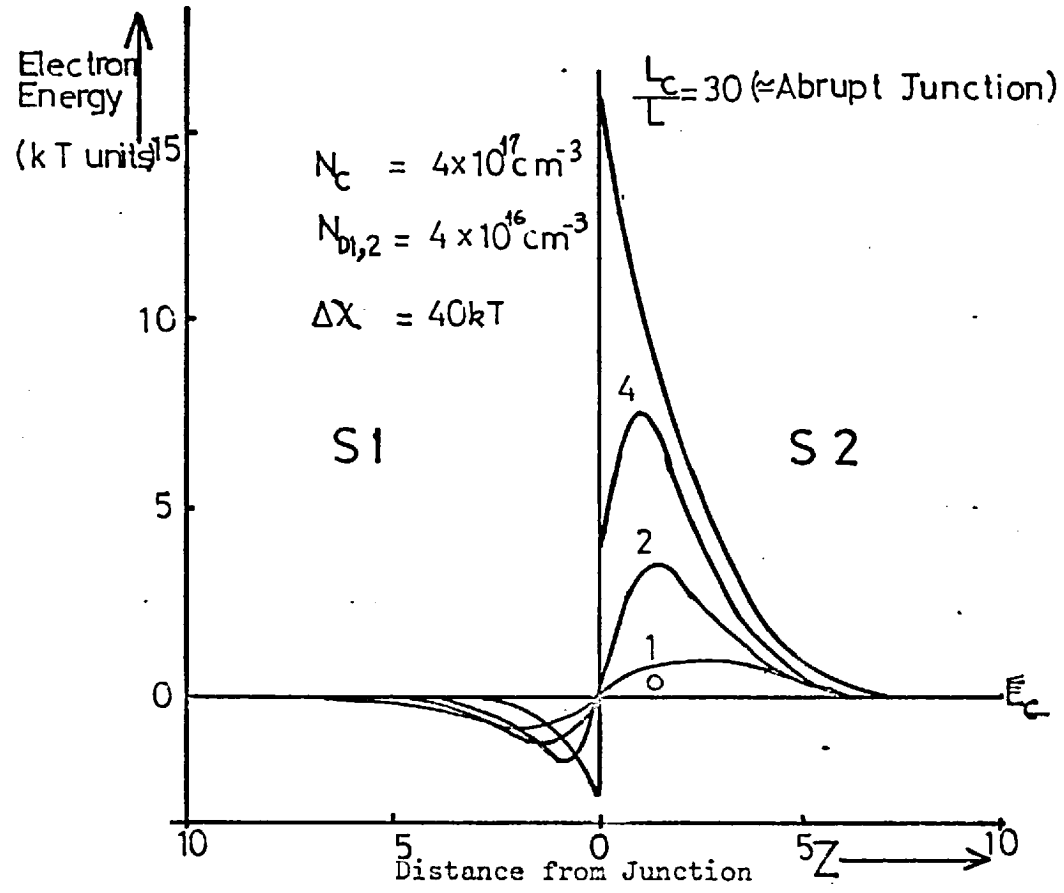


Fig. 5.14 Solution of the Conduction Band Edge in a Graded Heterojunction as a Function of the Grading Parameter Lc/L (After Oldham and Milnes, 1963)

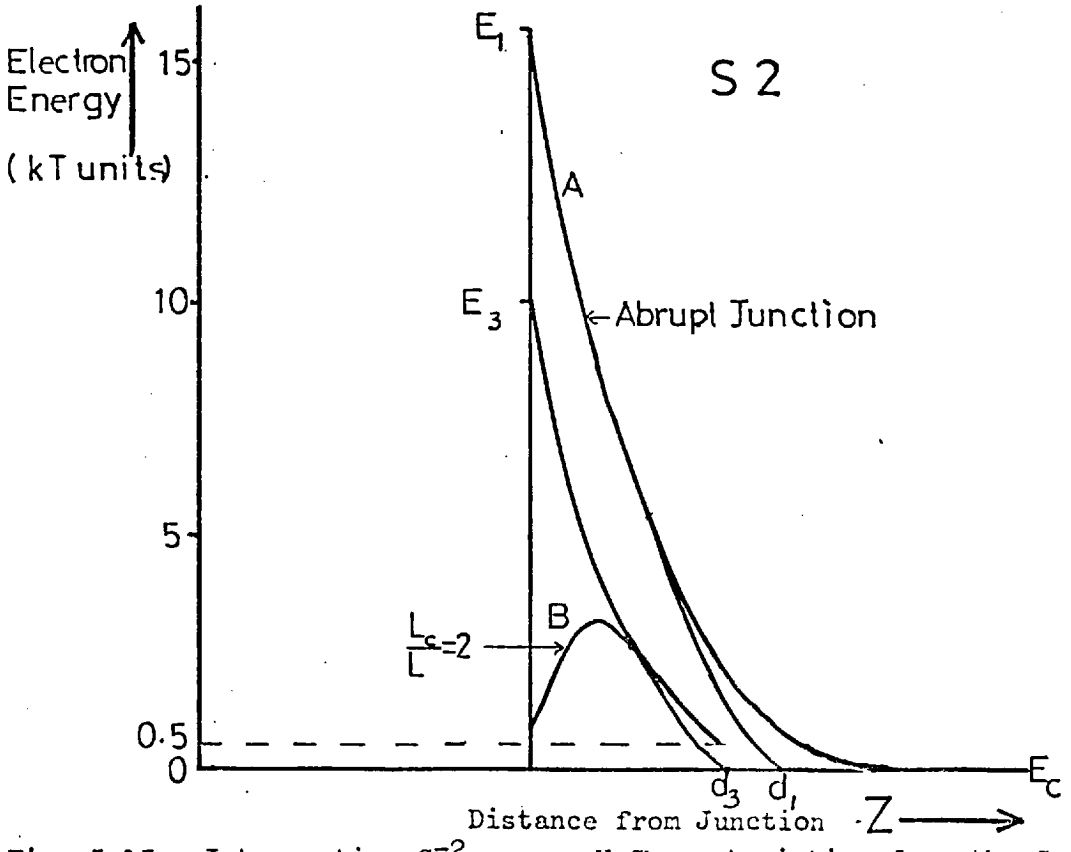


Fig. 5.15 Interpreting C^{-2} versus V Characteristics from the Conduction Band Edge of Fig. 5.14 (After Oldham and Milnes, 1963)

of χ across the junction. We may ask what would be the effect of variations of these parameters with position across the junction. If N_D is not the same in the two materials, but graded at the junction then the equation (5.36) will have to be modified to include an N_D position dependent term instead of the term '1', and new solutions will have to be sought.

Consider a simpler case of unequal but constant doping on either side of the z = o line. The doping in S1 (the high electron affinity side) is treated as N_D and a small error will result in the solutions. Alterations of mobility, effective mass or dielectric constant in S2 would not alter the solution of the equation to any large extent.

Oldham and Milnes interpreted reverse bias capacitance by referring to the curves A and B (fig. 5.15) representing the conduction band edges in the depletion layer of S2 for the abrupt and graded$\left(\frac{L_c}{L} = 2\right)$ junctions, where $\Delta\chi$= 20 kT. A parabola with the same height, E_1, as curve A is drawn to coincide with the upper limits of curve A, so that it intersects the zero energy level, at a distance, d_1, from the junction (i.e z = o). At this distance, d_1, curve A is $\sim$ 0.5 kT above its bulk value and defining the zero bias depletion layer width for the abrupt case. On curve B, the 0.5 kT value occurs at a distance d_2, from the junction. A parabola drawn from this point intersects the energy axis at an energy, E_2, greater than the barrier height but lower than $\Delta\chi$. Since the doping is constant and the capacitance is independent of the form of potential variation through the depletion region, then $1/C^2$ is propertional to the bias, V, whose gradient gives a measure of the doping concentration in S2. Extrapolating the $1/C^2$ versus V curve is equivalent to constructing the two parabolas. The zero bias capacitance is given by the relationship

$$C = \frac{\epsilon A}{d_{1,2}}$$

of curves 1 and 2 where A is the junction area.

5.3 Transport Mechanisms in Isotype Heterojunctions

There are at present several different theories to describe the mechanism of current flow in heterojunctions which have been adapted from homojunction theory with allowances for the discontinuities at the heterojunction interface. As a result of these parameter changes here, incident electrons have a high probability of reflection. In isotype heterojunctions the carrier transport is due solely to the majority carriers - in this study, electrons. These possible transport mechanisms are illustrated in Fig. 5.16 (after Price,1962) and include emission, diffusion and tunnelling elements. Fig. 5.17 shows the effect of interface states on the current flow. Note that the discontinuities contribute to significant carrier reflections which do not normally occur in homojunctions.

Forward current may be classified as thermal and non-thermal (or excess) currents. The first type deals with currents in which the carriers surmount the potential barrier to cross the junction and are temperature and voltage sensitive. The latter type deals with current in which the carriers partly tunnel through the potential barrier, and are very weakly temperature dependent.

5.3.1 Emission and Diffusion Models

The first model to explain current flow in isotype heterojunctions was presented by Anderson who expressed the current density in the absence of interface states from emission theory for metal semiconductor diodes as

$$J_E = A \exp\left(-\frac{qV_2}{kT}\right)\left[\exp\left(\frac{qV_2}{kT}\right) - \exp\left(-\frac{qV_1}{kT}\right)\right] \qquad (5.40)$$

where V_1 and V_2 are the portions of the applied bias appearing across

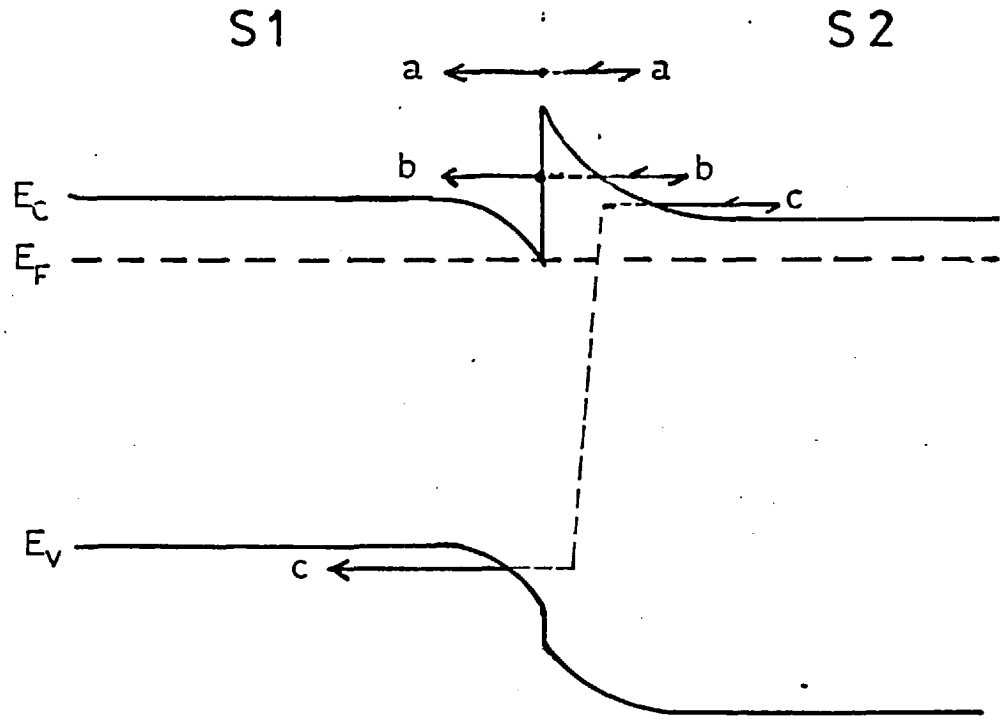


Fig. 5.16 Three Possible Carrier Transport Mechanism in an n-n Heterojunction without Interface States (a) Allowed-Allowed Transmission by Emisson-Diffusion, (b) Tunnelling Transmission, (c) Interband Tunnelling (doted line represents bias) (After Price, 1962)

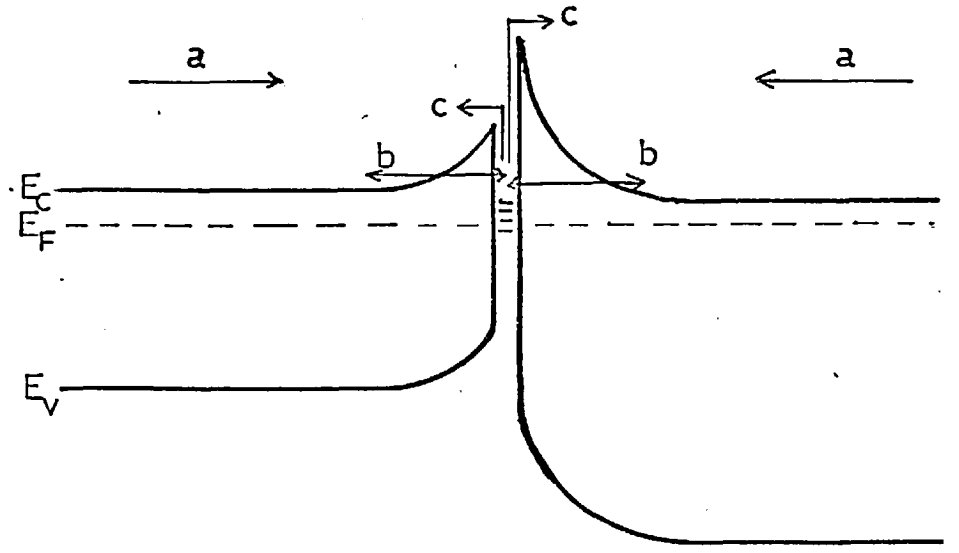


Fig. 5.17 Transport Mechanisms in an Abrupt n-n Heterodiode with High Interface State Density (a) Bulk Flux (Diffusion), (b) Tunnelling Into/From Interface States, (c) Emission Into/From Interface States.

the transition layers in S1 and S2 respectively,

$$A = Xq\, N_{D2} \left(\frac{kT}{2\pi m^*}\right)^{\frac{1}{2}} \quad , \left(\frac{kT}{2\pi m^*}\right)^{\frac{1}{2}} \text{ represents}$$

the average thermal velocity of carriers, X is the transmission coefficient for carriers.. The terms $\exp\left(\frac{qV_2}{kT}\right)$ and $\exp\left(-\frac{qV_1}{kT}\right)$ in equation (5.40) refer to forward and reverse bias respectively and describe exponential current variations with applied bias.

The transmission coefficient, X, has not as yet been measured for heterojunctions but has been used as a fitting variable to obtain agreement between predicted and experimental values. Van Ruyven (1972) suggested that a slight grading of the junction could perhaps produce an "anti reflection coating" for Bloch waves.

In this model it is assumed that most of the built-in voltage is supported in the wide-gap material S2 which is true except for the cases, $N_{D2} >> N_{D1}$ and for high forward bias. The forward current is controlled by V_2 (reverse current by V_1).

Other expression for emission current have been offered (Kumar, 1968 (b); Chang 1965; Fang and Howard, 1964) but are only slightly different and have been postulated to fit particular device properties. However, the expression for emission current does not describe very many of the devices quoted in the literature, since in some devices tunnelling of carriers through the spike barrier occurs and equation (5.40) does not make allowances for this effect. But the I-V characteristics of the GaAs-Ge isotype heterojunctions are in agreement with equation (5.40) and the $CdSe/CdS_xSe_{1-x}$ diodes are expected also to be represented by this equation.

Kumar (1968, b) presented in the same paper as the emission theory a generalized diffusion theory to describe current transport in n-n

heterodiodes.

$$J_d = \frac{\mu kT}{L_n} N_{D2} \; e^{-V_{D2}} \left[e^{V_2} - e^{V_1} - \left(\frac{N_{D1}}{N_{D2}} e^{V_D} - 1 \right) \left(1 - e^{-V_1} \right) \right]$$

$$\text{where } L_n = \int_{x_1}^{x_2} e^{\left\{ - V(x) - V(0) \right\}} dx \qquad (5.41)$$

However, it has been shown that the diffusion theory is inaccurate in predicting I-V characteristics especially at low voltage levels so this model will not be used in the analysis of $CdSe/CdS_xSe_{1-x}$ devices.

5.3.2 Tunnelling Model

It has already been mentioned that the emission models do not describe I-V characteristics of many heterojunction diodes, since the temperature term suggests far greater variation than what is actually observed. It has therefore been suggested that a tunnelling mechanismn may dominate forward characteristics of some devices.

An empirical equation has been presented by Newman (1965) from published I-V characteristics of many heterojunction pairs to describe temperature and boltage dependent behaviour

$$\text{i.e. } J = J_0 \exp \frac{T}{T_0} \exp \frac{V}{V_0} \qquad (5.42)$$

T and V are separate variables and V_0 may be regarded as indpendent of temperature and T_0 independent of voltage which suggests a tunnelling mechanism in place of an emission mechanism.

Price (1962) gave a wave mechanical treatment for the transport of Bloch waves through the crystal interface and introduced a transmission coefficient due to mismatch of electron wave functions for ingoing and outdoing waves at the interface. His voltage dependence of transmission

coefficient result is similar to the classical WKB approximation to tunnelling probability. Using the treatment of Rediker et al (1964) for tunnelling from the bottom of the conduction band, the voltage-temperature dependent tunnelling probability, P, is

$$P(\mathcal{E}) = \exp\left[- \frac{2}{h} \int_{x_1}^{x_2} (2m^* (E_B - \alpha qV)^{\frac{1}{2}}\right] dx \qquad (5.43)$$

where E_B is the barrier height between the limits x_1 and x_2 at any point x.

The total tunnelling current is obtained by integrating the product of tunnelling probability $P(\mathcal{E})$ and incident electron flux $J(\mathcal{E})$ over energies at which tunnelling occurs

$$\text{i.e. } I_T = \int_0^{E_B} T(\mathcal{E})\ J(\mathcal{E})\ d\mathcal{E}$$

The mathematics is complicated, but there are now several solutions available e.g. Zeidenbergs and Anderson (1967), Tansley (1966), Mammana and Anderson (1971). The model of Mammana and Anderson agrees to a fair approximation with the results for Ge-GaAs diodes over a relatively large bias range.

The current expression for tunnelling proposed by Van Ruyven is

$$I_T = I_0 \exp\left(\frac{E_{1,2}}{kT}\right) \exp\left[\alpha_f (V_D - V)\right] \qquad (5.44)$$

where $E_{1,2}$ is the activation energy for the two temperature regions, α_f is the factor related to tunnelling probability e.g. for a parabolic barrier $\alpha_f = \left[\frac{4m^*}{q^2 N_D}\right]$

These equations can all be approximated to the empirical expression

of Newman

$$I_T = I_0 e^{V/V_0} e^{T/T_0}$$

in which tunnel current varies exponentially with applied bias.

5.3.3 Reverse Bias Conduction

The theory of reverse currents is still relatively undeveloped although attempts have been made to derive expressions to fit experimental observations. Tansley (1971) suggested that"the forward characteristics represented the whole junction, but the reverse characteristics represented the properties of the worst point". He attributed soft breakdown, characteristic of all heterojunction diodes, to the diodes not being made with homogeneous surface properties. However, the main reasons for soft breakdown may be electron tunnelling through the conduction band spike from S1 to S2, interband tunnelling, surface leakage effects or ionization multiplication.

Like forward currents, reverse currents may be thermal or non-thermal; the former type resulting from thermal generation of carriers in or near the transition region which are removed by the field, contributing to current. Chang (1965) analysed reverse currents behaviour and found an exponential behaviour of V with I

$$J_R = J_0' \exp (- SV) \qquad (5.45)$$

where $S = \left(\frac{q}{kT}\right)\left(\frac{\beta}{2V_D^{\frac{1}{2}}}\right) - \left(\frac{q}{kT}\right)\left(\frac{\alpha}{2V_D^{\frac{1}{2}}}\right) + \left(\frac{1}{V_D}\right)$

and $J_0' = J_0 \exp\left(- q \frac{\alpha V_D^{\frac{1}{2}}}{kT}\right) \exp\left(\frac{q\beta V_D^{\frac{1}{2}}}{kT}\right)$

J_0 and S at each temperature are determined by extrapolating linear portions of the curve to zero voltage.

5.3.4 Effect of Interface States on Current Transport

The treatment of carrier transport in heterojunctions in which interface states are present depends on whether the density of the interface charge is sufficient to cause double depletion. If the interface charge is smaller than the 'critical' value then a model from those outlined in section 5.3.2 may be chosen to describe the junction, approximately. But, as the magnitude of the charge approaches this critical value, the expressions for current flow become less and less accurate. This is because interface states act as recombination centres of large cross-sectional area, trapping carriers. Or they may act as current paths for tunnelling currents.

If the interface charge density is high, then all the carriers traversing the interface are trapped and may subsequently be re-emitted over the barrier (Fig. 5.17) (Fig. 5.17b). Current transport for this double depletion model is complicated, however, solutions may be obtained with certain simplifying assumptions.

Oldham and Milnes (1964), applied a kinetic treatment to heterojunctions with large numbers of interface states to cause double current saturation while assuming long carrier mean free paths, small deviations from equilibrum and negligible carrier tunnelling and derived expression for current saturation as

$$F \simeq - F_{1,2} \exp\left(-\frac{qV_{D1,2}}{kT}\right)\left(1 - R_{1,2}\right)\left[\frac{\alpha_{1,2}(1-\alpha_{2,1})}{\alpha_{2,1}} + \alpha_{1,2}\right] \tag{5.46}$$

for both polarities of biases, where F_1 and F_2 are the bulk emission fluxes towards the barrier given by $\frac{1}{4}\bar{c}_1 n_1$ and $\frac{1}{4}\bar{c}_2 n_2$, and R_1 and R_2 are thereflection coefficients for the fluxes with energy sufficient to surmount the barriers, α_1 and α_2 are the interface state transmission

coefficients for the fluxes. This equation can be evaluated if R_1, R_2, α_1 α_2 are known. However, if α_1 and α_2 are small due to mass barrier reflections, then the equations are reduced to

$$\left.\begin{aligned} F &\simeq F_2 \exp\left(-\frac{qV_{D2}}{kT}\right)(1 - R_2)\,(1 - \alpha_1) \\ F &\simeq -F_1 \exp\left(-\frac{qV_{D1}}{kT}\right)(1 - R_1) \end{aligned}\right\} \qquad (5.47)$$

for positive and negative biases respectively, describing current saturations equivalent to two Schottky diodes back-to-back.

Conduction in Graded Heterojunctions

The conduction in macroscopically graded heterojunctions has been treated by several workers and Van Ruyven (1972) has given a comprehensive survey on the mechanisms of carrier transport in structures in which the level E_C, is different in the two materials (e.g. in anisotype heterojunctions) the model is illustrated in Fig. 5.18 and the equation for the electron current in n-type graded material is expressed as

$$j_n = -n\mu_n F - D_n \frac{dn}{dx} - \mu_n n\left[\frac{d\chi}{dx} - \frac{3kT}{2m^*_n}\left(\frac{dm^*_n}{dx}\right)\right] \qquad (5.48)$$

where F is the magnitude of the electric field the term $D_n \frac{dn}{dx}$ is the diffusion term. The position dependence effective mass term is often neglected because of insufficient experimental data of its form.

In this treatment there is no rectifying barrier in the conduction band edge in which case the effect of bias would cause less sensitive variations as compared to abrupt junctions in which the barrier occurs. Applying such a treatment to the $CdSe/CdS_xSe_{1-x}$ case would have little meaning since the conduction band edges in the two materials are almost the same height above the fermi level and this

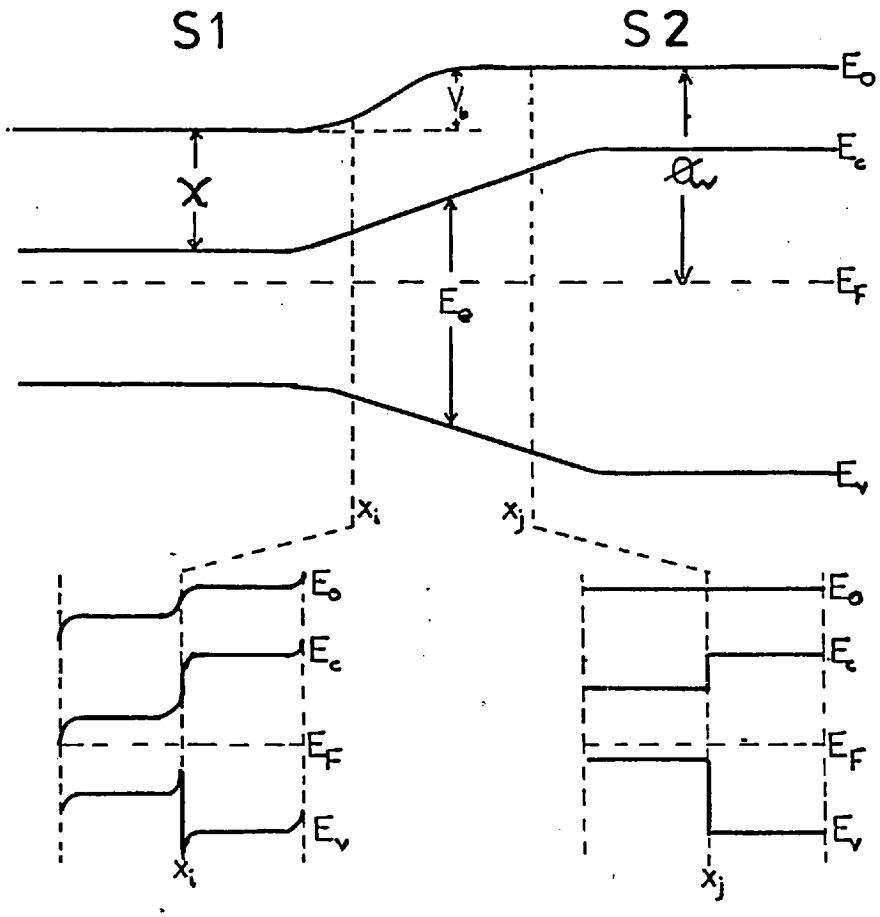


Fig. 5.18 Band Profile of Arbitrarily Graded Heterojunction (x_i -space-charge, x_j-space-charge-free cases) (After, Van Ruyven and Williams, 1967)

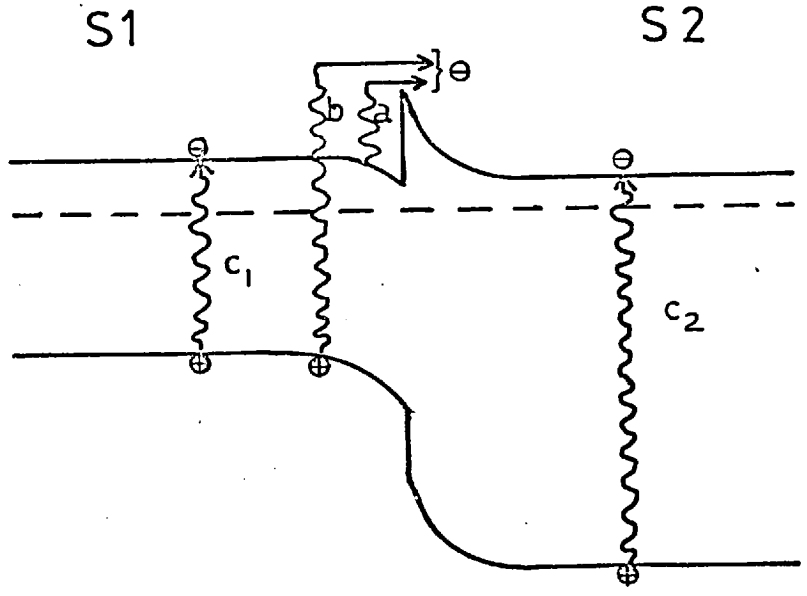


Fig. 5.19 Photoexcitation Mechanisms in n-n Heterodiodes (a) and (b) - Photoemission Processes (c) - Internal Processes

model implies ohmic conduction with no charge barrier. Since grading for the $CdSe/CdS_xSe_{1-x}$ diodes is confined within a few Debye lengths at the interface the abrupt junction conduction model of Section 5.2 will more accurately describe this pair than the model of above.

5.4 Photo-electronic Properties

Ideally when the heterojunction is illuminated, each absorbed photon generates an electron-hole pair, the electrons diffusing towards S2 and holes towards S1. This effective charge separation produces a photovoltage across the device. Some of these carriers may recombine during the diffusion process with carrier of opposite polarity or recombine at interface states, but others may pass the interface. A fraction of those electrons which pass the interface will have enough thermal energy to pass over the spike barrier, reaching the band edge of the other material as "hot" carriers.

The major elements contributing to photocurrent in n-n heterodiodes are illustrated in Fig. 5.19. Because $n_V > n_C$ then mechanism (b) is dominant.

Photo-electronic properties of isotype heterojunctions are not expected to be of any major importance so far as potential device application is concerned. However, these devices possess a few useful properties, the most important being the "window effect", first observed by Preston. This effect can be observed as the photoresponse from light in a suitable range of photon energies incident on the wide-gap materials, S2 perpendicular to the interface and illustrated in Fig. 5.20 Photons with energies less than the forbidden gap of S1, E_{G1}, are transmitted, while energies greater than E_{G2} are absorbed. However, photons with energies in the intermediate range are transmitted through S2 but are very heavily absorbed near the interface.

Tansley (1969) has dismissed isotype structures as being unsuitable for opto-electronic detectors in comparison with some anisotupe

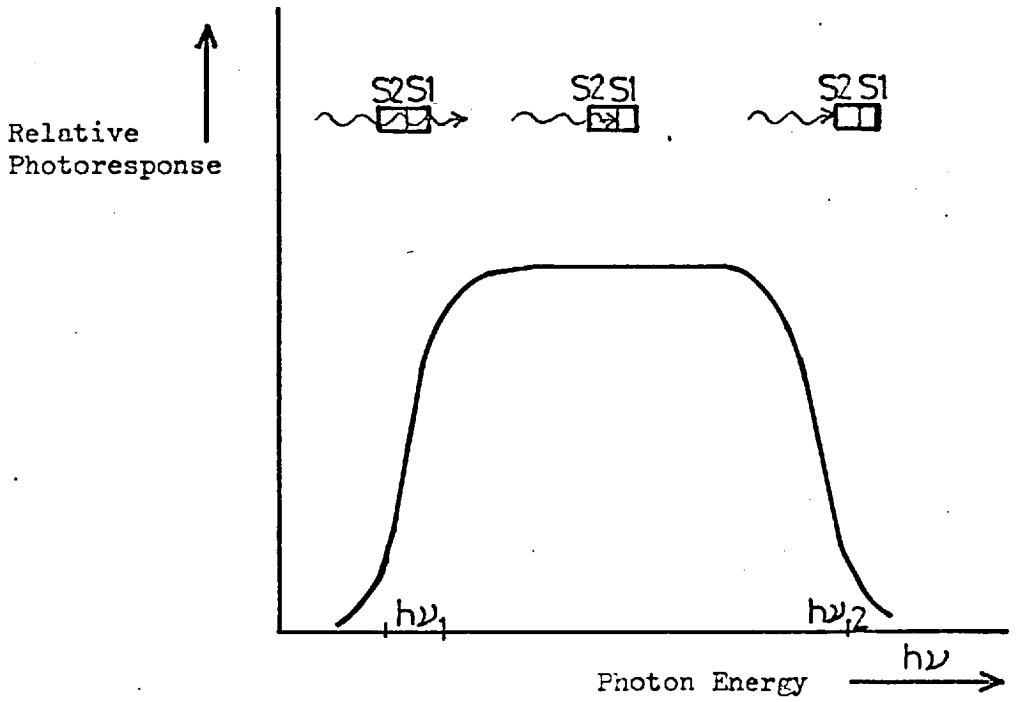


Fig. 5.20 Spectral Photoresponse Illustrating the "Window Effect".

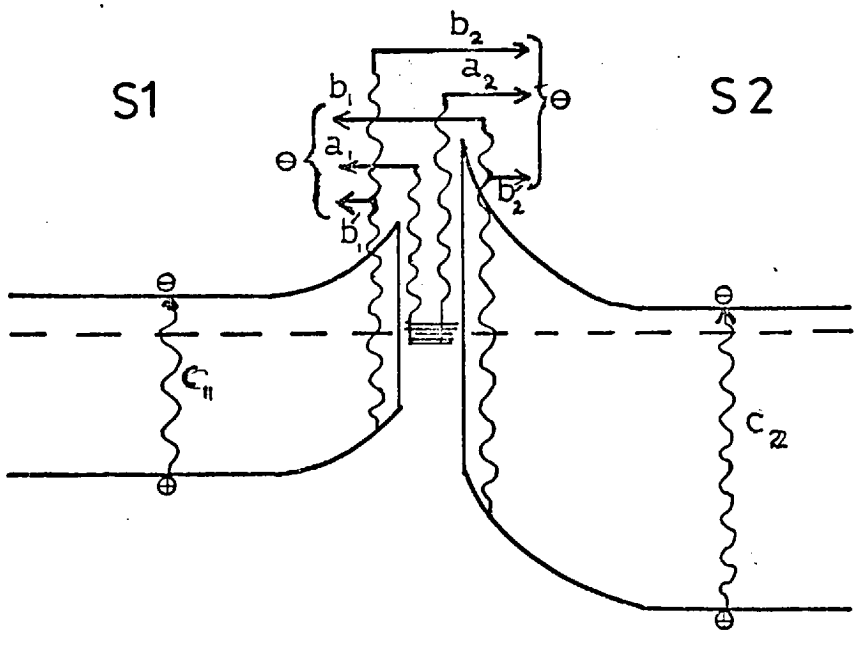


Fig. 5.21 Possible Photoexcitation Mechanisms in an Abrupt n-n Heterodiode Having Large Interface State Density

structures because the accumulation layer is incapable of supporting a large diffusion voltage, especially under reverse bias as compared with the equivalent depletion layer in the anisotype diode.

Interface states inevitably cause a reduction in the photo-conversion efficiency not only because of recombination losses, but also by distorting the band profile making efficient photo-emission less favourable. The band profile of an illuminated double-depleted n-n heterodiode is shown in Fig. 5.21. The processes in the wide-gap material, S2, dominates those in S1.

The sign reversal of the photoresponse observed in the double depleted nGe-nSi diodes fo Donnelly and Milnes (1966), Van Opdorp (1967, 1969) is direct evidence of the oppositely directed built-in fields on either side of the interface. In the diagram, process a_2 and b_2 give opposite photoresponse to a_1 and b_1; the sign reversal results as the dominant processes change from one to the other.

5.5 Conclusions

The Poissons equation for the isotype heterojunction of abrupt structures with and without interface states and of the graded structures has been solved numerically using approaches similar to those of Czerveny (1968) and Kumar (1968) (Abrupt case without interface states) and Oldham and Milnes (1963) (Graded Case). From these solutions accurate band profiles can be drawn and junction capacitance predicted. The C^{-2} against V plots are determined by the depletion layer in the wide-gap material.

Carrier transport mechanisms have not been fully developed and there are many theories to explain current flow. This is not surprising since the mechanisms of current flow can be very different for devices with slightly different properties. At low biases, because the barrier spike is narrow and thermal energy insufficient to emit many carriers over the top, tunnelling mechanisms may be important. At higher forward

bias, as the spike widens, the tunnelling probability is reduced; at the same time sufficient carriers will be thermally emitted over the barrier. At still higher forward bias, the spike becomes negligible in comparison to the step potential and current flow will be dominated by diffusion.

At increasing reverse bias Zener tunnelling will occur. It is therefore difficult to derive an expression to predict current over a full range of voltages. In addition, the reflection coefficient, X, has not as yet been verified for heterojunctions.

Interface states and grading at the junction are considered to degrade the performance of a device. Interface states distort the band profile, transforming an accumulation to a depletion layer, if present in sufficiently large numbers. They act as recombination centres and can deominate electrical behaviour particularly of isotype heterojunctions. Grading causes a reduction of the rectifying barrier in the conduction band edge at the interface. However, it also helps to remove strain at the junction during the growth process. It has been suggested that a slight grading at the junction can serve as an 'anti-reflection' coating for carriers. Tunnelling can also degrade the device by effectively reducing the barrier, giving rise to properties as 'soft' breakdown.

For $CdSe/CdS_xSe_{1-x}$ diodes, since the barrier height is greater than a few $\frac{kT}{q}$ units, and the depletion layer $\sim$ 0.5 μm, carrier transport is expected to be controlled by thermal emission. It was hoped that the dominant mechanism would be obtained from experimental I-V characteristics.

REFERENCES - CHAPTER 5

Blakemore, J. S. (1962) Solid State Physics. p.360 Pergamon Press.

Chang, L. L. (1965) Sol. St. Electron 8, 721.

Czerveny, S. I. (1968) Int. J. Electron 25, 65.

Donnelly, J. P., Milnes, A. G. (1965) Proc. IEEE 53, 2109.

Donnelly, J. P., Milnes, A. G. (1966) Sol. St. Electron. 9, 174.

Donnelly, J. P., Milnes. A. G. (1967) IEEE Trans. Electron. Devices ED-14, 63

Fang, F. F., Howard, W. E. (1964) J. Appl. Phys. 35, 612.

Hampshire, M. J., Wilson, G. A., Chadda, M. M. (1968) Brit. J. Appl. Phys. (J. Phys. D) 1, 853.

Hampshire, M. J., Tomlinson, R. D. (1970a) Sol. St. Electron 13, 41.

Hampshire, M. J., Tomlinson, R. D. (1970b) Proc. Int. Conf. Phys. Chem. Semicond. Heterojunctions Layer Structures, Budapest, 1970 2, 323.

Kumar, R. C. (1968a) Sol St. Electron 11, 543.

Kumar, R. C. (1968b) Int. J. Electron 25, 239.

Mammana, C. I. Z., Anderson, R. L. (1970) Proc. Int. Conf. Phys. Chem. Semicond. Heterojunctions Layer Structures, Budapest, 1970 1, 279. Hung. Acad. Sciences, Budapest, Hungary.

Newman, P. C. (1965) Electron. Lett. 1, 265.

Oldham, W. G., Milnes, A. G. (1963) Sol St. Electron. 6, 121.

Oldham, W. G., Milnes, A. G. (1964) Sol. St. Electron. 7, 153.

Perez, E. J. (1972) Ph.D. Thesis, Univ. of London.

Price, P. J. (1962) Proc. Int. Conf. Phys. Semicond., Exeter, 1962, p.99.

Rediker, R. H., Stopek, S., Ward, J. H. R. (1964) Sol St. Electron 7, 621.

Tansley, T. L. (1966) Phys. Status Solidi 18, 105.

Tansley, T. L. (1969) Optoelectronics 1, 143.

Tansley, T. L. (1971) Semiconductors and Semimetals, ed. Willardson, Beer 9, 293, Academic, N.Y.

Van Opdorp, C. (1969) Philips, Res. Rep. Suppl. No. 10.

Van Opdorp, C., Kanerva, J. K. J. (1967) Sol. St. Electron 10, 401.

Van Ruyven, L. J. (1964) Phys. Status Solidi 3, K109.

Van Ruyven, L. J. (1972) Annual. Rev. Mat. Sci. 2, 501.

Womax, J. F., Rediker, R. H. (1972) J. Appl. Phys. 43, 4129.

Zased, V. S. (1969) Sov. Phys. Semicond. 2, 1538.

Zeidenbergs, G., Anderson, R. L. (1967) Sol. St. Electron 10, 113.

CHAPTER 6 - RESULTS AND DISCUSSIONS

The electrical properties of the constituent materials and their alloys have been fully discussed in Chapter 3. The two materials are completely miscible and form alloys under suitable conditions, whose electrical properties vary approximately linearly with the anion molar ratios i.e. they obey Vegard's law.

In order to deduce accurately the band profiles for the heterodiodes, additional information is needed from heterojunction properties, in particular C-V measurements. This data enables values of contact potential, V_D, and hence ΔE_C and ΔE_V to be determined. These values are compared with the predicted ΔE_C from electron affinity differences.

A study of the band profiles and the analysis of I-V characteristics can determine the dominant type of charge carrier transport in this type of heterojunction. It was expected that for $CdSe/CdS_xSe_{1-x}$ diodes in which $x > \frac{1}{3}$, the emission model would be the most probable especially for low and moderate forward bias. At higher biases other types of mechanisms are possible.

Photoresponse measurements produced only limited information which included the energy gaps of the constituent materials and nature of the space charge region. The diodes exhibited only slight photosensitivity due to the absence of sufficient photosensitizing impurities e.g. halogen impurities. The photo-voltages generated when the samples were illuminated with a 'bright' tungsten filament bulb was only $\sim$2mV.

In attempting to give a rigorous analysis of $CdSe/CdS_xSe_{1-x}$ heterodiodes, it should be noted that of the numerous variables which affect the electrical properties of the devices only some can be reasonably well controlled. The variables of interest are:

(i) the quality, purity and stoichiometry of the grown crystals.

(ii) orientation of the substrates cut from these.

(iii) damage created by mechanical polishing.

(iv) effect of the chemical polish on the surface of the substrate.

(v) amount of desorption of impurity gases (e.g. O_2) prior to epitaxy.

(vi) effect of epitaxial conditions on the substrate (e.g. grading as a result of temperature or implantation).

(vii) effect of the substrate on the epitaxially grown film (e.g. mismatch dislocation).

(viii) crystalline properties of the epi-layer by sputtering.

(ix) mechanical strain caused by cooling from the growth temperature (due to differences in coefficient of expansion of the two materials).

(x) ohmic contacts and effective diode area.

Since comparison of the different types of diodes is very important in this analysis elaborate measures were undertaken to attempt to control as many of the important variables as possible in the fabrication of the devices.

There is little difference in the quality of the crystal substrates (Section 2.4) though carrier concentration varied from 5×10^{15} to 10^{16} cm^{-3}. Substrates were all cut in the basal plane so that the effect of crystal orientation on diode properties (Fang and Howard, 1964) was eliminated. Although three different chemical polishes were used on the CdS, CdSe and alloy substrates (Section 4.2) it is not believed that the 'cleaned' surfaces would vary greatly. However, adsorption coefficient of oxygen onto the basal plane of CdS and CdSe would depend on whether the Cd or the S/Se ions are on the surface. For Cd, the adsorption would be the same for both crystals. The adsorption for S is very small, but that for Se is unknown (Green, 1973).

Baking at 350°C at 10^{-5} torr for 2 hours, should desorb most of the adsorbed gases. It will be seen later that the conditions under which the epi-layer was grown gave rise to a grading in carrier concentration at the junction. The restivity of this layer, as discussed in Section 3. , was expected to be high, $\rho = 10^3 \Omega$-cm with $\mu_H \sim$ 10-20 cm^2/V-sec, giving a

carrier concentration of $\sim 5 \times 10^{14}$ cm^{-3}. This carrier concentration should have some effect on the forward bias current. The lattice mismatch between CdSe and CdS is 3.8% and, therefore, between CdSe and CdS_xSe_{1-x} will vary linearly with molar ratio, x to 0% when x = 0. However, many of the dangling bonds are likely to be saturated by residual O_2 and other impurity atoms so that the expected effect of lattice mismatch on electrical characteristics may be less. By using a slow cooling cycle (initially 20°C/hr) it was hoped that the amount of mechanical strain could be reduced, especially as the coefficient of expansion for CdS and CdSe are 4 and 4.8×10^{-0} C^{o-1} (at room temperature). A certain amount of elastic distortion of the lattice will result instead.

6.1 C-V Measurements and Deduction of Energy Band Profiles

6.1.1 C-V Measurements

The reverse bias junction capacitance, C, of the heterodiodes were measured by the method discussed in Section 4.5, and are illustrated in fig. 6.1 at frequencies in the range 1.6 KHz to 1 MHz. It can be observed that the capacitance decreases by a factor of approximately two as the frequency is increased from 1.6 to 1 MHz. This can be explained by the impurity levels in CdS_xSe_{1-x} substrates possessing individual time constants, some of which may be too long so that at high frequencies the trapping and releasing of carriers will not be able to follow the applied signal.

In determining the contact potential, V_D, of the devices it is normal to plot $1/C^2$ against applied bias at low frequencies (Hovel and Milnes, 1968) and the extrapolation of the straight line region of the graph to the V-axis gives a measure of V_D. This is illustrated in Fig. 6.2 for the $CdSe/CdS_xSe_{1-x}$ diodes, however, these values of V_D are not in agreement with predicted values, being much too large. If, however, log C-log $(V + V_D)$ plots are made, two straight lines of gradient $-\frac{1}{2}$ and $-\frac{1}{3}$ for high and low biases, respectively are observed. This indicates

Fig. 6.1a.

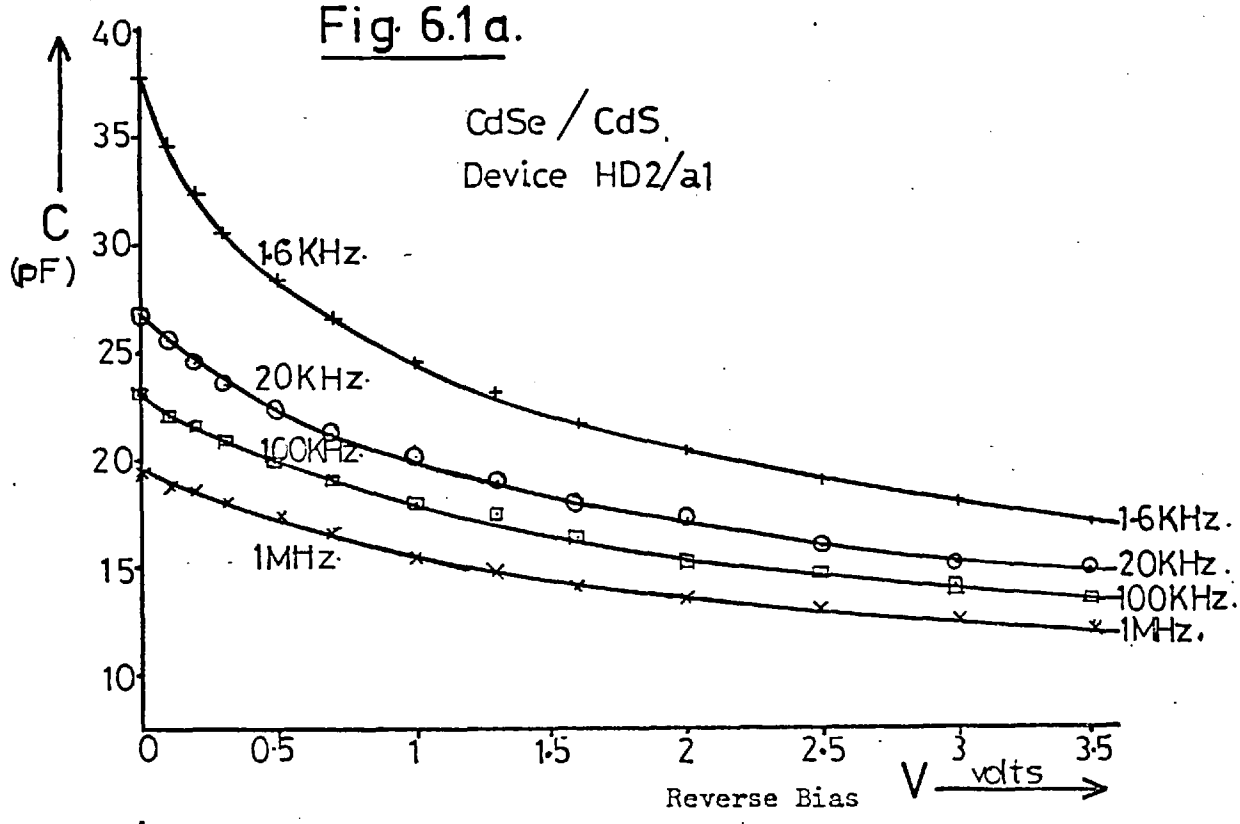
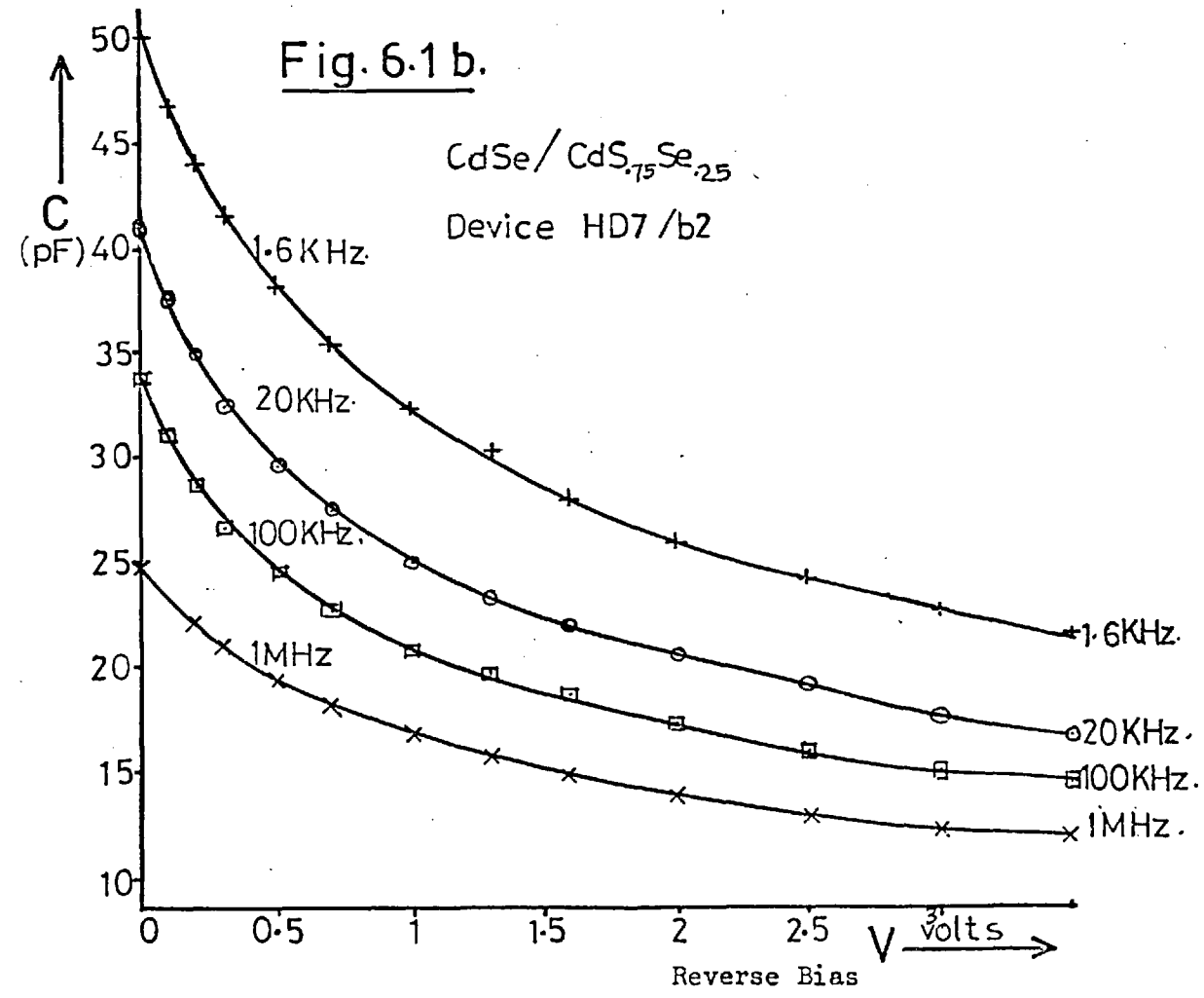
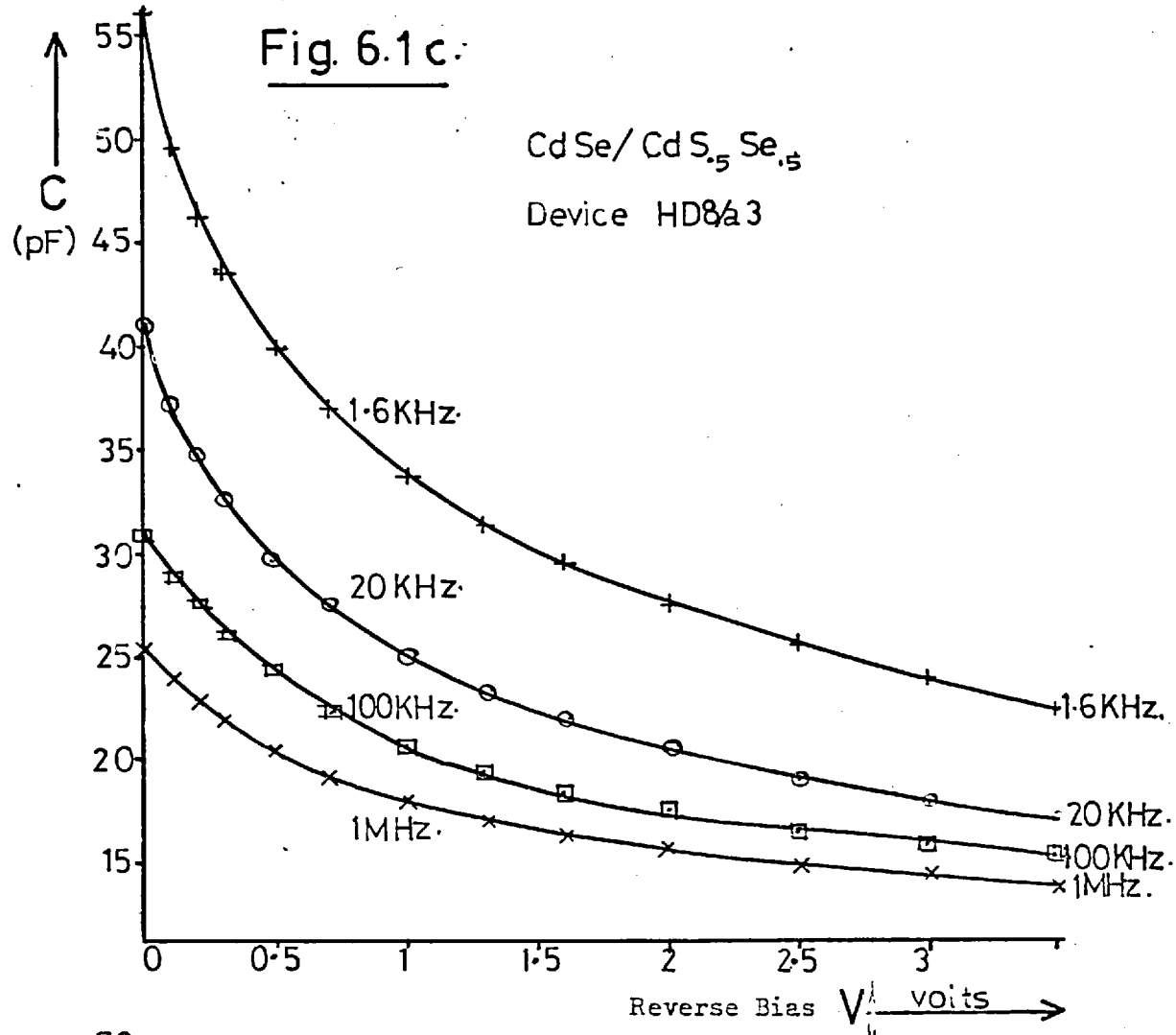


Fig. 6.1b.





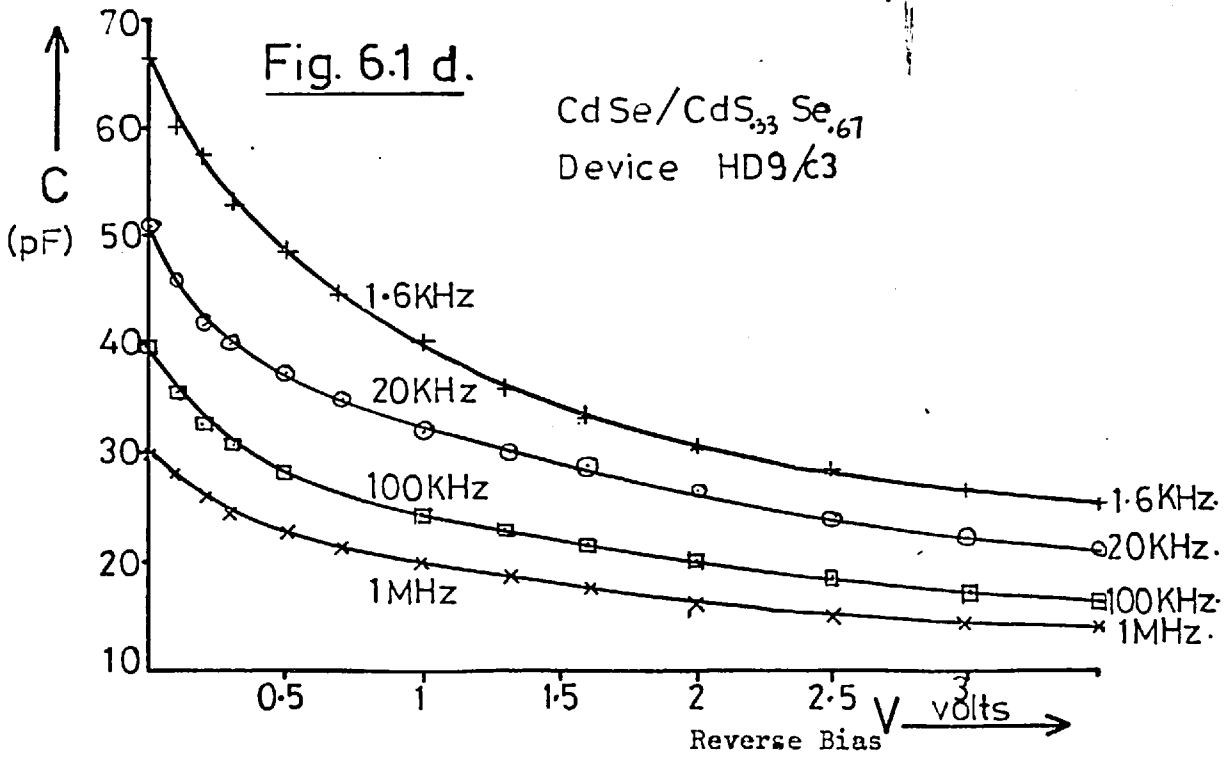


Fig. 6.1 C-V Characteristics of $CdSe/CdS_xSe_{1-x}$ Heterodiodes
(a) x = 1, (b) x = .75, (c) x = .5, (d) x = .33

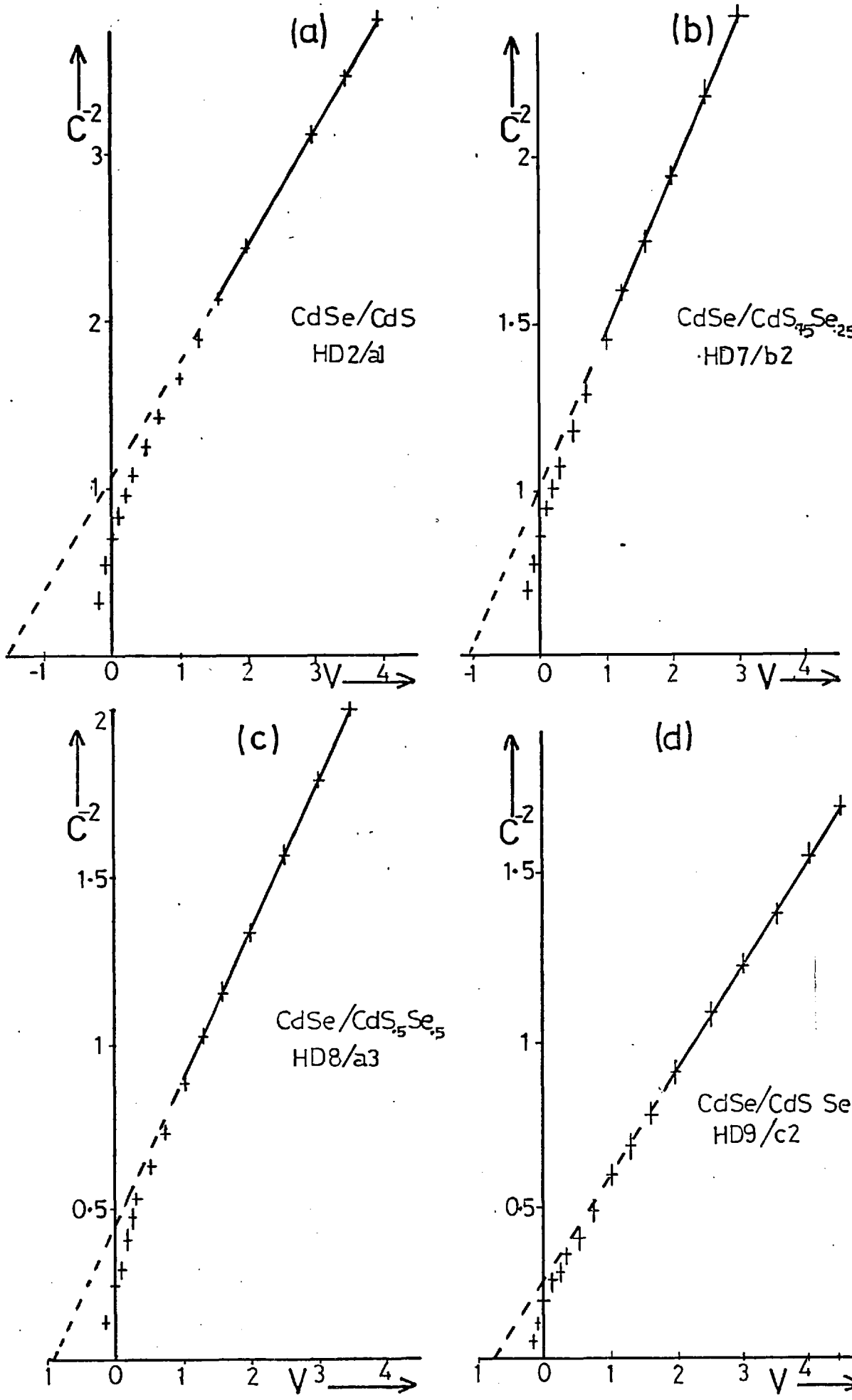


Fig. 6.2 Capacitance (of Fig. 6.1) Re-plotted as C^{-2}-V, (a) x = 1, (b) x = .75, (c) x = .5 (d) x = .33

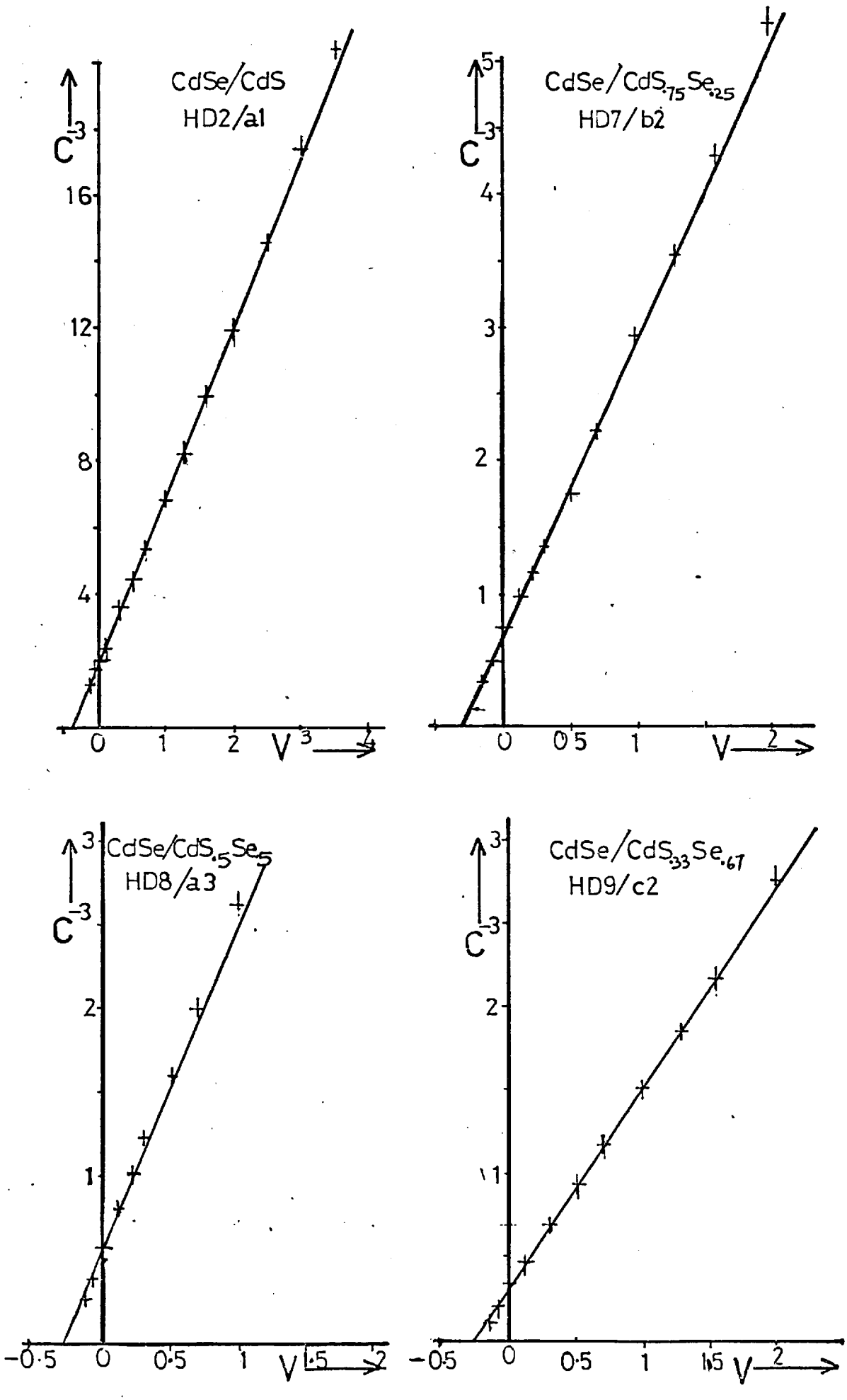


Fig. 6.3 Capacitance of Fig. 6.1 Re-plotted as C^{-3}-V

that the junction is graded linearly in carrier concentration over part of the voltage range (for the $-\frac{1}{3}$ gradient) and at the point of the change in slope corresponds to the superimposition of the depletion layer edge with the graded region edge.

The width of the grading in the depletion region is determined approximately by the relationship $x = \frac{\epsilon A}{C}$, where A is the diode area and C, the capacitance at a voltage corresponding to the change of slope. x is thus found to be ~ 0.5 μm for the devices.

At very low reverse and small forward biases, the depletion layer is small and the gradient of the log C-log V plots is further reduced to $\frac{1}{n}$ where $n>3$, indicating that the region here is becoming more graded (closer to the interface). A C^{-n} - V plot would then give a more accurate value of V_D than either a $1/C^2$ or $1/C^3$ plot. This is because an applied bias equal and opposite to V_D would reduce the depletion depth to zero making C infinite, and this voltage need not be that obtained by extrapolation of the $1/C^2$ or $1/C^3$ plots. However, at forward biases, capacitance values are difficult to measure accurately because of high conductances. In addition, because of non-negligible voltage drop in the accumulation layer, the change in capacitance is smaller than expected giving rise to a slightly higher intercept on the V-axis. This could be one reason why V_D values for all the diodes are higher than predicted values. Another explanation could be the presence of interface states which lead to a reduction in capacitance as they increase the depletion layer widths.

Many experimentalists who have obtained descrepancies between measured and predicted values at V_D have attributed this to presence of interface states and have ignored any possibility of shallow grading within or outside the edge of the zero bias depletion layer (Tansley, 1971; Demoulin and Van De Wiele, 1970; Van De Wiele and Van Overstraeten, 1967).

The values of V_D for the heterodiodes are measured experimentally by the extrapolation of the low voltage region of the $1/C^3$ versus V curves of Fig. 6.3. These values are only just higher than predicted values. The sloper of the $1/C^2$ versus V plots (of Fig. 6.2,) g, indicate doping levels in the substrates, S2, by $g = \frac{\partial(C^{-2})}{\partial V} = \frac{2}{A^2 q \epsilon N_{D2}}$. These values are listed in Table 6.1.

It should be noted that a graded heterojunction does not necessarily mean a grading in carrier concentration (see definition of pg. 1). If $N_{D1} \simeq N_{D2}$ for a heterojunction with grading in composition, then $1/C^2$-V plots are continuous straight lines to give correct values of V_D. Some authors have stated that if $1/C^2$-V gives a straight line, then the junction is abrupt; this is therefore not strictly true unless $N_{D1} \simeq N_{D2}$.

A grading in composition of the junction would have the effect of producing a reduction in the barrier height. This effect is not evident in determining V_D from $1/C^2$-V plots, but since other factors mentioned above have the effect of increasing V_D, a grading in composition over a few hundred Å units may not be detected.

The number of interface states is considered small compared to the critical value defined by equation 5-29, since capacitance measurements are not independent of bias at higher frequencies and the forward bias capacitance is very high.

When considering C-V measurements of $CdSe/CdS_xSe_{1-x}$ diodes as a function of molar ratios, x, it is observed that capacitance at a particular bias and frequency increases as x decreases (Fig. 6.1), because capacitance, C, given by a first order approximation $C^2 = \frac{Aq\epsilon N_{D2}}{2(V_D - V)}$ (more accurately when $N_{D1} > N_{D2}$) will depend on ϵ_2, and N_{D2} for the same diode area. For devices under consideration, ϵ_2 and N_{D2} increase while V_D decreases, as x becomes smaller, hence C increases.

6.1.2 Deduction of Energy Band Profiles of CdSe/CdS_xSe_{1-x} Heterodiodes

The room temperature equilibrum energy band profile of the CdSe/$CdSe_xSe_{1-x}$ diodes, assuming they obey the abrupt junction model is illustrated in Fig. 6.4 where the electrical parameters in the bulk of the CdSe layer is constant for all devices. The Table 6.1 lists the remaining values of the relevant properties for the substrates used.

The values of the electron affinities, X, of the different CdS_xSe_{1-x} substrates is very critical in determining shape of the band profiles for these diodes. Values of 4.79 and 4.95 were chosen from the literature for CdS and CdSe, respectively, as being the most quoted and a linear variation of X with molar ratio is assumed ΔE_C is therefore very small, and the barrier can change from positive reverse to negative reverse if x is inaccurate by 0.5% for the diode $CdSe/CdS_{\frac{1}{2}}Se_{\frac{1}{2}}$.

Due to the increase in both carrier concentration and dielectric constant as the molecular ratio x decreases, a larger proportion of the zero bias potential (determined by equation 5-17) is dropped across the accumulation layer S1, resulting in little variation of V_{D1} (See Table 6.1).

The position of the top of the rectifying barrier in the conduction band edge relative to the bulk level of conduction band in S1 (CdSe) will depend on the magnitudes of V_{D1} as compared with ΔE_C. In other words if $qV_{D1} < \Delta E_C$ then a positive reverse barrier exists. This occurs (see Table 6.1) when mole ratio $x > \frac{1}{2}$. When $x = \frac{1}{2}$, the height of the spike coincides with the level of conduction band in the bulk of S1. When $x < \frac{1}{2}$, then the spike appears below E_{C1} and a negative reverse barrier exists for the device. Hence, the expected carrier transport mechanisms would be the emission for devices with $x > \frac{1}{2}$ and diffusion for $x < \frac{1}{2}$.

If the junction is graded in material composition, as discussed in Section 5.2.3, then for rectification to occur, the graded width must be $\lesssim$ 0.1 μm as determined from equation 5-37. The junction width has become an important variable in this analysis and, therfore, great

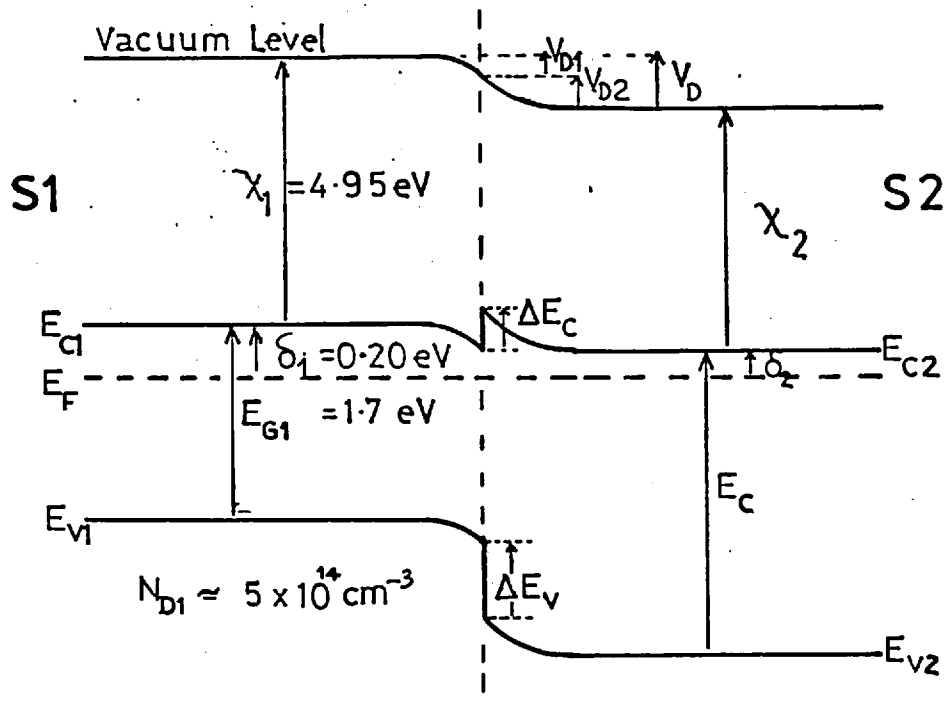


Fig. 6.4 Band Profile of the $CdSe/CdS_xSe_{1-x}$ Heterojunctions

Table 6.1 Electrical Parameters in Constructing the Band Profile

S2 Material	Carrier Conc. in S2 $\times 10^{15}$ cm^{-3} (a)	(b)	Electron Affinity in S2 (eV) (c)	ΔE_C (eV) (c)	δ_2 (eV)	ΔE_V (eV) (c)	V_D (volts) (d)	V_D (volts) (e)	V_{D1} (volts) (f)
CdS	5	6.8	4.79	0.16	0.16	0.56	0.20	0.35	0.09
$CdS_{3/4}Se_{1/4}$	6.9	7.5	4.83	0.12	0.15	0.42	0.17	0.25	0.09
$CdS_{1/2}Se_{1/2}$	8	8.5	4.87	0.08	0.14	0.24	0.14	0.25	0.08
$CdS_{1/3}Se_{2/3}$	10	12	4.91	0.04	0.13	0.14	0.13	0.2	0.08

(a) From Schottky diode measurements.
(b) From Slope of C^{-2}-V curves.
(c) Assuming Linear Variations with composition in substrate.
(d) From equation (5-18)
(e) From C^{-3}-V plots.
(f) From equation (5-17)

care was taken to determine its value.

The samples were cross-sectioned at an angle of abour 45^{o} to its edges and the junctions were investigated for grading. Scanning electron microprobe analysis could not resolve such a small length (Fig. 5a). The samples were also illuminated by incident light on a high powered microscope (magnification = 1.5K) (Fig. 5.6b) and regions at the interface were studies but no graded regions were observed. It can be inferred that if such a graded region existed, it would be < 500 Å. Investigators working on the CdSe/CdS system have, however, reported possible composition grading of the junction where epitaxy was performed at slightly elevated temperature (Gasanov et al, 1974).

6.2 I-V Characteristics

As mentioned earlier, the expected charge carrier transport mechanism is thermal in nature (i.e. mainly emission (for $x > \frac{1}{2}$) and diffusion for $x < \frac{1}{2}$).

All the devices fabricated, with the exception of the CdSe/CdS diodes exhibited rectification as observed on a Tektronix curve tracer 576 and illustrated in Fig. 6.6 for a typical CdSe/CdS diode. The semilogarithm dark forward I-V characteristics of each type of diode is shown in Fig. 6.7 and was obtained as described in Section 4.5 in the temperature range from 360^{o}K to 185^{o}K, by positively biasing the CdSe layer. The semilogarithm plots show strong thermal dependence of current. Such plots are normally used to determine the value of η from the emission or diffusion expression $I = I_0 \exp \frac{qV}{\eta kT}$, where η has a theoretical value between 1 and 2. However, the plots for all $CdSe/CdS_xSe_{1-x}$ diodes are not straight lines and even if tangential straight lines are drawn to the curves the value of n varies continuously from $\simeq 1$ to values > 10. Since all three carrier transport mechanisms in heterojunctions exhibit exponential dependence of voltage with current, it seems certain that the charge transport is space-charge-limited by

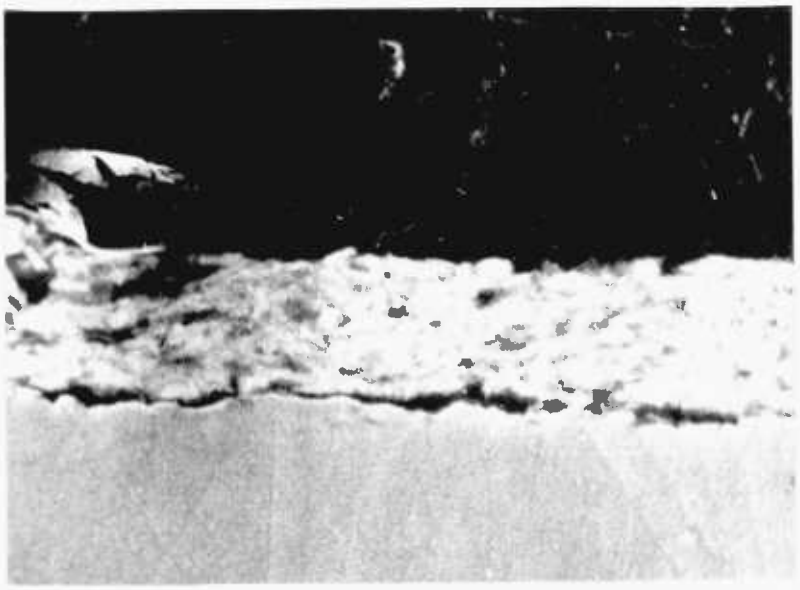


Fig 6.5a. SEM Photograph of the CdSe/CdS Interface.

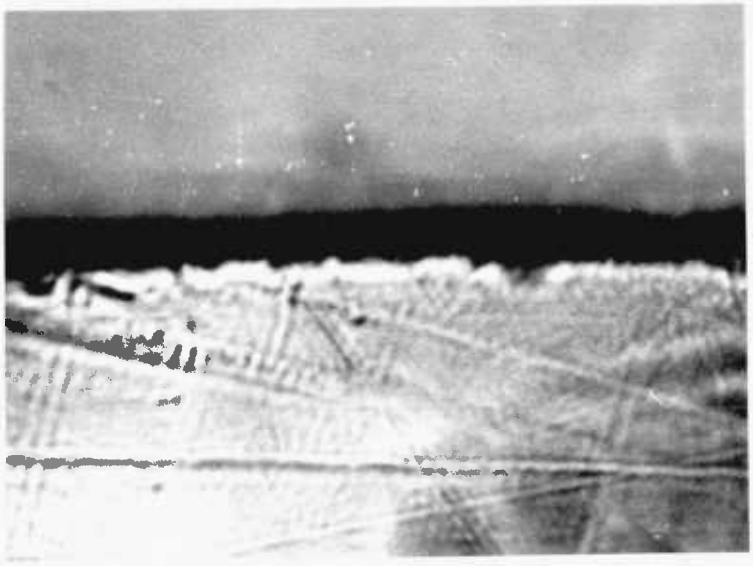


Fig 6.5 b. Optical Microscope Photograph of the CdSe/CdS Interface.

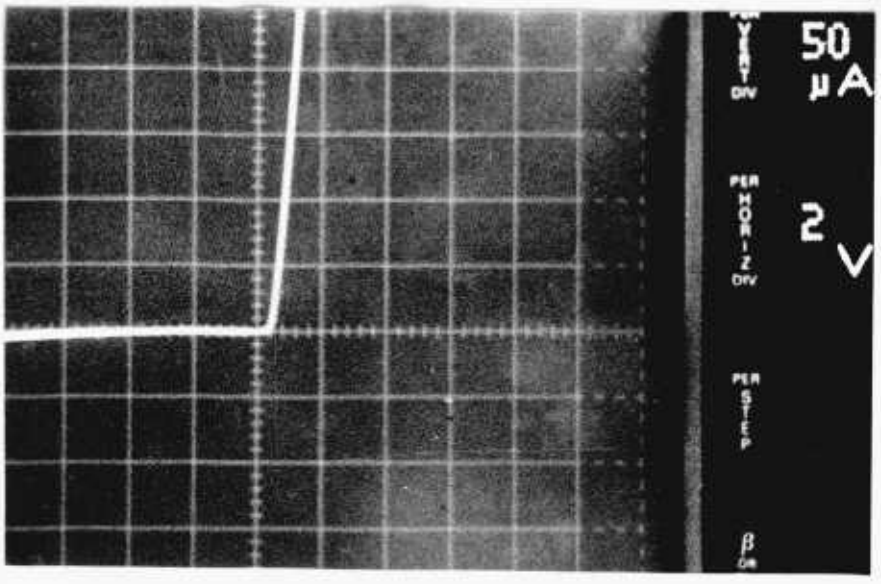


Fig 6.6. A Typical I-V Characteristic of a CdSe/CdS Heterodiode.

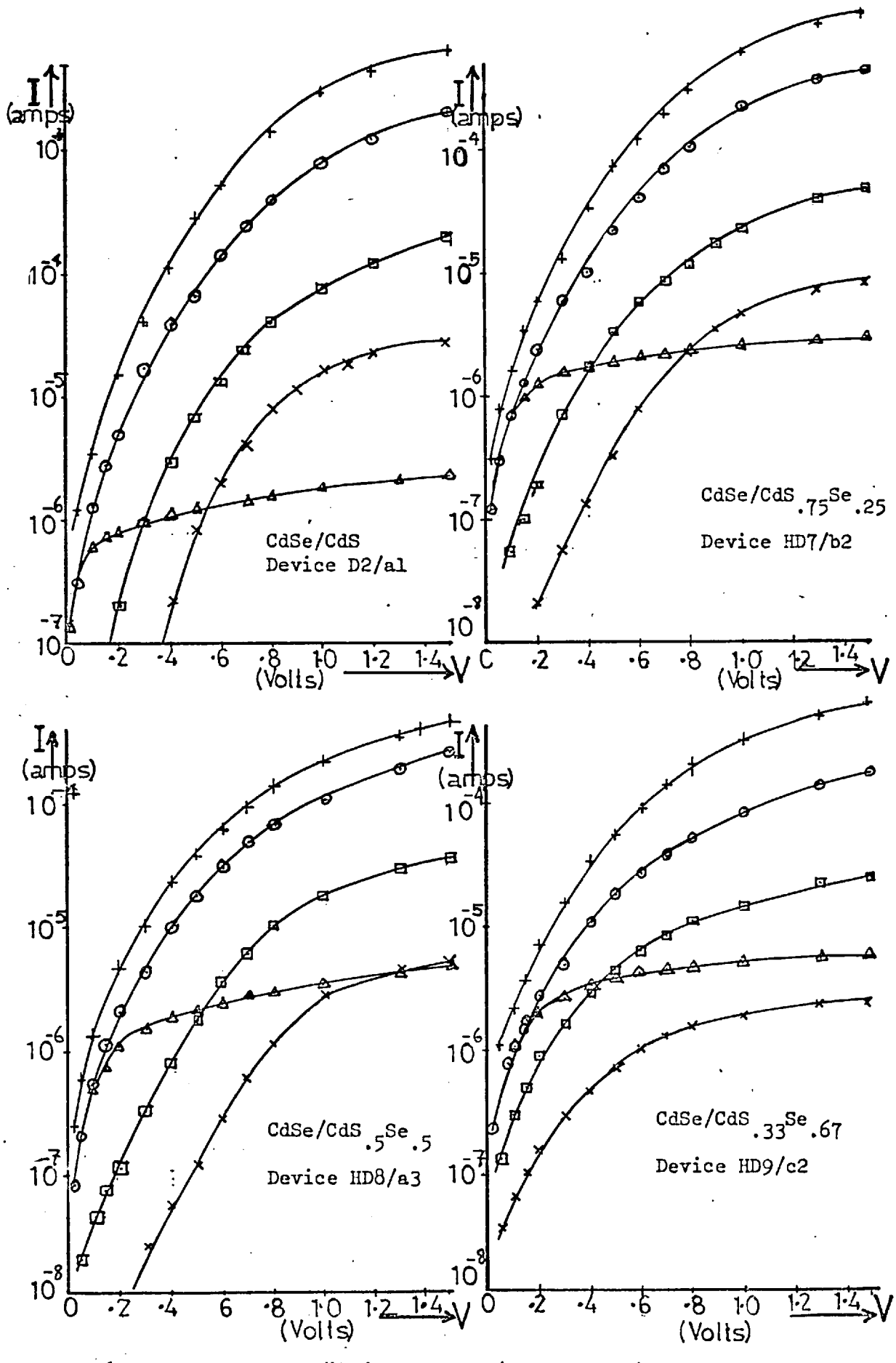


Fig. 6.7 I-V Characteristics of $CdSe/CdS_xSe_{1-x}$ Diodes

(Forward Current: + -330°K, 0 -298°K, -235°K, X-185°K)
(Reverse Current: -298°K

the highly resistive CdSe film. Such properties of CdSe/CdS diodes have been observed by Perez (1971), Pavlenko and Muzalevskii (1971), Konozenko et al (1970). In order to confirm a space-charge-limited mechanism it is necessary to replot I-V characteristics on a log-log chart as in Fig. 6.8 for the typical diodes at room temperature where different slopes are observed. The theory of space-charge limited currents has been explained in great details by such investigators as Lambert (1956) and Rose (1955) and as discussed in Section 3.8. Analysis of the graphs for the CdSe/CdS_xSe_{1-x} diodes (Fig. 6.8) shows an ohmic region (slope 1) for small voltages up to about 0.1 volt. This region has been explained by Hovel and Milnes (1968) for ZnSe/Ge as arising from surface leakage or from low level junction phenomena.

However, if grain boundaries do exist in these films across which carriers travel, then an ohmic region is obtained from barrier limited conduction at low biases. Fisher (1973) has shown that conductivity in thin CdSe films is limited by intercrystallite boundaries creating double potential barriers (the type described by Milnes, (1972) which affect current flow). The barriers under equilibrum and quasi-equilibrum conditions are illustrated in Fig. 6.9. In addition, since the resistivity of the CdSe film is high, suitably orientated grain boundaries will act as conduction paths.

The measured resistance of the ohmic region is high $\sim 10^5$ ohms being approximately 100 times larger than that of the CdSe layer. This can perhaps be explained as the transmission coefficient, X, of incident carriers at the interface being 10^{-2}.

Between 0.1 and 0.2 volts at forward bias, the slope of the curve changes to 2 and shows the current becoming space charge limited. Following this square law variation at $\sim$ 0.3 - 0.5 volts is a region where the current varies with voltage of powers from 3.5 to 2.4 for the devices and this represents the trap filling region. The current here is given

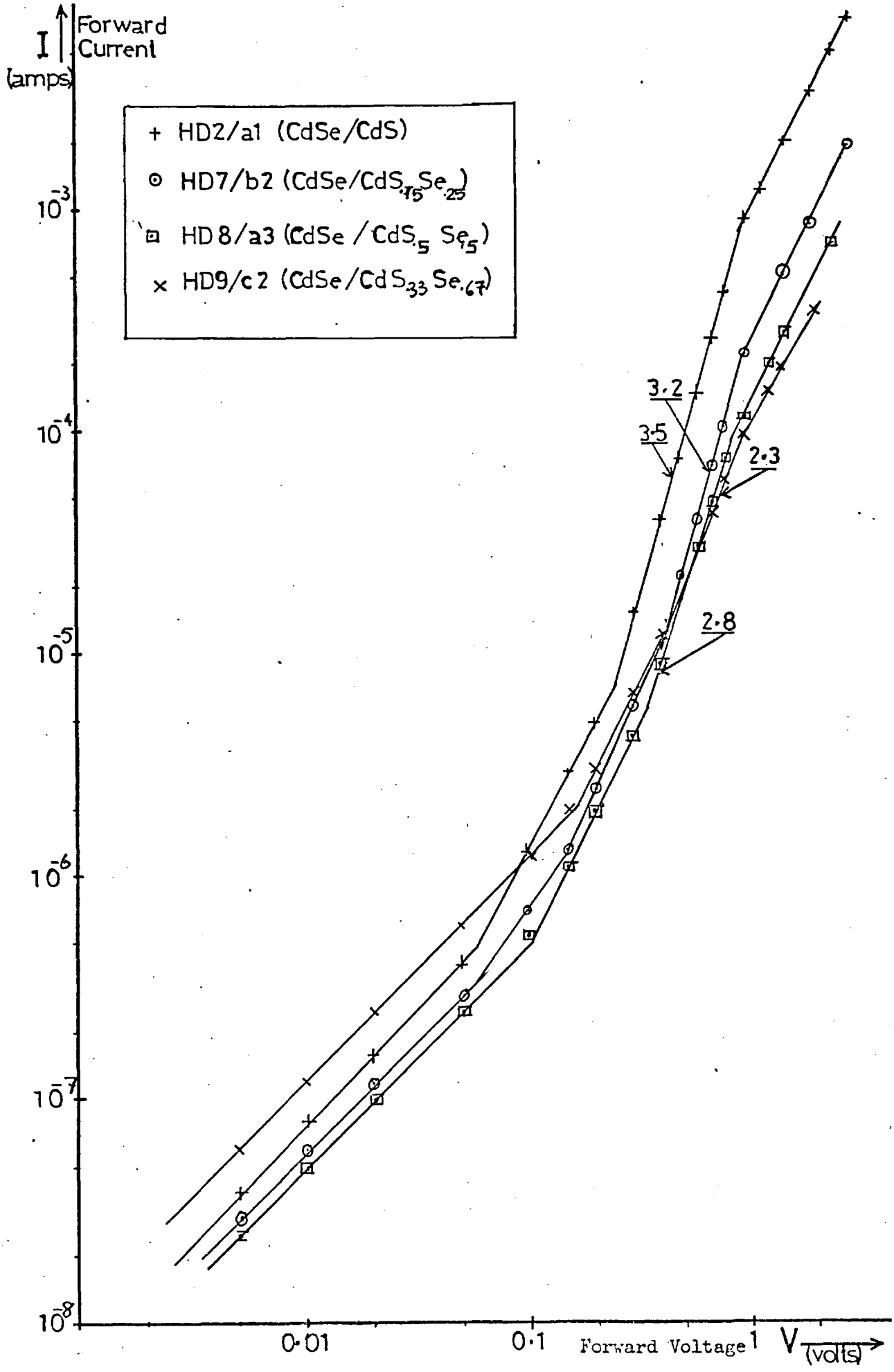


Fig. 6.8 Room Temperature Log I-Log V Characteristics of $CdSe/CdS_xSe_{1-x}$ Diodes

by the expression $J = \frac{9\mu\epsilon V^2}{8L^3}$ where L is the film thickness. When all the traps are filled i.e. when bias is just sufficient for this process, corresponding to voltage V_{TFL} of values $\sim$ 1 volt, the power returns to 2, and the current is described as trap-filled, space-charge-limited and the total trap density is given by $N_t = \frac{V_{TFL}}{qL^2}$. The value of N_t is approximately 5×10^{14} for the devices. It should be noted that as molar ratio x, decreases, so does the barrier height and hence, more voltage is dropped across the film, making N_t values here more accurate. Returning to the trap filling region, it is not understood why the slope decreases from 3.5 to 2.4 as x is reduced from 1 to $\frac{1}{3}$. Another point worth noting is that as x decreases, the transmission coefficient, X, should increase and, hence, the ohmic region should be higher. For devices where x = $\frac{3}{4}$ and $\frac{1}{2}$, this is not observed, the ohmic part being lower. A possible explanation for this is that the CdSe film thickness is probably greater for these devices.

It is thus observed that the forward I-V characteristics is due essentially to the bulk properties of the CdSe layer, so the transport properties, due solely, to the junction, cannot be determined. Although no rectification was observed for the CdSe/CdSe devices, which was expected, a value for the resistivity of the CdSe layer was estimated as $\sim 10^3$ Ω- cm.

If the temperature dependence of current is examined for fixed bias voltages then the slope of $I / \frac{1}{T}$ graph for a crystalline semiconductor would give a measure of the activation energy $(E_C - E_D)$ i.e. the energy between donor level and bottom of the conduction band. This energy for the $CdSe/CdS_xSe_{1-x}$ diodes (Fig. 6.10) is roughly estimated as (0.26 $\pm$ .03) eV at a low bias value of 0.2 volts, and is larger than the predicted value of (0.15 $\pm$ 0.02) eV associated with selenium vacancies since CdSe grows naturally with excess Cd. Since no donors are associated

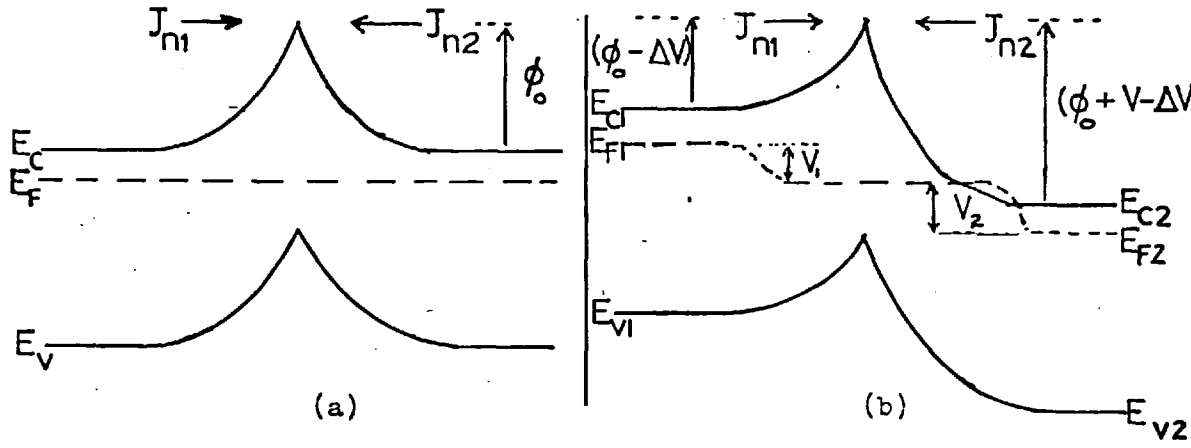


Fig. 6.9 Proposed Barrier Limited Conduction in the CdSe Epi-layer under (a) Equilibrum (b) Quasi-Equilibrum Conditions (After Miles, 1972)

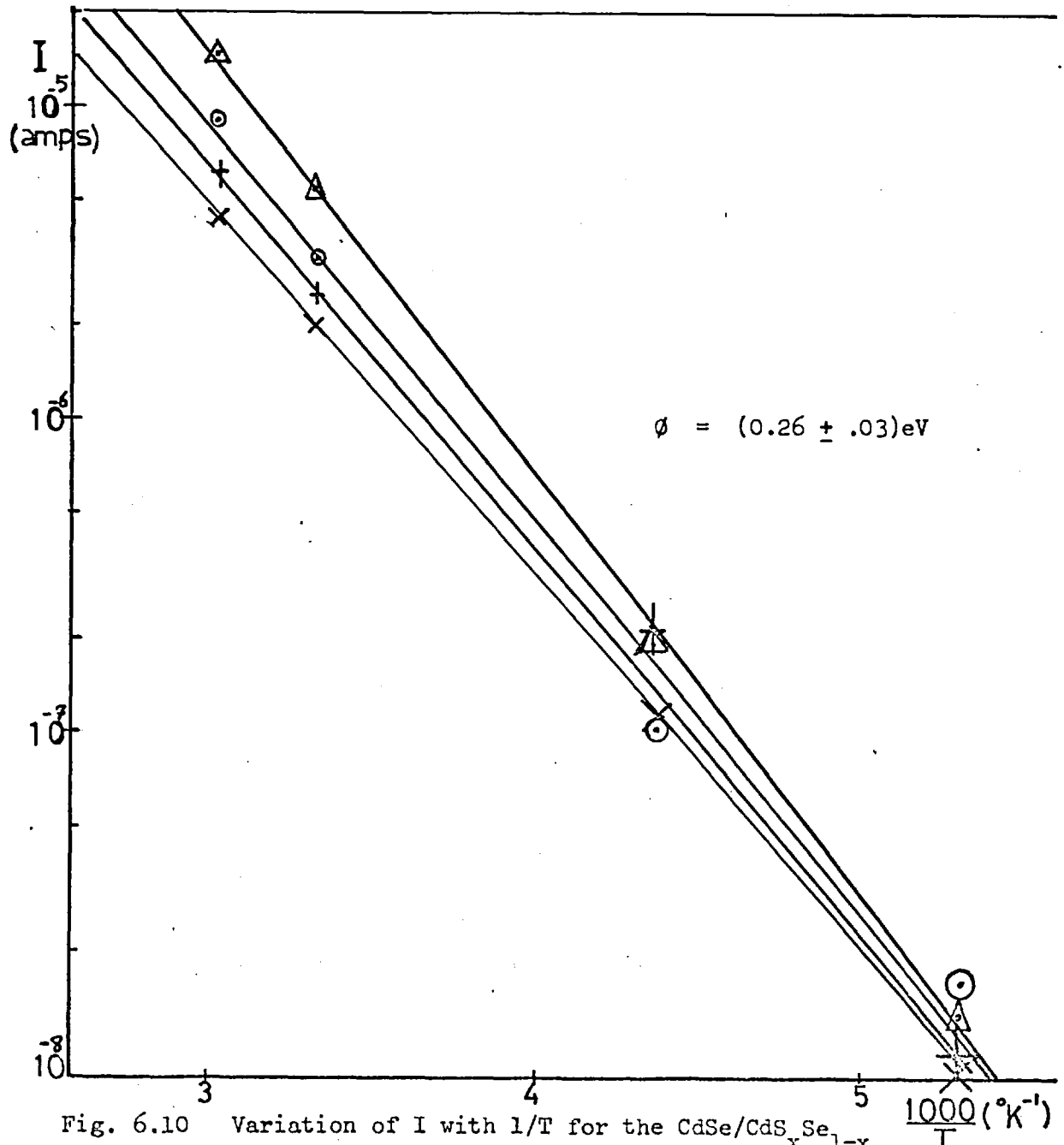


Fig. 6.10 Variation of I with 1/T for the $CdSe/CdS_xSe_{1-x}$ Devices

with the 0.26 eV level, it further suggests the existence of grain boundaries giving rise to double potential barriers in the CdSe films. Similar results have been obtained for evaporated CdSe films on glass substrates after being annealed by Fisher (1973) and Yates (1974). At higher voltages the activation energy becomes smaller. Note that because of the unexplained decrease in power of V for the trap filling region as x decreases no significance can be attached to the results for diodes at higher voltages.

The reverse bias I-V characteristics are of less importance than the forward characteristics and, as Tansely, (1971) suggests, show the worse device properties. However, the room temperature reverse I-V curves for each device is shown (together with the forward currents) in Fig.6.1 showing an ohmic region followed by current saturation with a slight excess current. The diodes exhibit soft breakdown because of the reasons mentioned in Section 5.3.4.

The rectification ratios of current at a particular bias of 1 volt are 470, 100, 31 and 16 for x = 1, .75, .5, .33 respectively. This is understandable since the spike barrier in the conduction band edge becomes smaller as x is reduced.

6.3 Spectral Photoresponse

Using the experimental arrangement of Fig. 4.8 and the method described in Section 4.5, the spectral photoresponse of the unbiased CdSe/CdS_xSe_{1-x} heterodiodes were measured and the results are shown in Fig. 6.11.

It wasobserved that as x decreased, the spectral band-width becomes narrower from the low wavelength end while that at the high wavelength end remains approximately fixed. The photoresponse measurements confirm an accumulation depletion structure. The signal was attenuated in forward bias and amplified in reverse bias, as expected.

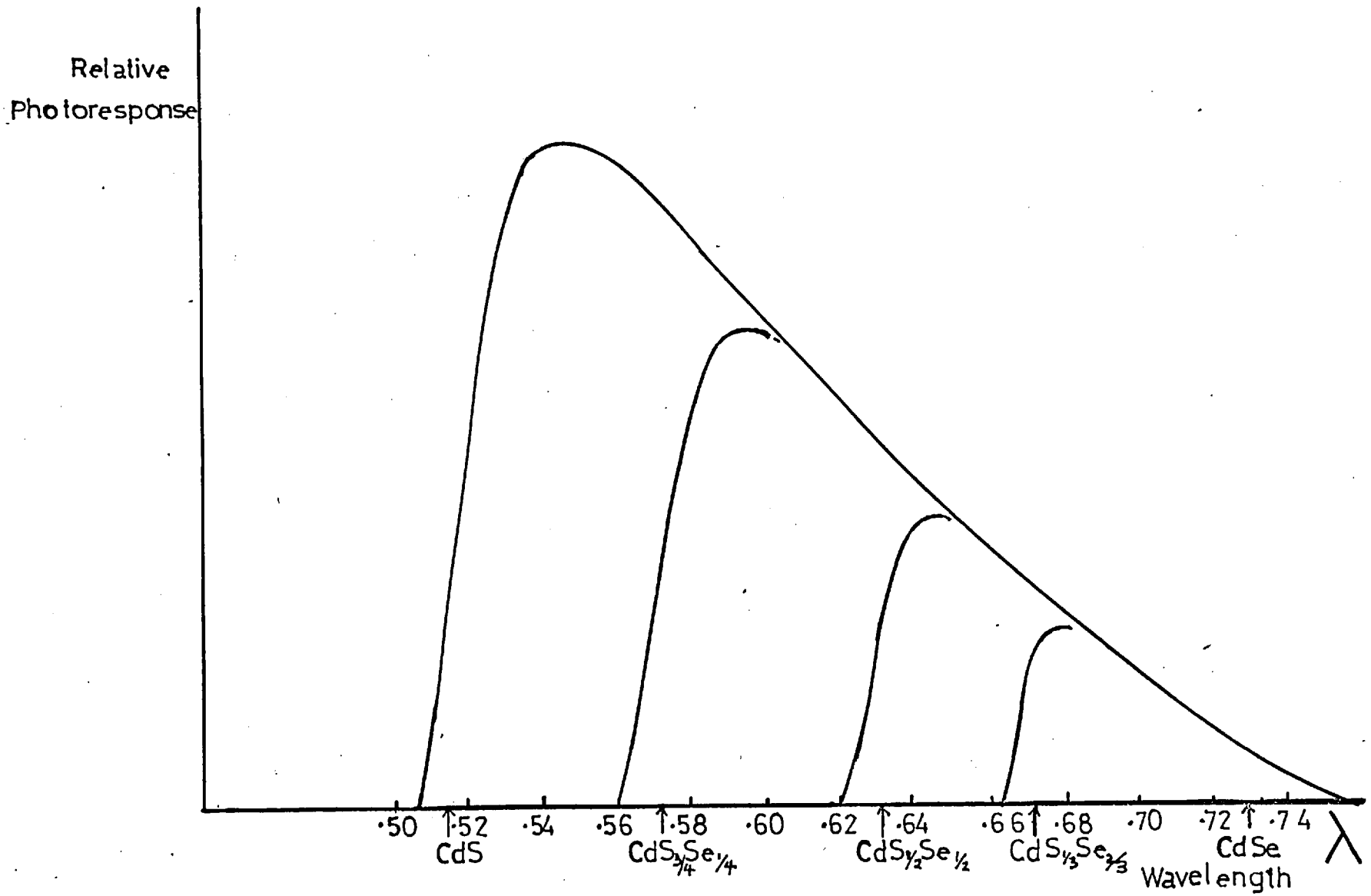


Fig. 6.11. Spectral Photoresponse of $CdSe/CdS_xSe_{1-x}$ Heterostructures at Room Temperature.

REFERENCES - CHAPTER 6

Demoulin, E., Van De Wiele, F. (1970) Proc. Int. Conf. Phys. Chem. Semicond. Heterojunctions Layer Structures, Budapest, 1970 2, 267. Hungary Acad. Sciences, Budapest.

Fang, F. F., Howard, W. E. (1964) J. Appl. Phys. 35, 612.

Fisher, J. (1973) M. Phil. Thesis, Univ. of London.

Gasanov, H. G., Magomedov, X. A., Magomedov, M. A. (1964) Izvestiya - Vysshikh Uchebnykh 7, 129.

Green, M. (1973) Private Communication.

Hovel, H. J., Milnes, A. G. (1968) Int. J. Electron 25, 201.

Konozenko, I. D., Kushneir, S. Ch. Musalevsky, E. A., Ostranitza, A. P., Petrenco, N. S., Pavlenko, A. A. (197) Proc. Int. Conf. Phys. Chem. Semicond. Heterojunctions Layer Strucutres, Budapest, 1970, 1, 221. Hung. Acad. Sci. Budapest.

Lampert, M. A. (1956) Phys. Rev. 103, 1648.

Miles, (1972) Ph.D. Thesis, Univ. of London.

Pavlenko, A. A., Muzalevskii, E. A. (1971) Sov. Phys. - Semicond. 4, 1373.

Perez, E. J. (1972) Ph.D. Thesis, Univ. of London.

Rose, A. (1955) Phys. Rev. 97, 1538.

Tansley, T. L. (1971) Semiconductors & Semimetals 7A, 293.

Yates, H. (1974) Project (Material Section) Univ. of London.

Van De Wiele, F., Van Overstraeten, R. (1967) Electron. Lett. 3, 218.

CHAPTER 7 - CONCLUSION

Good quality single crystal boules of CdS, CdSe and the alloys were reproducibly grown by the modified Piper-Polich vapour-phase transport technique under the conditions of diffusion-limited growth with slightly supersaturated vapours, (Ballentyne et al, 1970).

The electrical and crystallographic properties of the alloys were similar to those of the parent materials, though generally varying in magnitude lineraly with the molar ratio of S to Se.

The boules provided suitable substrates for hetero-epitaxy involving CdSe growth by r.f. sputtering to form $nCdSe/nCdS_xSe_{1-x}$ structures. The conditions necessary for good epitaxial growth unfortunately produced grading in carrier concentration at the junction due to inter-diffusion but there was no noticable grading in the composition of the bulk materials.

The Poisson's equation for isotype heterojunction was solved numerically for both the abrupt case with and without interface states and for the graded case using similar approaches to Czerveny (1968), Kumar (1968) (for the abrupt case) and Oldham and Milnes (1963) (for the graded case). This study provided a good understanding of the space-charge regions and gave the necessary information for constructing the band profiles, and the capacitance-voltage behaviour of isotype hetero-junctions. In the absence of interface states, these heterojunctions closely resembles the Schottky contact (especially when $N_{D1} > N_{D2}$). When interface states are present, arising from lattice mismatch, and represented in a constant monopole model, the value of V_{D1} in the accumulation layer is reduced while that in the depletion layer increases. If this interfacial charge is of sufficient magnitude, the accumulation layer is transformed to a depletion layer and the device can be represented by two Schottky contacts back-to-back. Oldham and Milnes (1964) suggested that if the lattice mismatch is $>1\%$ then interface states

would play a dominant role. When applying these theories to the CdSe/CdS system where lattice mismatch is $\simeq 4\%$, the experimental results indicated a minor role for these states. (It is expected that as the bonds in the substrates are mostly ionic, the number of 'dangling bonds' will be lower for a given lattice mismatch than that for covalent materials). Similar conclusions, derived from I-V, C-V and photoresponse measurements were obtained for the mixed crystal substrates. This independance of dangling bond concentration may be attributed to the dangling bonds being 'saturated' during CdSe growth (as the pressure was only 10^{-5} torr) perhaps by adsorbed impurities e.g. oxygen, thus greatly reducing the interface state density.

The expected variations of electrical properties with lattice mismatch between the CdS_xSe_{1-x} substrates and the CdSe epi-layer were, therefore, not observed. However, the observed variations of electrical properties with the different CdS_xSe_{1-x} substrates resulted mainly from their bulk properties. For instance, the observed variations of capacitance with substrate composition was due to change in the height of the rectifying barrier, mainly from electron affinity variations, (assumed to vary linearly with x) shown in Fig. 6.3 and Table 6.1. The discrepancies between observed and theoretical values of built-in-voltage, V_D were attributed partly to non-uniform grading in carrier concentration at the junction and partly to small amounts of interface states. The measured height of the rectifying barrier indicated negligible composition grading at the junction. This result was confirmed by microscope studies.

The 'window effect' was illustrated in the photoresponse measurements (Fig. 6.11) on the heterodioes, the cut-off frequencies closely relating to the band-gap of the materials. Further variations with substrate composition were due to the built-in voltages (i.e. magnitude of the photovoltage). The photovoltage signal was shown to attenuate under forward-bias and amplified under reverse-bias. These measurements confirmed

the proposed accumulation-depletion model across the interface for all the $CdSe/CdS_xSe_{1-x}$ devices.

The expected dominant charge carrier transport mechanism in the $CdSe/CdS_xSe_{1-x}$ structures, since the barrier height $> \frac{kT}{q}$ and depletion layer ~ 0.5 μm, was thermal emission over the barrier - a model adopted from homojunction theory. However, the forward current showed space-charge limited behaviour, due to the high resistivity of the CdSe layer and made it extremely difficult to analyse the junction characteristics. One obvious solution to the problem would have been to decrease the resistivity of the CdSe epi-layer provided that this is not too great so as to alter the transport mechanism across the junction.

Forward current measurements indicated the presence of grain boundaries in the CdSe epi-layer, across which the carriers would flow. This would undoubtedly severely perturb the periodic lattice giving rise to Tamm-like states.

The fabrication method gave reliable and reproducible results from which properties were associated with the devices rather than the fabrication steps. Thus direct comparison could be made between different $CdSe/CdS_xSe_{1-x}$ devices.

The devices fabricated in this work, unfortunately, did not exhibit any favourable properties which could be exploited for commercial applications. The important properties viz rectification, switching, photovoltage could not compete with the already available Si, Ge, GaAs, homojunctions and Schottky diodes. The $CdSe/CdS_xSe_{1-x}$ showed only a very small photovoltage. However, heterostructures incooporating either one of these materials with a p-type material e.g. CdTe, would be expected to exhibit pronounced photovoltage properties. Such devices may have applications as commercially viable solar energy converters.

APPENDIX A Purity of Starting Materials Used for the Growth of CdS, CdSe and CdS_xSe_{1-x} Crystals.

A1 'Optran' Cadmium Sulphide Polycrystalline Lumps Typical Mass Spectrographic Analysis (in p.p.m units)

Uranium (U)	<0·02	Ruthenium (Ru)	<0·1
Thorium (Th)	<0·02	Molybdenum (Mo)	<0·1
Bismuth (Bi)	<0·02	Niobium (Nb)	<0·01
Lead (Pb)	<0·04	Zirconium (Zr)	<0·04
Thallium (Tl)	<0·02	Yttrium (Y)	<0·02
Mercury (Hg)	<0·06	Strontium (Sr)	<0·02
Gold (Au)	<0·02	Rubidium (Rb)	<0·06
Platinum (Pt)	<0·06	Bromine (Br)	<0·4
Iridium (Ir)	<0·04	Selenium (Se)	<2
Osmium (Os)	<0·04	Arsenic (As)	<0·02
Rhenium (Re)	<0·04	Germanium (Ge)	<0·2
Tungsten (W)	<0·06	Gallium (Ga)	<0·03
Hafnium (Hf)	<0·06	Zinc (Zn)	<4
Lutetium (Lu)	<0·02	Copper (Cu)	0·03
Ytterbium (Yb)	<0·06	Nickel (Ni)	<0·08
Thulium (Tm)	<0·02	Cobalt (Co)	<0·02
Erbium (Er)	<0·06	Iron (Fe)	<2
Holmium (Ho)	<0·02	Manganese (Mn)	<2
Dysprosium (Dy)	<0·06	Chromium (Cr)	0·06
Terbium (Tb)	<0·02	Vanadium (V)	<0·02
Gadolinium (Gd)	<0·08	Titanium (Ti)	<0·02
Europium (Eu)	<0·04	Scandium (Sc)	<0·2
Samarium (Sm)	<0·08	Calcium (Ca)	1
Neodymium (Nd)	<0·4	Potassium (K)	0·4
Praseodymium (Pr)	<0·02	Chlorine (Cl)	<0·1
Cerium (Ce)	<0·2	Sulphur (S)	Base
Lanthanum (La)	<0·01	Phosphorus (P)	0·06
Barium (Ba)	<0·2	Silica (Si)	<2
Caesium (Cs)	<0·02	Aluminium (Al)	0·4
Iodine (I)	<0·2	Magnesium (Mg)	<0·2
Tellurium (Te)	<0·06	Sodium (Na)	0·6
Antimony (Sb)	<0·04	Fluorine (F)	<0·1
Tin (Sn)	<0·06	Oxygen (O)	—
Indium (In)	<0·2	Nitrogen (N)	—
Cadmium (Cd)	Base	Carbon (C)	—
Silver (Ag)	<0·04	Boron (B)	<0·3
Palladium (Pd)	<0·08	Beryllium (Be)	<0·02
Rhodium (Rh)	<0·02	Lithium (Li)	<0·04

A2 'Vactran' Cadmium Selenide Typical Emission Specification

Assay (ex Cd)	99.8%
Silica	trace
Aluminium	slight trace
Zinc	slight trace
Manganese	slight trace
Copper	partial trace

APPENDIX B Purity of Cadmium Selenide of Sputtering Tartet Material

Cadmium Selenide (Nordiko Ltd)

Copper	$<.0001\%$
Iron	$<.0003\%$
Nickel	$<.0001\%$
Lead	$<.0001\%$
Volatiles	$<.02\%$